LOW SALINITY WATER ALTERNATE GAS INJECTION PROCESS FOR ALASKAN VISCOUS OIL EOR

By

Kushagra Saxena, B. Tech.

A Thesis Submitted in Partial Fulfillment of the Requirements

for the Degree of

Master of Science

in

Petroleum Engineering

University of Alaska Fairbanks

May 2017

APPROVED:

Mohabbat Ahmadi, Committee Chair

Shirish Patil, Committee Co-chair

Abhijit Dandekar, Committee Member

Robert Brugman, Committee Member

Yin Zhang, Committee Member

Abhijit Dandekar, Chair

Department of Petroleum Engineering

Douglas Goering, Dean

College of Engineering and Mines

Michael Castellini, *Dean of the Graduate School*

Abstract

Carbon dioxide has excellent oil swelling and viscosity reducing characteristics. CO_2 injection alternated with water has shown substantial incremental recovery over waterflood for the Alaska North Slope (ANS) viscous oil reservoirs. However, for any project, the ultimate CO_2 slug size is finite and once the apportioned solvent volume is used up, the reservoir oil rates gradually revert to the low waterflood rates during the later life of a field. Low salinity waterflooding (LSWF) has also shown some promise based on corefloods and single well tracer tests in North Slope light oil reservoirs. However, two challenges impede its implementation as a standalone enhanced oil recovery (EOR) option on the North Slope: 1) slow response; the delay prolonged with increasing oil viscosity and 2) large upfront investments for the processing and transport of source water.

This study proposes a hybrid EOR scheme, the low salinity water alternate gas (LSWAG) process, for the viscous fields of the ANS. The process was modeled by coupling geochemical and ion exchange reactions to a CO_2-WAG type pattern model of the Schrader Bluff O sand. The Schrader Bluff reservoir has been classified suitable for low salinity EOR based on its permeability, temperature, clay content, and oil and formation water properties. Oil recovery through wettability alteration was modeled through ion exchange at the clay sites. Multiphase compositional flow simulation was run using numerical dispersion control.

LSWAG forecast for 50 years following 36 years of high salinity waterflood recovered 15% OOIP more oil over high salinity waterflood and 4% incremental over high salinity WAG. This translates to an improvement of 58% and 11% over waterflood and conventional WAG respectively. Higher oil rates were observed during later life due to increased oil relative permeability caused by the low salinity mechanism. Furthermore, very low solvent utilization values were seen for LSWAG which can be tied to the higher ultimate oil recovery potential of using low salinity water over conventional waterflood. In summary, LSWAG outperformed LSWF and conventional WAG by synthesizing the oil swelling and viscosity reduction advantages of CO_2 with lower residual oil benefits of LSWF, while overcoming the challenges of the late response of LSWF and low waterflood oil rates during later life in a conventional WAG flood.

Dedication

To my Guru His Holiness Sri Sri Ravi Shankar who has made my life a living miracle

and

To my loving family who helped me keep faith in my moments of doubt

Table of Contents

Page

List of Figures

Page

List of Tables

Page

Acknowledgements

This study is the result of hard work and religious dedication to learning the science and art of Reservoir Simulation and, in turn producing something useful for the future of Alaskan viscous oil. Many hurdles were crossed, a few of which were more complex than anticipated. In retrospect, I could not have crossed some of them without seeking help from highly knowledgeable academic professionals, industry experts, and genuinely good people.

First and foremost, I would like to lend my deepest gratitude to Dr. Mohabbat Ahmadi, my committee chair for accepting me as a student. Dr. Ahmadi has always been very kind and considerate in his dealings and put a lot of faith in me. He gave me lot of breadth and freedom to take the research in my direction of interest. He would try and understand complex concepts related to enhanced oil recovery (EOR) modeling and history matching and always helped me out with a huge heart. I am thankful to him for providing me with funding during the last phase of my research.

I wish to thank Dr. Shirish Patil for the time he spent with me as the co-chair for this thesis. Dr. Patil provided invaluable assistance when needed during his time at the University of Alaska Fairbanks and King Fahd University of Petroleum and Minerals (KFUPM) in Saudi Arabia, where he is now Saudi Aramco Chair Professor of Petroleum Engineering. He also funded a much-needed trip to Houston, TX for a training with CMG that brought new life into this research. His assistance and contributions from a 12-hour time zone difference are greatly appreciated. In this regard, I would also like to thank KFUPM for allowing Dr. Patil to dedicate his time to this effort while he is working there.

Dr. Abhijit Dandekar also lent his unconditional support as a committee member both academically and nonacademically. The brainstorming sessions with him during the committee meetings brought about some of the best ideas incorporated into this thesis. His keen insight into rock on fluid properties saved me from a few potential pitfalls. I am also thankful to him for providing me funding for the first two semesters of my program.

I would also like to thank committee member Dr. Yin Zhang for his active participation in the committee meetings and the one-to-one meetings in his office. He helped make a broad roadmap for this research during its initial phases and provided valuable tips on history matching which made the process far less cumbersome.

Modeling the low salinity water alternate gas was a complex process and I was very fortunate to have the expert guidance of Dr. Robert Brugman (CMG) as a committee member. I am very grateful to him for kindly agreeing to serve on my committee when I requested him during my training in CMG. Dr. Brugman is an expert in pressure-volume-temperature (PVT) simulation and modeling miscible gas injection processes. His guidance on modeling CO_2 based processes in CMG accelerated my learning and helped me achieve a lot more in the allotted time frame.

I am extremely grateful to Jim Erdle (CMG) for donating four parallel processing GEM licenses for me to work with for my thesis. This saved me lot of simulation run time and again, enabled me to accomplish much more than I would have achieved without parallel processing power.

Vikram Chandrasekar (CMG) provided valuable support on my queries regarding low salinity waterflooding modeling in GEM. His detailed clarifications regarding the usage of certain low salinity waterflood keywords made this process very simple for me. I am very thankful to him for his support of my research.

I extend my thanks to Kiran Venepalli (CMG) who also helped me understand different modules in CMG. His guidance was instrumental in the decision to go to Houston for a training with CMG, and I appreciate his efforts toward the donation of parallel processing licenses to my department.

When modeling the Schrader Bluff reservoir, I received valuable guidance and input from Dr. Samson Ning (retired BP). In the absence of reservoir modeling data, his suggestion on using representative petrophysical properties and bottomhole well conditions played a key role in constructing a representative reservoir model. I am very grateful for his support.

I am also very thankful to Frank Paskvan (BP) who verified the performance forecasts for the different EOR models simulated and for bringing to my awareness the potential corrosion issues due to CO_2 usage as a solvent.

I would like to thank Dr. Catherine Hanks for her teachings on reservoir characterization and integration of geological data for reservoir modeling. These concepts have gone a long way in my pursuit to model the Schrader Bluff sands as accurately as possible with limited data.

I am also very grateful to Dr. Debasmita Misra for providing me Teaching Assistantship for one semester. I learned a lot through serving as a TA for his course on Subsurface Hydrology.

I am grateful to the Art of Living, a Humanitarian non-governmental organization, for helping me see life through the right perspective. I am thankful to my Art of Living teachers who helped push wisdom in my life. The knowledge and practices I learned through them helped keep stress at bay, which has been pivotal in me achieving my highest potential.

Last but not the least, I am blessed to have a loving and supporting family like mine. What they have done for me, nobody else could do.

CHAPTER 1 INTRODUCTION

Until recent years conventional, light crude oil has been abundantly available and has easily met the world demand for this form of energy. Over the past two decades, however, worldwide demand for crude oil has increased substantially, and hence, the supply of conventional oil is depleting fast. This rapid decline and the reduced availability of economically recoverable conventional oil has led to consideration of unconventional energy sources that have been insufficiently utilized, among which heavy crude oil and natural bitumen are perhaps the most readily available to supplement short- and long-term needs (Meyer et al., 2007). Innovation in enhanced oil recovery (EOR) techniques will be required to meet future demands of hydrocarbon fuels, and hence the oil and gas industry will inevitably have to focus on increasing the oil recovery of currently producing reservoirs as well as unconventional oil and gas resources via research and technological innovation.

The Alaska North Slope (ANS) contains vast resources of viscous and heavy oil primarily concentrated in the Upper-Cretaceous and Lower-Tertiary Schrader Bluff/West Sak and Ugnu reservoirs respectively. The total in-place resource for these reservoirs combined is estimated to be about 26 billion barrels (Bidinger and Dillon, 1991). To date about 150 million barrels of oil have been produced from the ANS viscous oil pools (Thyne, 2016). The in-place oil is viscous in the Milne Point Unit (MPU), with oil viscosity averaging around 150 cp in the Schrader Bluff sands. Viscosities increase as depth to the pay zones decrease with the concomitant increase in proximity to the permafrost and hence, lower reservoir temperatures. Live oil viscosities of the order of 50,000 cp have been measured in the overlying colder Ugnu reservoir (Hulm et al., 2013). Recovering the viscous to heavy oil economically from these shallow pools requires a combination of innovative EOR schemes and intelligent horizontal/multi-lateral well placement, which can contact a larger portion of the reservoir as compared to vertical wells, thereby reducing costs in the long run.

Thermal methods have proven very effective for heavy oils to substantially increase recovery over a waterflood. However, 1,800 feet [549 m] of permafrost above these viscous oil sands has always kept the applicability of thermal methods under question. Studies have been done for chemical Enhanced Oil Recovery (EOR) processes (Kumar and Mohanty, 2010, Seright, 2010) but they have not been

very successful at the field scale. Lack of close well spacing, high required water quality, expensive chemical and water treatment costs, and logistical issues make them unattractive on the ANS.

Due to the lack of a market for transporting gas to consumers, much of the gas produced is injected back into the reservoir. Its injection as a water alternating gas (WAG) has met success at the field scale to recover additional oil left behind after a waterflood. WAG combines the increased microscopic displacement efficiency of a gas with the improved macroscopic sweep of water. Furthermore, it has been shown that oil viscosity can be reduced by 90% after multiple contacts even in very viscous reservoirs where complete miscibility is not possible (Ning et al., 2011). This process has been termed Viscosity Reduction WAG, or simply VRWAG.

Usually, the gas injected may be lean or it may be enriched with intermediate components to enhance its miscibility with the reservoir oil. Additionally, the increased benefits of CO_2 based solvents as viscosity reducing injectants (VRI) have been established over and above those of CH_4-based ones. Carbon dioxide has phase behavior very similar to propane but is substantially cheaper. This makes CO_2 an attractive solvent for achieving miscibility and reducing in-place oil viscosity. Other benefits include low solvent utilization and CO_2 sequestration. The Prudhoe Bay reservoir has approximately 5 trillion cubic feet of CO_2 that may become available once the gas sales start (Ning et al., 2011).

Efforts have also been made to evaluate the prospect of a surfactant based-WAG, or SAG, for the viscous oil of the North Slope. This is being done to remedy the problem of the unfavorable mobility ratio of CO_2 with viscous oil. Foams have been shown to reduce the effective permeability of gas considerably (< 10%); this is more pronounced in unconsolidated sands (< 5%) (Bernard and Holm, 1964). Secondly, foams are anticipated to improve the solvent utilization beyond that of the WAG process. The Schrader Bluff sands are heavily stratified with high permeability zones. In-situ foams may reduce the mobility of CO_2 in these high permeability zones thereby arresting CO_2 viscous fingering considerably. However, the economic viability of this process i.e., increased oil recovery versus the added cost of surfactant remains a concern.

Among the various EOR options considered, low salinity waterflooding has also been tested at the lab scale, as well as single well chemical tracer tests (SWCTT) (McGuire et al., 2005a, Jerauld et al.,

2006, Lager et al., 2008, Patil et al., 2008b, Seccombe et al., 2008). Injection of water of significantly lower salinity than that of the connate water disrupts the ionic chemical equilibrium between the ions in solution and the ones that are attached to the mineral (clay) surface. This results in a shift of wettability towards a more water-wet state, causing higher oil recovery. The Schrader Bluff oil pool in the Milne Point Unit and the adjacent time-equivalent West Sak oil pool in the Kuparuk River Unit have been identified as top candidates for low salinity waterflooding among a pool of 32 fields on the North Slope (Thyne, 2016). The screening criteria used was based on factors such as field estimated ultimate recovery (EUR), recovery factor at EUR, permeability, oil composition, and reservoir temperature.

In comparison, it is estimated that low salinity waterflooding may yield relatively lower recovery at any time/injected volume compared to WAG. However, in the light of economics, it may be the more practical option given the cheap and easy availability of low salinity water from the Prince Creek aquifer that overlies the Schrader Bluff formation (McGuire et al., 2005a) compared to gathering and transporting CO_2 from Prudhoe Bay. Furthermore, pumping and treating water may be cheaper than compressing and recycling gas. However, in contrast to the fast oil production response from the WAG process, the delayed oil response in a low salinity waterflood poses economic hurdles. The oil market also plays a significant role, as more expensive methods may be sustained only at higher oil prices.

1.1 Outline of Present Research

The main objective of this research was to evaluate the applicability and performance of low salinity waterflood cycled with CO_2 using a typical WAG design for the Schrader Bluff reservoir on the North Slope, Alaska. The key objectives of this study are as follows:

1. Model the petrophysical properties and characterize a quarter pattern with 2000 ft [610 m] horizontal wells in the Schrader Bluff OA sand.
2. Tune the equation of state for an 18°API, 76 cp viscosity Schrader Bluff oil.
3. Validate the simulation and fluid model by matching a benchmarked waterflood and carbon dioxide WAG performance done for a type pattern model for the same reservoir sand.

4. Develop the low salinity EOR models – low salinity waterflood and low salinity CO_2-WAG – by coupling geochemistry with the gross simulation model.
5. Analyze performance forecasts for different recovery models and evaluate potential challenges of using carbon dioxide as a solvent.

1.2 Summary of Subsequent Chapters

This thesis is divided into eight chapters. Chapter 2 consists of a detailed literature review describing the global distribution of heavy oil. The Alaskan viscous oil pools are discussed and the Schrader Bluff reservoir sands are described in detail. A detailed screening of various enhanced oil recovery (EOR) methods is discussed and the suitability of the water alternate gas (WAG) and low salinity waterflooding processes is established for the Alaskan reservoir conditions.

Chapter 3 discusses the construction of a type pattern model (TPM) for the Schrader Bluff OA sand in detail. In the absence of detailed petrophysical data, modeling of the heterogeneous rock properties through integration of MATLAB's reservoir simulation tools, statistical techniques, and representative well logs is described. The relative permeability correlation to generate oil-water and gas-liquid tables is also described, along with the length and orientation of the wells in the simulation model.

Chapter 4 discusses the workflow for modeling the Schrader Bluff viscous oil equation of state (EOS). Using limited PVT data, the characterization of a 10 component, 18 °API, and 76 cp viscosity fluid is described. The tuned fluid model's interaction with carbon dioxide is also examined and the mixture's unusual PVT behavior for the Schrader bluff conditions is also established through PVT simulation.

Chapter 5 describes the methodology used to tune the uncertain reservoir model parameters, such as absolute and relative permeability variables, by calibrating the simulation model to a benchmarked waterflood and CO_2-WAG performance done in a previous study for a similar TPM of Schrader Bluff.

Chapter 6 describes the development of the low salinity EOR model by coupling geochemical and ion exchange reactions with the base model. In the absence of clay distribution data, the use of porosity as a proxy is described. A detailed review of basic ideas and concepts behind reaction path modeling, as well as the simulator capabilities and limitations for modeling the low salinity process,

are discussed. Finally, wettability alteration based on the cation exchange process is shown. Incorporation of a hybrid mobility weighing numerical scheme to control dispersion and improve resolution over grid cells is also mentioned.

Chapter 7 evaluates the performance of the waterflood models and compared with that of the WAG models, including low salinity EOR models. In addition to from producing oil rates and recoveries, other production parameters such as water-cut and gas-oil ratio (GOR) are also assessed for the simulations. Model-wide monitoring of aqueous components is done and their activity is interpreted. Potential corrosion issues due to CO_2 in the effluent stream are discussed and a workflow for a possible solution is described.

Chapter 8 presents the main findings of this work and discusses key observations. This is followed by a set of recommendations for future work that can carry this study forward to enhance the reservoir modeling approach and gain deeper insight into the feasibility of low salinity processes.

The Appendix has the output of the formation water that was equilibrated in a geochemical modeling package, PHREEQC. This was used to identify key aqueous reactions to include in the geochemical model.

CHAPTER 2 LITERATURE REVIEW

Seventy percent of the world's oil resources are heavy and viscous (Alboudwarej et al., 2006). These are difficult and costly to produce and refine. It is estimated that there are 9-13 trillion barrels of heavy oil, extra heavy oil and bitumen globally. With high oil demand and lack of availability of "easy" conventional oil, the industry focus in many parts of the world is shifting to exploitation of heavy oil. Heavy oil is defined as having 22.3°API or less. Extra-heavy oils have 10°API gravity or less and are denser than water. By contrast, conventional oils such as Brent or West Texas Intermediate crudes have densities from 38 to 40°API, while the Dubai benchmark crude has an oil density of 31°API (Petroleum.co.uk, 2015).

The property that most affects producibility and recovery of heavy oil is its high viscosity. Viscosity of conventional oils ranges from 1 cp, the viscosity of water, to about 10 cp. The viscosity of heavy and extra-heavy oils may range from less than 20 cp to more than 1,000,000 cp (Alboudwarej et al., 2006). Live oil viscosity in the Ugnu field in Alaska is as high as 50,000 cp (Hulm et al., 2013). Bitumen, the most viscous hydrocarbon, is solid at room temperature; however, it softens readily when heated. Many countries have recognized the valuable role heavy oil promises to play in the future of the oil industry. These countries are moving to increase their production, revise reserve estimates, test new technologies and invest in infrastructure to ensure that their heavy oil resources are not left behind.

2.1 Distribution of the Vast Resource

The largest heavy oil accumulations occur in supergiant, shallow deposits trapped on the flanks of foreland basins. Foreland basins are huge depressions that are formed when a subducting tectonic plate downwarps during an orogeny. Marine sediments in the basin source hydrocarbons migrate updip into sediments eroded from newly built mountains. The Ugnu heavy oil field on the Alaska North Slope (ANS), for example, is composed of a succession of marine and nonmarine sequences deposited from south to north from the nascent Brooks Mountains during the Cretaceous and Tertiary (Hulm et al., 2013). The updip traveled oil resides in shallow, cool sediments where it undergoes biodegradation, the main cause of formation of heavy oils (Alboudwarej et al., 2006).

2.1.1 Global Distribution

The Orinoco heavy oil belt in Venezuela with 1.2 trillion barrels [190 billion m^3] of extra-heavy, 6 to 12° API oil (Alboudwarej et al., 2006), is the largest known individual petroleum accumulation in the world. Accumulations totaling 1.7 trillion barrels [270 billion m^3] occur in the western Canada basin in Alberta combined. The total heavy oil resources in all deposits of western Canada and eastern Venezuela total 5.3 trillion barrels. Substantial extra-heavy oil resources also occur in the North Caspian Sea (421 billion bbl) and in the Volga-Ural deposits (263 billion bbl) in Russia (Meyer et al., 2007). Region-wise split for heavy oil and bitumen deposits are shown in Table 2-1.

Table 2-1 Regional distribution of heavy oil and natural bitumen (billion barrels)

Region	Heavy Oil, OOIP	Bitumen, OOIP
North America	650	1671
South America	1099	2070
Europe	75	17
Africa	83	13
Transcaucasia	52	430
Middle East	971	0
Russia	182	296
South Asia	18	0
East Asia	168	10
Southeast Asia and Oceania	68	4
TOTAL	**3366**	**4311**

2.1.2 Alaskan Viscous Oil Pools

The Alaska North Slope contains vast resources of heavy oil primarily concentrated in the West Sak, Milne Point, and Ugnu reservoirs. There are five major viscous oil fields producing in Alaska: Schrader Bluff, West Sak, Orion, Polaris, and Tabasco. The West Sak and Ugnu heavy oil reservoirs lie within the Kuparuk River Unit (KRU). In this unit, the Ugnu reservoir is the shallowest heavy oil deposit that overlies the West Sak formation. The Schrader Bluff viscous oil formation overlies the Kuparuk River formation and underlies the Milne Point Unit (MPU), while the Orion and Polaris heavy oil belts are classified under the Prudhoe Bay Unit (PBU). The estimated total oil in place

within these reservoirs amounts to 20–25 billion barrels, with about two-thirds of the heavy oil lying under the Kuparuk River Unit (Patil et al., 2008a).

2.1.3 Schrader Bluff/West Sak Sands

The informal terms Schrader Bluff and West Sak denotes a sequence of stratified sands deposited during the Late Cretaceous below the present Kuparuk River and Milne Point Units, respectively. Collectively, they are part of the Schrader Bluff Formation in the Colville group. From West to East, the formation top lies at depths ranging from 2400–3800 ft [732–1158 m] subsea true vertical depth (SSTVD) beneath the KRU (Targac et al., 2005) and 3500–4500 ft [1067–1372 m] beneath the MPU (Smalley et al., 1997), respectively. From bottom to top, the sand members represent a transition from inner-shelf deposition to shallow marine or delta front (Werner, 1987), typical of an upward cleaning gamma ray log. The formation dips gently North-Northeast at 130 ft/mile [25 m/km] below the KRU (Werner, 1987) while increasing to 170 ft/mile [32 m/km] beneath the MPU (Smalley et al., 1997). The sands are very fine- to fine grained, moderately sorted, and contain interbedded siltsones and mudstones (Werner, 1987). Quartz is the dominant mineral while feldspars and lithic rock fragments are also present. Mica is present in small amounts, while traces of glauconite have been observed in some core samples. The clay matrix consists of kaolinite, illite, and chlorite and varies between 5–30% of the total rock fragment.

2.1.3.1 Schrader Bluff O Sands

The Schrader Bluff sand sequence is broadly divided into two sand packages: N sands and O sands. The shallower N sands are subdivided into six reservoir intervals. These multiple sand sequences are 5–15 ft thick and have permeabilities in the range of 5 mD–5 D, respectively (Smalley et al., 1997). The lower sand package, O sands, is the focus of interest for this study. These are found at depths between 3,900 ft and 4,200 ft [1,189 m and 1,280 m] beneath the MPU S-Pad and are subdivided into seven separate reservoir horizons, namely, from top to bottom: OA, OBa, OBb, OBc, OBd, OBe, and OBf (McGuire et al., 2005b). Figure 2-1 shows the sand package correlation for the Schrader Bluff O sands under the Milne Point and Prudhoe Bay units and the corresponding West Sak sands under the Kuparuk River unit.

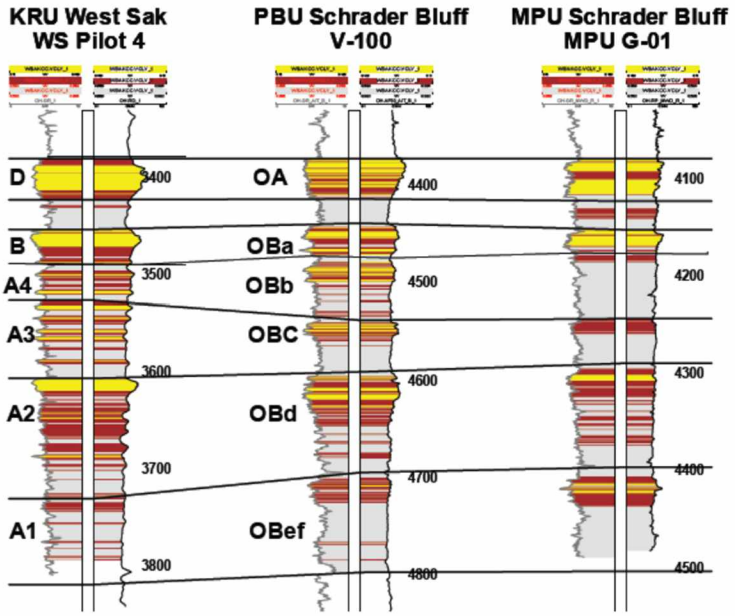

Figure 2-1 Cross-section of the Schrader Bluff O sands

The O sands have porosities in the range of 25–35% (McGuire et al., 2005b). Permeabilities in the reservoir intervals vary from 50–400 mD with the higher end representing blocky to fining upwards facies within the discrete sand units. The average reservoir pressure is about 1,790 psia at 4,000 ft [1,219 m] SSTVD. The reservoir temperature is approximately 82° F at this depth.

2.2 Schrader Bluff Fluid Properties

The Schrader Bluff reservoir is undersaturated by approximately 500 psia, with no gas cap (Strycker and Wang, 2000). Oil in the O sands is of better quality than the shallower N sands. Oil gravity in this interval ranges from 18 to 21.5°API while viscosities are between 30 and 45 cp. The fluid resembles that of a typical heavy oil, with a low gas-oil ratio (100–200 scf/STB) and low formation volume factor (FVF) (1.04–1.08 RB/STB).

Compositionally, Schrader Bluff live-oil has about 30% C_1 and is dominated by a large fraction of C_{7+} (about 67 mole percent) (Strycker and Wang, 2000). C_2–C_6 are present in negligible amounts, suggesting high biodegradation. Thus, the produced gas is primarily methane. While carbon dioxide and nitrogen may be present in trace quantities, hydrogen sulfide is absent from the compositional makeup.

The formation water salinity increases with depth from the southwest to the northeast part of the unit and averages around 27,000 ppm of total dissolved solids. The average NaCl equivalent salinity is 20,000 pm (Strycker and Wang, 2000). Smalley et al. (1997) report the formation water salinities in excess of 30,000 ppm in the northwest part and less than 10,000 ppm in the southwest part of the MPU. It is proposed that fresh water may have entered the formation from the southwest, where it crops out, facilitating biodegradation in the shallower, up-dip parts of the reservoir with greater access to the influx.

In general, this shallow belt of sands provides an environment conducive to the formation of viscous to heavy oil. The final composition of the viscous crude and its characteristic high densities and viscosities vary with depth and also laterally within a sand unit as it traverses down-dip. Furthermore, the low temperature and pressure conditions, the degree to which it has been degraded, and the presence of a 1,650 ft [500 m] layer of permafrost at about 1,200 to 1,700 ft [365 to 520 m] (Hallam et al., 1992) below the surface make this reservoir a challenging candidate demanding suitable recovery methods to develop it.

2.3 Recovery Methods

Heavy oil recovery methods are classified into two main types based on temperature: (1) thermal and (2) non-thermal (cold) methods. This is because viscosity, which plays a key role in the transport of heavy oil, is highly influenced by temperature. Heavy oil become less viscous when heated. Thermally assisted methods are used when the oil viscosity is so high (usually greater than 20,000 cp) (Chmielowski, 2013) that it needs to be heated to make it mobile. On the contrary, when the viscosity is low enough to allow economic extraction of oil, cold production methods – those that do not require the addition of heat – are preferred.

2.3.1 Non-thermal (Cold) Methods

2.3.1.1 Mining

Mining, the original cold method of heavy oil recovery, occurs in open-pit mines (Alboudwarej et al., 2006). Mining bitumen sands is common in Canada and in Russia, where heavy oil has been recovered by subsurface extraction. The open-pit method requires a substantial large volume of reserves to make

it economic. Such a method is practical only in Canada where the surface access and volume of the shallow oil deposits (estimated at 176 billion barrels) make it commercially feasible.

Oil sands are recovered by trucks and shovel applications and subsequently transported to processing plants where gravity separation of bitumen from sand takes place in warm water. The bitumen is upgraded to form synthetic crude oil by diluting with lighter fractions. This method is the primary choice of operators wherever helpful conditions are encountered due to a high recovery rate: greater than 80% of the hydrocarbons (Alboudwarej et al., 2006). However, only reserves down to about 246 ft [75 m] can be accessed from the surface. Unfortunately, these make up only 20% of the heavy oil share. In 2014, Canadian oil sands production was 1.98 million bbl/day. This is expected to grow to 3.7 million bbl/day by 2020 and 5.2 million bbl/day by 2030 (CERI, 2014).

2.3.1.2 Primary Cold Production

It is also possible to produce heavy oils from boreholes by primary cold production. A large part of the oil in the Orinoco heavy oil belt in Venezuela and fields in offshore Brazil is recovered by cold production (Alboudwarej et al., 2006). As the oil is heavy and lacks mobility, horizontal and multilateral wells are drilled to contact as much of the reservoir as possible. Viscosity is reduced using diluents, such as naphtha, and once oil flows from the reservoir into the wellbore, artificial lifts such as electrical submersible pumps (ESPs) and progressive cavity pumps (PCPs) are employed to lift the hydrocarbons to the surface for transport to an upgrader. This method is advantageous due to its lower capital expenditure relative to thermally assisted processes however, the low recovery factor (6 to 12%) warrants switching to a more efficient recovery technique early in the life of the field. Furthermore, increasing fluid viscosity arising due to mixing and shearing of oil-water emulsions in pumps and tubulars poses an additional challenge.

2.3.1.3 Waterflooding

Waterflooding is perhaps the most widely applied cold method in heavy oil fields. Beliveau (2009) reviewed 37 waterflood projects in viscous oil reservoirs. 28 of the 37 fields are in Canada, with the oil viscosity varying from 5 cp (Midale field, Saskatchewan) to 1,935 cp (Buffalo Coulee, Saskatchewan). It is observed that expected oil recovery increases with increasing volumes of water injected. Also, in contrast to conventional light oils, the expected ultimate recovery (EUR) from a viscous oil field usually comes at very high water cuts, and the recovery factor decreases with

increasing oil viscosity. This is because water is much more mobile than viscous oil and causes viscous fingering in waterflood fronts, resulting in poor sweep efficiency. The success of a water flood project is contingent on the following factors: well spacing, facility design, throughput of injected water, voidage replacement, economic water-oil ratio limit, reservoir surveillance quality, and flexibility in adjusting the flooding pattern (Beliveau, 2009).

2.3.1.4 Cold Heavy Oil Production with Sand (CHOPS)

Recently, a new cold production method, cold heavy oil production with sand (CHOPS), has found acceptance as a primary production method in many heavy oil fields. It is a prospective primary recovery technique for developing the Ugnu heavy oil deposit on the Alaska North Slope (Pospisil, 2011). Numerous fields in Canada are employing this method, where oil and associated gas is produced along with 10% sand cut (Alboudwarej et al., 2006). In this process, gas exsolving from the oil that is depressurized helps destabilize and move sand grains. A unique feature of this process is the creation of channels, called wormholes, in the reservoir due to sand movement, which creates a growing zone of high permeability around the well and assists fluid mobility. The sand and liquids are extruded in the wellbore due to differential pressure. Gravity separation at the surface separates sand and oil and the sand is disposed of into permeable strata. CHOPS requires multiphase pumps that can handle sand, oil, and gas, and has been applied in fields with oil viscosity from 50 cp to 15,000 cp.

Deliberate production of sand, however, causes operational problems, the majority of which are related to pump failures (Dusseault, 2007). Frequent plugging of perforations by sand, especially small ports with large sand grains, leads to a gradual decline in production. In addition to perforation plugging, near-wellbore sand recompaction also causes cessation of production in wells. Recompaction can be attributed to the decline of solution-gas bubble drive that causes the sand to stop moving and recompact (PetroWiki, 2015a). Due to the increased pressure differential near the wellbore, water coning problems have also been observed in a part of Alberta's Lindbergh field, and have been reported to adversely affect productivity.

2.3.1.5 Vapor-Assisted Petroleum Extraction (VAPEX)

Vapor-assisted petroleum extraction (VAPEX) (Alboudwarej et al., 2006) involves the injection of a miscible solvent, usually propane at its dew point, which causes a reduction in the viscosity of heavy

oil. The method can be applied one well at a time as well as in well pairs. In single wells, the solvent is injected from the bottom of a horizontal well. In the double-well case, solvent is injected into the upper of a pair of parallel horizontal wells, much like the steam assisted gravity drainage (SAGD) process. Once produced, valuable gases are scavenged by inert gas injection. Vapor-assisted petroleum extraction (VAPEX) has been tested in Canada. Using propane, however, makes the cost of injected gas per barrel of oil recovered critical for the economic success of a VAPEX project (Talbi and Maini, 2003). For reducing project costs, CO_2 has also been tested for the VAPEX process. CO_2 is cheaper than propane and equally soluble in reservoir oil. Consequently, a mixture of propane and CO_2 further decreases the heavy oil viscosity.

2.3.2 Thermal Methods

Thermal methods, like their cold cousins, have their own advantages and limitations. Thermal-assisted methods yield a higher recovery factor than cold production methods (except for mining), but the costs associated with heat generation and water treatment are also high.

2.3.2.1 Cyclic Steam Stimulation (CSS)

Cyclic steam stimulation (CSS) is also known as the steam soak or huff and puff process. It is a single-well method that is applied in stages. Steam is injected after which the soaking or waiting period begins, in which the oil heats up. The heated oil with reduced viscosity is produced, along with water (condensed from steam), and separated at the surface. The process then repeats again. The method works well in stratified reservoirs and may yield recovery up to 30% OOIP (Alboudwarej et al., 2006). Some researchers, however, have a different take on CSS and have observed that the maximum recovery with CSS is relatively low and seldom exceeds 20% OOIP (Das, 1998). A common practice is to do steam flooding after CSS, which may yield a significant additional recovery. However, when the oil is highly viscous, this technique is generally not recommended. The Cold Lake field in Alberta is an example of CSS application (Alboudwarej et al., 2006).

2.3.2.2 Steamflooding

Steamflooding is another thermal method. It is essentially a multiwell process (Alboudwarej et al., 2006). Steam is injected into injector wells that are spaced out in a variety of location patterns. Steamflooding can achieve high oil recoveries up to 50% OOIP (Ali, 1974); however, this process requires good inter-well communication so that steam can be injected at effective rates.

Steamflooding has been successfully applied in heavy oil fields in California. Recoveries above 60% OOIP have been reported (Matthews, 1983): 60% at South Belridge (4,000 cp oil), 62% at Yorba Linda (85 cp oil), 65% at Mt. Poso (20 cp oil), 65% at Midway-Sunset (4,000 cp oil), and 68% at Kern River (4,000 cp oil). Though efficient at recovering oil, this method has certain challenges: gravity override of the low-density steam, reservoir heterogeneities, and monitoring/controlling the steam front (Alboudwarej et al., 2006).

2.3.2.3 Steam Assisted Gravity Drainage (SAGD)

Steam-assisted gravity drainage (SAGD) is gaining acceptance as the preferred method for extra-heavy oils. SAGD has been employed in numerous fields in Canada, including MacKay River and Christina Lake (Alboudwarej et al., 2006). In this process, a pair of parallel horizontal wells is drilled, one on top of the other, with about 16 to 23 ft [5 to 7 m] of clearance in between. Steam is injected into the upper well, which heats the heavy oil and lowers its viscosity. Due to gravity drainage, the mobilized oil flows down towards the lower horizontal producer. Sometimes, a solvent is used to establish initial communication between the injector and the producer. The estimated recovery factor for this method is between 50 and 70%. However, formation layering can significantly influence SAGD recovery. Simulation studies of the applicability of SAGD in the Ugnu Sands in the Alaska North Slope (ANS) have been done (Sharma et al., 2002). Recovery nearing 70% has been reported where a horizontal steam injector and a horizontal oil producer were placed in the upper and lower layer, respectively, of a two-layer homogeneous reservoir model. However, Ugnu sands are very heterogeneous. Sharma et al. (2002) observed substantive decline in SAGD efficiency with higher permeability anisotropy (less than 0.6) as well as lower permeability in the bottom section of the reservoir. It was concluded that the steam rising rate and the oil drainage rate were both impaired by vertical permeability reduction. Reduced permeability in the bottom layer resulted in poor drainage by the producing well located in the low permeability layer.

2.3.2.4 In-Situ Combustion

In-situ combustion is usually applied when dealing with highly viscous oils. It is also known as fireflooding, and is essentially a multiwell process (Alboudwarej et al., 2006). In this technique, a combustion front is initiated at an air-injection well which propagates to a producing well. Oil viscosity is reduced by the heat produced by the combustion process. However, in-situ combustion burns some of the oil left behind in the reservoir as residue. Due to combustion, cracking happens,

which upgrades the crude, separating small molecules from large ones. This process is mostly unstable. However, in the Suplacu de Barcău field, Romania, a large scale fireflooding operation has been operating since 1964 (Alboudwarej et al., 2006).

2.3.3 Challenges with Thermal Methods

Despite the apparent success of thermal processes for the recovery of heavy oil and bitumen, they suffer from inherent disadvantages. The applicability of steam-based recovery processes become limited for thin reservoirs due to heat losses to the base and caprock (Das, 1998). Steam as an EOR agent loses its economic viability in very deep formations, typically greater than 3,280 ft [1,000 m], and in those less than 33 ft [10 m] thick (Mangalsingh and Jagai, 1996). In formations that contain swelling clays, in-situ condensation of steam can cause severe permeability blockage near the production well. A simulation study of the SAGD process for the recovery potential of the Ugnu Tar Sands, Alaska North Slope showed great promise, but the optimistic results were fused with the danger of possible formation damage when steam was injected (Kamath et al., 1995). For steam processes, about 30% of the capital investment is used for the steam generation facilities (Das, 1998). The recycling of produced water is also an issue, as it requires elaborate processing. The disposal of waste water may also pose a threat to the environment. Limited area and operational hazards concerns may interdict the implementation of a steam project on offshore platforms. Furthermore, thermal well completion and other surface and subsurface accessories cost several times more than normal well completion. Many heavy oil and bitumen reservoirs are underlain by aquifers. In such reservoirs, SAGD may lose thermal energy released by condensation of steam to the underlying water and become uneconomic.

Oil production on the Alaska North Slope (ANS) is bound by another constraint – that of permafrost. Permafrost is ground that is always frozen throughout the year. On the Alaska North Slope, the thickness of this layer varies from just below 1,000 ft [304 m] to over 2,000 ft [608 m] in some areas. Here, the permafrost forms a continuous layer of frozen soil that consist of coarse sand, gravel, and conglomerates in the shallower part and silty sand, silt, and claystones in the deeper parts. In the Kuparuk River Unit (KRU), the depth of the "ice-bearing" permafrost varies from 1,200 to 1,700 ft [365 to 520 m]. Within the area containing the thick Ugnu accumulation, the permafrost thickness averages about 1,650 ft [500 m] (Hallam et al., 1992). The temperature at the base of the ice-bearing

permafrost interval is about 31°F [-0.5°C]. Under certain temperature and pressure conditions, gas hydrates are known to exist within and near the base of the permafrost.

An anticipated difficulty in producing oil through the permafrost region is its thawing around the producing oil wells. The recent emphasis on decreasing the footprint using directional drilling from closely spaced wells on small well pads has contributed to thawing of annular regions in permafrost around warm production wells. In the process of drilling a well, injecting a hot fluid, or extracting oil, natural gas, or formation waters, fluid circulating through the wellbore transfers the heat from warm formations (200°F [93°C] bottomhole temperature) at deeper depths to colder formations near the surface. Although the reservoir temperature in the shallower Ugnu sands is much lower and varies from 45°F [7°C] in the west to 65°F [18°C] at the eastern boundary (Hallam et al., 1992) due to the presence of permafrost, lower West Sak sands and reservoirs in the Prudhoe Bay unit have much higher temperatures (Gondouin and Fox III, 1991, AOGCC, 2012a). The heat from the warm fluid is conducted radially through the casing, thawing the annular area. Any thawing that occurs at the cement-permafrost interface would destroy the cement bond (Couch and Watts, 1970). Thawing of permafrost in the layers near the surface will result in sloughing of the soil around the wellbore. This can impose mechanical stresses on the casing and result in irreparable damage necessitating premature abandonment of the well. In view of the tremendous drilling and completion expenses encountered in the Arctic, this is obviously undesirable.

2.3.4 Chemical Flooding

In light of the above issues and challenges in producing heavy- and extra-heavy oil from the Alaska North Slope (ANS) fields, it is clear that the well-established thermal recovery methods cannot be applied. Chemical methods, although they are not considered suitable for oil viscosities over one or two hundred cp, have been applied with decent success in heavy oil fields in Canada. Two main chemical EOR processes are polymer flooding and alkaline-surfactant-polymer (ASP) flooding. Polymer based methods are applied with the objective of increasing the viscosity of injection water, thereby improving the mobility ratio and subsequently, improving the macroscopic sweep of a waterflood. Schematically, ASP covers two different processes. The surfactant assists in reducing the interfacial tension between water and oil, thereby reducing the residual oil saturation. For a first class of ASP processes, the addition of an alkaline agent such as NaOH promotes the formation of in-situ

surfactants when oil is reactive, which helps reduce the quantity of surfactant required to lower the interfacial tension. For the second class of ASP processes, the alkali decreases surfactant adsorption.

Delamaide et al. (2014) gave a review of 23 chemical heavy oil EOR projects in Canada, 12 of which were polymer-based and 8 were ASP-based methods. The most successful of them was the Pelican Lake project. Here, a polymer flood pilot was initiated following a low primary recovery – 5 to 10% OOIP – in a thin reservoir, approximately 5 m, with high oil viscosity in the range of 800 to 80,000 cp. The operators estimate the increase in recovery factor as 20 to 30% OOIP. In the Mooney Bluesky (Black Pearl) field, modeling studies indicated polymer flood recovery between 17 and 25% OOIP for the heavy oil field, where oil viscosity varies from 300 to 1,500 cp at reservoir temperature. Here, polymer injection was started after early water breakthrough of a waterflood pilot. The Seal Bluesky field had extra-heavy oil of 5,000 to 12,000 cp dead-oil viscosity. A polymer flood pilot with 3 injectors and 4 producers – all 4,593 ft [1,400 m] long horizontal sections – was initiated. Improved mobility resulted in oil rates increasing from approximately 30 bbl/day up to a maximum of 135 bbl/day in one of the wells and from approximately 50 bbl/day to a maximum of 155 bbl/day in another one. The estimated incremental recovery (IR) from this project is 8.8% OOIP. In the Taber South Manville B field, the incremental recover due to an ASP flood, followed by a 32 cp polymer flood, is estimated to be 11.1% OOIP. The dead oil viscosity for this field is 120 cp. Similar results for an ASP flood have been observed in the Suffield Upper Manville UU. The live oil viscosity ranges from 180 to 250 cp. According to the operator of this field, the expected recovery factor for primary + waterflood is 20% OOIP, and the incremental recovery due to the ASP flood is over 10% OOIP.

2.3.5 Challenges with Chemical Methods

Chemical EOR is effective when the pay zone is thin, and has been the preferred choice over thermal methods to develop heavy oil fields consisting of thin sand-shale sequences. Although efforts have been made to increase the use of polymer and ASP floods in other parts of the globe, they have been met with limited success. Surfactant flooding has difficult flood-design considerations of chemicals and setting up an ASP project usually warrants large capital requirements (Shahid et al., 2013). It is very sensitive to local reservoir heterogeneities. The reaction of alkali with minerals in the connate water and reservoir rocks may impact the flood process negatively. Surfactant loss due to chemical retention is common. This happens in the reservoir due to precipitation, adsorption, and phase partitioning into a slow-moving phase. Deterioration of the composition of the chemical slug may

happen because of chemical retentions, and leads to a poor displacement efficiency. Furthermore, alkali is not soluble in hard brines (Delamaide et al., 2014); hence, salinity is also a point of concern. ASP flood offshore projects are even more difficult to implement due to highly deviated wells, larger well spacing, sophisticated logistics, incremental costs, and limited slots on the platform (Shahid et al., 2013).

Polymer flooding, like surfactant flooding, has its own limitations. In many instances, in-situ cross-linking of the polymer causes a permeability reduction in the reservoir. High temperature and high salinity are challenges for conventional polymer flooding (Alomair et al., 2014). Polymer flooding is suitable for cases where viscosity is lower than 100 cp, temperature lower than 200°F [93°C], water salinity lower than 100,000 ppm, and formation permeability higher than 20 mD. The increased viscosity of the polymer solution sometimes makes it difficult to recover oil from smaller pores. This problem is aggravated in heavy- and extra-oil reservoirs. In a high temperature, high salinity (HTHS) environment, the polymer loses its mechanical and chemical stability. Furthermore, the high cost of chemicals stymies the applicability of this process in contrast with other methods like water alternate gas (WAG).

The major problem in using chemical methods on the ANS is the close well-spacing required for the success of the project. The Ugnu and the Schrader Bluff formations both have thick sand sequences (AOGCC, 2012b, Hulm et al., 2013). As such, the natural tendency of the water is to sweep the lower parts of the reservoir; adding a high molecular weight polymer would only make it denser. When the well spacing is large, oil in the lower sections may be swept, however, the upper section of the pay zone away from the injection well may not be contacted.

2.4 Choosing a Recovery Method

For developing the heavy and extra-heavy oil fields of Alaska, in view of recovery efficiency, production rates, reservoir characteristics, permafrost constraints, and economics, a suitable recovery technique would aim at lowering the in-situ oil viscosity without increasing the reservoir temperature. Here, water-alternating-gas (WAG) and vapor extraction (VAPEX) (Patil et al., 2008a) seem to be the more favorable methods for ANS field conditions. VAPEX utilizes injecting a mixture of propane or butane at its dew point and a non-condensable gas, like methane, in a similar way as steam is injected in SAGD using a horizontal well (Mokrys and Butler, 1993). While the non-thermal nature

of this method may appeal at first glance, and though it may be economical, it may face the same limitations as SAGD as far as reservoir heterogeneities are concerned. Once the oil is deasphalted, its downward mobilization to the producer will be contingent on vertical permeability. Furthermore, permeability reduction using a mixture of propane and methane may not be as significant as using propane and CO_2, or CO_2 alone for that matter (Talbi and Maini, 2003). WAG using CO_2 appears to be a suitable tertiary recovery method to extract heavy oil form the Alaska North Slope fields.

2.4.1 Water-Alternate-Gas (WAG) Flooding

WAG is a tertiary recovery technique that involves injecting alternate slugs of gas and water into the reservoir to recover additional oil left behind by water injection. The WAG injection was proposed initially to improve the sweep efficiency of gas injection, mainly by using water to control the mobility of the displacing gas and to stabilize the front. Because gasflooding leaves lower residual oil than waterflooding, and three phase zones may obtain lower remaining oil saturation, WAG has the potential for increased displacement efficiency (Christensen et al., 2001). Hence, the WAG injection combines both the benefits of improved microscopic displacement efficiency and an improved macroscopic sweep due to gasflooding and water injection, respectively. It has been shown that WAG injection results in a lower residual oil saturation than for waterflood or gasflood, owing to the effect of three-phase and cycle-dependent relative permeability (Skauge et al., 2007). WAG has the potential to recover oil by contacting unswept zones, especially the attic or cellar oils, as gas segregates to the top and water accumulates at the bottom. This results in improved recovery compared to that of waterflooding alone.

Due to alternate water and gas cycles, a complex saturation pattern is observed during the WAG process (Christensen et al., 2001). This is attributed to the cyclic increase and decrease of the two saturations during their injection cycles. The WAG mechanism at the microscopic scale that gives rise to the alternating increase and decrease of the saturation of the two phases has been explained by Minssieux and Duquerroix (1994). The first striking feature observed in the WAG process is that the pressure drop increases periodically during the imbibition sequence after a gas slug. This is because during imbibition, only a fraction of gas in place can be replaced by water, resulting in only a limited increase in water saturation, while the gas relative permeability practically drops to zero at the water front. Such hysteresis in the gas flow, causes a "stop-and-go" aspect of gas and water production. Following a pseudo steady-state of flow, gas production increases during each subsequent drainage

cycle. Water injection following the gas slug also causes gas trapping along the porous medium. Consequently, a high gas saturation is observed during initial gas breakthrough (Minssieux and Duquerroix, 1994).

The effect of trapped gas on reduction of residual oil saturation has been observed by several authors (Kyte et al., 1956, Champion and Shelden, 1989, Skauge et al., 2007). Land (1968) suggests an optimum gas saturation that would result in the lowest possible residual oil saturation following an imbibition process, such as waterflooding. The author acknowledges that the residual saturation of a three-phase system occupies the same volume as that of a two-phase system, i.e., trapped gas occupies pore space that would be occupied by trapped oil if gas was not present. A subsequent imbibition process would then strip at least a part of the trapped gas, leaving a lower residual oil saturation than would have been obtained in the absence of trapped gas. However, the author also mentions the adverse impact of increasing gas saturation on oil relative permeability. The decrease in relative permeability to oil would result in an unfavorable mobility ratio that would adversely affect the displacement efficiency. This would result, at a given water-oil ratio, in a larger hydrocarbon saturation left unrecovered by water displacement. According to the author, only after infinite throughput of water, that the maximum benefit of increased gas saturation will be realized. This, of course, is not possible on a practical level. An optimum gas saturation exists for maximum oil recovery that depends on both rock and fluid properties. Lighter oils, however, derive greater benefit than heavier ones (Land, 1968).

2.4.1.1 WAG Classification

WAG processes can be grouped in many ways. The most common is to distinguish between miscible and immiscible displacements as a first classification.

Miscible WAG (MIWAG) – Miscible displacement happens when the gas is injected at a pressure greater than the minimum miscibility pressure (MMP) of the reservoir oil. The minimum miscibility pressure is the pressure, at constant temperature, at which first- or multiple-contact miscibility (dynamic miscibility) between the injected solvent and the in-situ oil can be achieved. Ideally, at minimum miscibility pressure, the interfacial tension is zero and no interface exists between the fluids (Schlumberger, 2015). The MMP can be estimated from published correlations; measured in a PVT cell; estimated from correlations using an equation of state (EOS); and measured in a rising bubble

apparatus, from slim tube tests, or from core displacement studies (Mungan, 1991). The following criteria are used to describe miscibility:

1. A recovery of 85% or more of the oil in place at solvent breakthrough
2. Single phase observed at the core outlet
3. At least 95% recovery at 1.2 pore volume of solvent injection.

The MMP is directly proportional to the reservoir temperature and to the amount of C_5-C_{30} components in the hydrocarbon mix (Holm, 1987, Orr Jr. and Silva, 1987). Studies have shown that a miscible process recovers more oil than an immiscible one (Madarapu et al., 2002). In a miscible process, displacement generally occurs via a condensing or a vaporizing mechanism. In condensing gas drives, the in-situ generation of miscibility occurs due to gradual enrichment of reservoir fluids in intermediate components of a solvent, to a point where the injected solvent and enriched oil become fully miscible. In the vaporizing drive, the in-situ generation of miscibility occurs due to extraction of intermediate components of the reservoir fluid by the solvent and its gradual enrichment with these intermediates as it flows in the reservoir (Sharma et al., 1995). Extensive experimental and theoretical studies on miscible WAG have been published in literature (Holm and Josendal, 1982, Gorell, 1988, Sharma et al., 1995, Khataniar et al., 1999, McKean et al., 1999, Jiang et al., 2012). However, the fluid and reservoir conditions in the shallow, viscous to heavy oilfields on the Alaska North Slope (ANS) usually render the gas injection process immiscible for pure solvents (Ning et al., 2011). Therefore, MIWAG is not the topic of research for this study and a detailed review of MIWAG cases has not been presented.

Immiscible WAG (IWAG) – In the case of an immiscible water-alternating-gas (IWAG) process, gas and water are injected alternately at a pressure less than the MMP. This is done until a certain predetermined amount of gas is injected, and then water is injected continuously. Subsequently, the reduced-viscosity oil is driven by water injection, resulting in a waterflood with an improved mobility ratio. This type of WAG process has been applied with the aim of reducing viscosity (Spivak et al., 1990) and improving frontal stability for contacting unswept zones. IWAG has been implemented in reservoirs where gravity-stable gas injection cannot be applied because of gas resource constraints or in low dip reservoirs having strong heterogeneity. In addition to sweep, the microscopic displacement efficiency is also improved (Christensen et al., 2001).

Swelling is an important compositional effect that takes place during an immiscible gas flood (Skauge et al., 2007). If the oil is undersaturated at the reservoir pressure or if gas injection increases the reservoir pressure, the volume of gas dissolved in the oil will increase until the oil is saturated at that pressure (PetroWiki, 2015b). The increased volume of gas in solution in the oil causes the oil formation volume factor (FVF) to increase. This phenomenon, known as swelling, causes oil to occupy more volume for a given mass or mole, and is known to increase the efficiency of the gas-oil displacement process (Sankur et al., 1986, Holm, 1987, Minssieux and Duquerroix, 1994, Li et al., 2011, Ning et al., 2011). Oil swelling and viscosity reduction usually go together in improving the mobility of the in-situ oil.

Stripping is another key compositional aspect of the immiscible gas-oil displacement process that happens due to the vaporization of the intermediate hydrocarbon components (C_3 through C_8) by the injected gas (PetroWiki, 2015b). In immiscible gas-oil displacements using carbon dioxide, nitrogen, or a combination of these gases with methane (such as 88% flue gas and 12% CO_2), vaporization of various hydrocarbon components until gas-oil equilibrium is reached at reservoir conditions may also be achieved. The Hawkins nitrogen injection project is a testimony to this (Carlson, 1988). Carbon dioxide has phase behavior like propane (PetroWiki, 2015b), and can extract a substantial amount of hydrocarbon components from the oil at reservoir conditions. The extent of the stripping effect also depends on the oil composition. Immiscible gas-oil injection projects have been applied in reservoirs having a range of oil gravities from 24 to 43° API or more (Christianson, 1977, Carlson, 1988, Ma and Youngren, 1994). In all cases, the stripping effect increases the recovery of hydrocarbons from the oil reservoir. Minssieux and Duquerroix (1994), however, observed only negligible stripping of the light ends of the reservoir oil of a 34°API crude and 2.5 cp viscosity. The injection gases used for their coreflooding experiments were dry gases, methane, and nitrogen.

It is difficult to distinguish between miscible and immiscible WAG injections (Christensen et al., 2001). In many cases, a multi-contact gas-oil miscibility may have been obtained, but much uncertainty remains about the actual displacement process. This is predominant where the reservoir pressure at the start of the gas injection cycle may be below the MMP, but not too much. This may cause the gas to be miscible near the injection well, where pressure may be higher than the average reservoir pressure and quite possibly close or higher than the MMP as well. However, further away from the injection well, towards the producer, the pressure would decrease causing the gas to lose

miscibility. It has not been possible to isolate the degree of compositional effect on oil recovery by WAG injection. Most of the miscible projects are repressurized to bring the reservoir pressure above the minimum miscibility pressure (MMP) of the fluids. However, failure to maintain sufficient pressure may cause loss of miscibility and the WAG process may oscillate between miscible and immiscible gas during the life of the oil production.

Christensen et al. (2001) have given an excellent review of approximately 60 WAG projects. In most of the cases, additional recovery by the WAG process was reported to be about 5%. However, incremental recovery from several fields, including Rangely Weber, Dollarhide, and Slaughter Estate have been up to 20%. Among the various projects reviewed by the authors, 10 were planned to be immiscible and 47 were planned to be miscible. Of these, two had not been classified. Most cases reviewed were high permeability reservoirs. Some cases of very low permeability chalk, e.g., the Daqing field, have also been reviewed. 33 projects had been applied in sandstone formations, while 12 fields were dolomite, 5 fields were mainly limestone, and 6 applications had been characterized as carbonate sequences. Except for Juravlevsko-Stepanovskoye and Ekofisk, all projects in carbonate rocks had been miscible WAG. CO_2 had been the choice of gas for dolomite reservoirs, except for Fenn Big Valley and Jay Little Escambia. Both hydrocarbon and non-hydrocarbon gases have been tested in sandstone, carbonate, and limestone reservoirs.

Hybrid WAG – In this process, a large fraction of the pore volume of the gas is continuously injected to about 20% to 40% HCPV and the remaining fraction is then injected using the WAG technique at a specific WAG ratio. This technique has the advantages of early production response, better injectivity, and minimizing water blocking. On the other hand, it has the disadvantages of poor sweep efficiency and less efficient use of the gas. A description of a successful hybrid WAG process is given for the Denver Unit, which is located in the Wasson field of west Texas (Tanner et al., 1992). A simulation study involving a four to six years continuous CO_2 injection, followed by a 1:1 conventional WAG, had been done. Early production response and ultimate recovery over continuous CO_2 injection and 1:1 conventional WAG have been reported. The early response is attributed to the continuous CO_2 injection, whereas the WAG portion provided the increased sweep performance that led to higher ultimate recovery.

The hybrid WAG process may not be beneficial in case of heavy and extra-heavy oils, however. Due to the adverse mobility contrast of the gas with the in-place oil, gas injected before initiating the WAG

process may result in premature gas breakthrough and result in the production well "gassing out". The increased production response observed in the Wasson field may not happen, leading to inefficient utilization of the gas ahead of the water-front. The same problems of continuous gas injection would apply for heavy and extra-heavy oil cases. Furthermore, the benefit of an early production response also may not be observed for heavy oils (Rojas and Ali, 1988).

Surfactant Water Alternate Gas (SWAG) corresponds to the simultaneous injection of gas and water into the reservoir. The first SWAG project was carried out in the Seelington Field in 1962 (Christensen et al., 2001). Due to a loss in injectivity, the project was unsuccessful. Since that time, SWAG has been tested in Rangely Weber, Kuparuk, and Joffre Viking as a pilot project, and the reports from these fields have been optimistic. In the Joffre Viking field, after a preliminary comparative study between WAG and SWAG, it was concluded that SWAG injection gave the best recovery. Dual-injection strings for gas and water injection, respectively, were used to carry out the SWAG pilot. In the Rangely Weber field, SWAG was implemented to optimize the injection because the wells were switched manually between gas and water cycles. Even though a more stable GOR, as compared to the WAG process, was observed, oil recovery due to SWAG increased only slightly (0.5% OOIP). There were two disadvantages with this method as well: (1) injection instability that necessitated increased monitoring of the injection system and (2) increased corrosion problems as the mixing of CO_2 gave carbonate acid. As such, a drastic decrease in the SWAG injectivity was not observed. In the Kuparuk pilot, it was desired to have only one injection system, instead of separate gas and water systems. Thus, the surface-mixed CO_2-water mixture was pumped directly to the injection site. Reduced injectivity was observed when the gas fraction of the injection mixture was increased.

Tapered WAG involves increasing the WAG ratio and/or reducing the gas slug size with increasing WAG cycles. This technique is important in view of keeping field GOR within manageable limits and more efficient utilization of the solvent. In addition to improving the solvent utility, the tapered WAG process allows more wells to be on gas injection for a given supply of injection gas (Hadlow, 1992). Tapering the WAG ratio has proven effective in reducing CO_2 production and increasing the effectiveness of CO_2 injection. This is usually achieved by either increasing the WAG ratio, reducing the gas slug sizes, or both as WAG injection continues beyond two or three cycles.

A description of effectiveness of increasing the WAG ratio has been pointed out by Hadlow (1992): a case in the Rangely Unit operated by Chevron. To reduce CO_2 production, the operator increased the WAG ratio in a stepwise manner at predetermined solvent bank sizes. After injecting 30% HCPV of CO_2 at 1:1 WAG ratio, Chevron switched to 2:1 WAG until 40% of HCPV of CO_2 was injected. From 40% to 50% HCPV, a 3:1 WAG ratio was utilized, followed by chase water. A sharp increase in the slope of the incremental recovery line following the change in WAG ratio from 1:1 to 2:1 on a plot of cumulative incremental oil production in %OOIP versus HCPV of solvent injected was observed.

Similar results have been seen in the Kuparuk River Unit, ANS, where reducing the gas slug size was effective in controlling produced GOR (Ma and Youngren, 1994). A field test involved six injectors in mature IWAG areas with definite GOR interactions with offset producers. Four wells were tested with smaller slug sizes: two each at 2% HCPV and 1.5% HCPV respectively. The WAG ratio for these wells remained at 1:1. The remaining two wells were tested with a 2:1 WAG ratio, while the gas slug sizes remained at 3% HCPV. It was observed that smaller gas slug sizes were effective in reducing the peak GOR response.

2.4.2 Carbon Dioxide as an EOR Solvent

CO_2 injection is the most widely used gas injection EOR process. As per the Worldwide EOR Survey 2014, in the US there were 127 CO_2 miscible and 9 CO_2 immiscible projects, compared to 12 hydrocarbon miscible, 2 hydrocarbon immiscible, and 9 nitrogen immiscible projects (Koottungal, 2014). On the North Slope, CO_2 emissions derive mainly from gas turbines which provide power for gas compression. Some 15 Megatons CO_2 per year are produced. Furthermore, there is approximately 5 trillion scf of CO_2 in the Prudhoe Bay reservoir (Ning et al., 2011). With cost effective extraction technology, this CO_2 becomes a valuable EOR solvent while the reservoir takes on value as a sequestration site. CO_2 has three attributes namely, viscosity reduction, underground sequestration, and lower cost, that would make it an attractive EOR solvent on the Alaska North Slope (McKean et al., 1999).

Viscosity Reduction – The use of ESPs results in bottomhole pressures as low as 500 psia. The already low production rates are further exacerbated by increased oil viscosity around the wellbore due to production below the bubble point. Numerical simulation indicates that the arrival of injected

CO_2 at the producers will reduce viscosity and promote increased production rates (McKean et al., 1999). The application of CO_2 EOR for viscosity reduction has been well documented in the literature (Klins and Ali, 1982, Holm, 1987, Chung et al., 1988, Moffitt and Zornes, 1992, Emadi et al., 2011). Rojas and Ali (1988) conducted subcritical CO_2-brine displacement experiments on two Aberfeldy heavy oil samples of 1,080 and 4,900 cp viscosity, respectively. The swelling factors observed following the saturation of cores with CO_2 were 1.17 and 1.14 [17% and 14% volume expansion], respectively for the two samples. The high solubility of CO_2 was able to decrease the viscosity considerably from 1,080 cp to 47 cp (95.6% reduction) in sample 1 and from 4,900 cp to 82 cp (98.3% reduction) in sample 2. Spivak et al. (1990) reviewed the Wilmington Tar V immiscible CO_2 flood project and reported that a 10-fold viscosity reduction is possible by CO_2. Ning et al. (2011) conducted laboratory experiments that included two four-step backward multiple-contact experiments (MCE) using pure and enriched CO_2 on the viscous oil of the Alaska North Slope to investigate the phase behavior of CO_2 and live reservoir oil fluid. The enriched CO_2 had 85% CO_2 and 15% natural gas liquids (NGLs). It was observed that pure CO_2 reduced the oil viscosity from 122 cp to 7 cp and the NGL-CO_2 mixture could reduce the oil viscosity from 122 cp to 6 cp. Li et al. (2011) examined the enhanced swelling effect and viscosity reduction of CO_2-saturated heavy oil. By conducting displacement tests on a Lloydminster heavy crude, they found that in an immiscible displacement, viscosity of oil was lowered by dissolution of CO_2 in heavy oil. This resulted in lower oil saturation by displacing water. They observed that the dissolution of CO_2 in the reservoir oil can be further enhanced by addition of alkane solvents like C_3H_8 and n-C_4H_{10} to the CO_2 stream.

Underground Sequestration – The CO_2 sequestration capacity of reservoirs has become valuable as industries are pursuing challenging CO_2 reduction targets. If reservoir architecture and oil to injectant mobility are favorable, the sweep efficiency can be high, resulting in a high retention of CO_2. A study sponsored by the International Energy Agency (IEA) suggests that EOR has more potential to sequester CO_2 than previously thought (McKean et al., 1999). The work attributes a global storage capacity of 61 Gigatons to this option, based on a utilization factor of 6,000 scf/STB [0.3 tons/STB]. This utilization factor is the calculated average of 16 CO_2 EOR projects in the USA. Because it represents the net utilization (i.e., recycled CO_2 is not included), this is a measure of CO_2 sequestration efficiency.

Cost – CO_2 shows good, propane-like miscibility with crude oil, and is less expensive than other similar miscible fluids. Natural gas enriched with heavier hydrocarbons like propane is miscible with oil but is also a valuable commodity. On the other hand, underground deposits of CO_2 are relatively inexpensive. Prudhoe Bay has 5 tcf of CO_2 as 12% of the gas cap composition (Ning et al., 2011). These are naturally occurring sources of the CO_2 that can be extracted economically in large quantities, making it a viable choice (NETL, 2010). CO_2 produced by human activities, as in gas-fired turbines, has been viewed as a prospective and inexpensive source on the ANS (Strycker and Wang, 1999).

2.4.3 CO_2 Water Alternate Gas EOR

In laboratory studies as well as in field cases, the efficiency of CO_2 as a miscible and immiscible flooding solvent is well established (Mungan, 1991). CO_2 displacement in the laboratory or in the field can happen by one of the following modes: CO_2 stimulation, continuous CO_2 injection, CO_2 slug process, simultaneous injection of CO_2 and water, and alternating injection of CO_2 and water. It is generally regarded that a miscible CO_2 flood recovers more oil than an immiscible one. This argument has been supported by various researchers (Holm, 1987). The efficiency of the miscible CO_2 WAG flood at the field scale (Mungan, 1991) is testimony to the fact that there are a large number of miscible projects as compared to immiscible ones. The Alaska North Slope is no exception to this. McKean et al. (1999) have given an evaluation of a CO_2 miscible gas injection scheme to enhance viscous oil recovery from the Schrader Bluff reservoir at Milne Point. Simulations on a fully compositional model indicated net incremental oil production of 7 to 12% (incremental oil minus injected NGL), concomitant with a reduction in oil viscosity from 45 to 3 cp.

The main mechanisms associated with the immiscible CO_2 flooding process are oil viscosity reduction, oil phase swelling, and solution gas-oil drive during pressure blowdown (Mangalsingh and Jagai, 1996). These mechanisms are important depending on whether the CO_2 displacement is miscible or immiscible. In the reservoir, the forces controlling the displacement of heavy oil by CO_2 and water are: viscous, capillary, diffusive, gravitational, and inertial (Rojas and Ali, 1988). Heavy oil is generally found in shallow reservoirs where sand is unconsolidated. Here, flow of CO_2 is likely to be laminar given low or moderate superficial velocities. The highly viscous-oil displacement in unconsolidated sands is a weak function of capillary forces. Neglecting capillary and inertial forces,

only the viscous, gravitational, and diffusive forces dominate the heavy oil displacement by CO_2 and water.

Klins and Ali (1982) presented numerical simulation results and compared them with those obtained in laboratory investigations and field observations. They found that over the viscosity range of 1 to 1,000 cp, carbon dioxide was superior to natural depletion, inert gas injection, and waterflooding (when oil viscosity was over 70 cp). The incremental recovery over waterflooding was as much as 9%, being greater for more viscous oils. Oil saturation was found out to be an important factor, as oil recovery decreased sharply with decreasing oil saturation. The effect of critical gas saturation was also noted. Viscous oils showed a 27% increase when critical gas saturation was varied from 0 to 10%. This again testifies to the role of trapped gas in the pores assisting oil recovery.

Madarapu et al. (2002) conducted a simulation study to evaluate the miscible and immiscible solvent injection process for the Schrader Bluff crude. The solvents studied were CO_2, Prudhoe Bay gas (PBG), a mixture of 85% CO_2 and 15% natural gas liquids, and a mixture of 50% PBG and 50% NGL. During the immiscible slug process, CO_2 and PBG failed to show any significant incremental recovery (IR), even with a 20% PV slug size. This was attributed to channeling and gravity override. It was observed that the slugs quickly channeled throughout the reservoir and the recovery from the immiscible process was dominated by the waterflood following the solvent slug. Miscible slug injection on the other hand, showed a much better performance. 5% PBG/NGL and CO_2/NGL solvent slugs were simulated under miscible conditions alternating with water for WAG ratios of 2, 5, and 10. A decrease in incremental recovery was observed with increasing WAG ratio, as the total volume of solvent injected decreased. At a WAG ratio of 10, PBG/NGL WAG had 11% IR, whereas CO_2/NGL yielded 7.5% IR. Since the immiscible slug showed essentially the same performance as waterflood, it was not studied for the WAG process.

While the immiscible slug showed poor performance in terms of oil recovery due to uncontrolled mobility, alternating the CO_2 slug with water may have reduced the gas relative permeability due to the presence of three-phase saturations inside the pore space. This is known to increase oil recovery (Skauge et al., 2007). Mungan (1991) showed that achieving miscibility was not essential to recovering incremental oil, since oil swelling and viscosity reduction were the most significant factors in recovering additional oil. Choosing a WAG scheme (miscible or immiscible), however, depends on oil composition, reservoir pressure and temperature, composition of injected gas, and project

economics. Khataniar et al. (1999) conducted experiments to investigate the performance of CO_2 injection and miscible WAG processes for the tertiary recovery of Schrader Bluff viscous oil. From slim tube tests, CO_2 was found to be immiscible with the Schrader Bluff oil at reservoir conditions. Enrichment with at least 15% natural gas liquids was needed to achieve dynamic miscibility with the in-place crude. The shallower Ugnu reservoir has even heavier oil; in some parts, live oil viscosities exceed 50,000 cp (Hulm et al., 2013). The fluid in this reservoir is too heavy to achieve miscibility at reservoir conditions. The carbon dioxide density required for achieving miscibility at a certain temperature and pressure increases with increasing amounts of C_{31+} in the reservoir fluid (Holm, 1987). Due to the high MMP of heavy oils, combined with the relatively low reservoir pressures prevailing in shallow deposits, achieving miscibility with CO_2 is not expected. Many authors have corroborated this contention (Emadi et al., 2011). CO_2 immiscible flood then becomes a viable option to test in these heavy and extra-heavy oil sequences.

Ning et al. (2011) presented results for a laboratory as well as a reservoir simulation study on an immiscible viscosity reducing WAG (VRWAG) for the Schrader Bluff fluid. The viscosity of a 122 cp oil reduced to 17 cp and 6 cp b using pure CO_2 and enriched CO_2 (85% CO_2 + 15% NGLs) as solvents, respectively. Numerical simulation for a 76 cp crude showed a 9.8% OOIP incremental recovery (IR) over waterflood using CO_2 and a 15.7% OOIP incremental recovery using enriched CO_2. CO_2 utilization ratios of 8.5 and 6.3 Mscf/STB were obtained for 50 years of performance forecasts, which are similar to the miscible gas EOR in the deeper light oil reservoirs on the ANS.

2.4.4 CO_2 Mobility Issues

Carbon dioxide is a low viscosity fluid that has high relative mobility in contrast to the in-situ oil. At reservoir conditions, CO_2 viscosity is 10 to 50 times lower than that of conventional light oil (Bernard et al., 1980). The ratio with heavy oil is even more drastic, with the viscosity ratio of the in-place oil and CO_2 on the order of 1,000 to greater than 10,000. This unfavorable mobility ratio causes fingering and channeling of CO_2 in highly permeable strata and bypassing of oil due to crossflow, and has been seen in several field cases (Holm, 1987). Even when miscibility is achieved, significant crossflow of mobilized oil can happen because of fluid pressure gradients and the effects of capillary and buoyant forces between porous layers of a reservoir where vertical permeability exists. Viscous fingering causes early CO_2 breakthrough (and hence, high gas processing costs), high CO_2 utilization ratios, delayed CO_2 production, depressed oil production rates, and consequently, low hydrocarbon

recovery. These problems are exacerbated when an injection well is perforated in two or more producing zones (Enick and Olsen, 1993). CO_2 tends to flow preferentially through highly permeable strata. These may be portions of the reservoir that have been effectively waterflooded. This results in the gas bypassing the lower permeability sections of the reservoir which may contain more recoverable oil. Thus, optimistic oil recoveries obtained in laboratory experiments on small diameter linear corefloods are never achieved on a field scale.

Graue and Blevins (1978) reported the CO_2 flooding performance in a watered-out area in the SACROC Unit, Texas. The data and simulation results suggested that the flooding mechanism was not strictly miscible displacement. They found evidence of CO_2 dissolving rock and aggravating the effect of heterogeneities and the tendencies of CO_2 to channel. The CO_2 requirements to give an incremental recovery of 4 to 6% OOIP were large – 15 to 20 Mscf/STB – for a 30% PV of CO_2 slug. This recovery efficiency was uneconomic at $14.85, the prevailing price per barrel of oil at the time (Graue and Blevins, 1978).

A similar case of early CO_2 breakthrough and poor reservoir sweep due to an unfavorable mobility ratio was observed in the miscible CO_2-WAG ($WACO_2$) EOR in the Joffre Viking field, Canada (Stephenson et al., 1993). In this project, a CO_2 flood pilot was tested on two adjacent inverted five-spot patterns. The pilot CO_2 response time gave an indication of CO_2's tendency to override and the ineffectiveness of the water-alternate-gas scheme for mobility control. Pilot wells typically experienced CO_2 breakthrough in approximately 6 months, when the original $WACO_2$ design study anticipated the CO_2 response time to be between 12 to 18 months. In contrast, a well abutting the border of the two patterns produced significant volumes of CO_2 within 3 months of CO_2 injection. In fact, only the top one-third of the reservoir was contacted by CO_2.

Because CO_2 is a costly fluid compared with water, various methods have been used to minimize the amount of CO_2 required to recover a barrel of oil. In one method, a slug of CO_2 is used rather than continuous CO_2 injection. The CO_2 slug is displaced by water. In another method, CO_2 slugs are injected with the production wells shut in to avoid severe pressure sinks and accompanied CO_2 channeling. Alternate slugs of CO_2 and water have been most successful in recovering incremental oil. The water reduces CO_2 mobility, but it also traps oil, increases water flow, and decreases extraction of hydrocarbons from in-situ oil by CO_2 (Shelton and Schneider, 1975, Bernard et al., 1980, Walsh et al., 1989).

2.4.5 Foams for Mobility Control

Considerable research on testing foams for gas mobility control was initiated in the 1960s. Studies in the lab and field indicate that foam is a better mobility control agent than water (Bernard and Holm, 1964, Bernard and Jacobs, 1965, Albrecht and Marsden, 1970). Foam is formed by successively injecting a surfactant solution and gas into a porous medium. Foams in the reservoir can be formed in two ways (Hoefner et al., 1995): (1) surfactant-alternate-gas (SAG) injection and (2) coinjection. While coinjecting the surfactant, brine, and gas mixture produces a more effective foam due to more intimate mixing, using multiple dilute aqueous slugs of surfactant alternating with CO_2 (SAG) allows for better injectivity as foam components are injected separately from (and ahead of) the injection gas. Foams of 85 to 90% gas have an inherent advantage over water for mobility improvement. Furthermore, foam's viscosity is greater than that of its components and increases with capillary diameter. Both these factors are favorable for improved oil recovery, as increased viscosity of the displacing agent results in an improved mobility ratio and better sweep (Bernard et al., 1980). Hoefner et al. (1995) have described foams as conformance and mobility control agents. Near-wellbore, foams preferentially reduce flow to higher permeability strata and act as conformance, or profile-control agents, whereas foams that propagate some distance into the formation help in controlling CO_2 mobility. According to the authors, foam is best suited to applications where total blocking of high permeability channels or "thief" zones is not desired or feasible. In their opinion, foams for injection-gas profile improvement in the reservoir are suitable when treating:

1. Multizone or thin intra-zone thief intervals
2. Thief zones that are not vertically isolated from CO_2 target zones
3. Thief zones potentially contributing to pattern oil production
4. Thief zones not otherwise treatable with more-permanent methods.

Bernard and Holm (1964) have shown that foams decrease the effective permeability of porous media to gas. In a laboratory experiment on consolidated Berea sandstone cores and unconsolidated sandpacks, they observed the specific permeability to nitrogen reduced from 100 and 146,000 mD for the consolidated and unconsolidated sands, respectively, to less than 1% of its value. In many cases, the gas permeability was practically zero. Foam reduced the gas permeability of loose sand to a much greater degree than tight sand. Furthermore, it has also been established that foams increase the trapped gas saturation (Bernard and Jacobs, 1965), thereby reducing the effective permeability to

water indirectly. On the other hand, the trapped gas phase is also not continuous, and consequently does not permit high permeability to gas either. However, it was noted that the presence of oil in the porous medium reduced the effectiveness of foams in reducing gas permeability. The permeability reduction to gas was observed only after continuous injection of the foaming agent. The presence of oil also impacted the increase in trapped gas saturation negatively. While injecting foam on a continuous basis was feasible on the lab scale, this practice in a field may be uneconomical.

Dellinger et al. (1984) demonstrated the utility of cosurfactant stabilization in linear, two-phase flow tests through tight, unconsolidated sandpacks using brine and gas. Nitrogen was used instead of CO_2, as initial experiments showed a wide varying CO_2 solubility with pressure. A solution containing 0.45% Alipal CD-128™ and 0.05% Monamid 150-AD™ decreased gas mobility over 100-fold. Alone, Alipal CD-128™ reduced the gas mobility by a factor of 10 when compared with gas mobility in the presence of brine only. It was observed that the effect of foam was time-independent, indicating good foam stability. The addition of Monamid 150-AD™ to Alipal CD-128™ reduced the foam height slightly compared to when Alipal CD-128™ alone was used, but increased the foam stability. Furthermore, it was seen that maintaining a pH of 2.5 resulted in the surfactant's retention of its foaming properties for extended periods of time. It was noted, however, that adsorption effects of foam in the porous media lowered the efficiency and required a slightly larger amount of foam to be injected. A surfactant concentration in the range of 0.5 to 1.5% was found adequate to overcome any adverse effects of adsorption (Dellinger et al., 1984).

In addition to laboratory experiments, foams have been tested in several field projects for gas mobility control. An application of a surfactant foam for CO_2 mobility control in a high permeability channel has been well described by (Martin et al., 1995) for an inverted nine-spot pattern in the East Vacuum Grayburg/San Andres Unit (EVGSAU) in the Delaware basin. The reservoir was characterized by 9 units (units A to I from top to bottom), of which subzone C2 in Unit C was a high permeability channel of 200 mD, as compared to an average of 23 mD for other units. Before the foam project, most of the gas channeled directly into a producing well connected to this unit. Thus, a large volume of CO_2 was produced within a very short span of commencing the WAG process. The oil production rate was low, at 5 bbl/day accompanied with a high bottomhole pressure (BHP). A production log run during a flow test indicated that the high BHP caused severe crossflow and exit of fluids at the bottom of the borehole. This had severe safety and workover implications. A short surfactant alternate gas (SAG)

cycle comprising three days of a 2,500 ppm Chevron Chaser CD1045™ solution at 1,000 bbl/day followed by 12 days of CO_2 at the same rate showed a positive oil response and reduced CO_2 production. An increase in elapsed time between WAG injection cycle and saturation changes observed in unit C2 provided evidence of diversion of injected fluids away from this zone. Cumulative CO_2 production as well as peak CO_2 response from the affected well dropped to half over a 10-month period. However, only a slight increase in oil production rate was observed.

Smaller SAG cycles reduce CO_2 injectivity and improve sweep. This fact has also been supported by Hoefner et al. (1995). In a study on CO_2-foam field trials in the East Mallet Unit (EMU), Texas, several coreflood experiments were performed to characterize the relative effects of (1) surfactant-alternate-gas (SAG) vs coinjection, (2) SAG slug size and frequency, and (3) coinjection foam quality. It was observed that smaller SAG cycles reduced injectivity to a greater degree than larger ones. As the SAG cycle increased, the CO_2-foam behavior approached that of coinjection. However, longer SAG cycles reduced CO_2's mobility farther into the core than shorter ones. Following lab experiments, four trials were performed in the EMU to compare the effects of SAG and coinjection strategies. SAG was carried out in the first trial. It reduced gas injectivity and hence, gas production, whereas it increased oil production. Coinjection done in the second trial showed more or less the same production response as that obtained from SAG. However, coinjecting the foam mix was found to be operationally difficult. In the fourth trial, the coinjection process (that was implemented after an initial SAG process) had to be terminated because of operational problems. It was observed that coinjection gave high CO_2-foam quality and was very cost-effective in reducing CO_2 injectivity.

CO_2-foams have been extensively used for recovering conventional oil. However, not much literature is published for their application to heavy oil reservoirs. Emadi et al. (2011) discuss one such case. In a series of experiments carried out in a high-pressure environment on transparent micromodels, the performance of subcritical CO_2 and CO_2-foam in heavy oil was investigated visually. The results showed that CO_2-foam can significantly improve recovery of viscous oils and also reduce the quantity of CO_2 injected. It was observed that a surfactant solution preflush before foam flooding sped up the process of foam generation and the subsequent displacement process. In these micromodel tests, it was revealed that in addition to improving the macroscopic sweep, the micro-scale displacement and sweep also improved through a number of pore scale mechanisms. These mechanisms inherent of interconnected pores, in combination with the improved sweep, resulted in a high oil recovery of

90%. However, it was also noted that the displacement efficiency was contingent on the formation of a strong and stable foam. For cases where stable foam was not generated, the oil recovery efficiency dropped drastically.

While some foam tests have been successful, some others have not produced expected results. As reported by Stephenson et al. (1993), following the poor WACO_2 sweep performance in two adjacent pattern pilots (A and B) in the Joffre Viking field, Canada, foam was tested in pattern B. After a successful injectivity test, an extended field test was planned and implemented. Approximately 10,000 kg (100% active) of a 0.2 wt% surfactant solution was injected simultaneously with CO_2. The reservoir was pre-flushed and conditioned with a 900 kg of 0.5 wt% surfactant solution. The initial increase in the bottomhole pressure (BHP) was akin to that observed in the injectivity test however, within 3 weeks of injection the increase in BHP ceased and a pressure plateau was reached. Simulation studies, on the other hand, had predicted a continuous rise in the BHP if a cylinder of foam was continuously expanding away from the injection wellbore. While the GOR didn't increase during the test, sulfur hexafluoride tracer that was injected with the CO_2 foam was detected at a pattern B producer within 3 weeks. Other producers in the pattern saw tracer response within 2 to 3 months, thus establishing early gas breakthrough. It was concluded from the extended field test that foam did not propagate a significant distance into the reservoir. The modest rise in oil production observed was attributed to the additional CO_2 injection.

Henry et al. (1996) describe another field implementation of CO_2 foam, where foam stability issues resulted in less-than-expected results. Operators in the Wasson ODC Unit, Texas were facing severe gas recycling problems due to CO_2 cycling in a high permeability zone in the reservoir. A tracer test using fresh water and fluorescent dye had verified the existence of the thief zone. About 3,000 barrels of 0.5 wt% Chaser CD1045™ surfactant was injected directly into the identified thief zone. This was done by utilizing crossflow within the wellbore due to the pressure differential between the tighter and more permeable strata. Reduced CO_2 cycling was observed by comparing injection and production rates pre- and post-foam injection. The gas breakthrough time also increased from 8 to 22 days. However, no significant improvement in the sweep efficiency was seen after the foam treatment, as no additional CO_2 was retained in the reservoir as compared to the no-foam case. Had the sweep improved, a lower produced gas volume should have been observed at the producer, indicating that CO_2 had been diverted to other reservoir areas to recover additional oil. Furthermore, the reduction

in CO_2 injectivity was only short-term, as CO_2 injection rate gradually increased with time. This was attributed to the degradation of the foam bank due to bubble collapse and dehydration. The authors also report that the foam treatment was uneconomical, as recycling the gas was a cheaper option than managing 3,000 barrels of 0.5 wt% surfactant.

The aforementioned two incidents bring to light an inherent limitation of using foams for gas mobility control: weak mechanical and chemical integrity. An excessively large volume of continued surfactant solution has to be injected to reap the expected benefits of gas diversion and gas mobility control (Bernard and Holm, 1964, Bernard and Jacobs, 1965, Martin et al., 1995, Henry et al., 1996), as dissipation and disintegration of foams happens away from the injection wellbore. This effect is more pronounced at elevated reservoir temperatures. From a heavy oil development standpoint, achieving the desired mobility ratio may warrant even larger volumes of stronger surfactant solutions in contrast to light or black oils. This may make the foam injection process uneconomical compared to other recovery options. However, mobility control of CO_2 is critical for improving sweep efficiency and optimization of CO_2 storage capacity. Because surfactant based foams are thermodynamically unstable, their long term stability becomes a limitation for field application and is, in general, difficult to maintain (Yu et al., 2012). This happens especially when the foam contacts the in-place oil. Under high reservoir temperatures, the surfactants tend to degrade before they have fulfilled their long-term duty. Furthermore, surfactant losses in the reservoir due to adsorption on the rock surface result in more-than-anticipated chemical requirements in CO_2 foam flooding and are thus, a major constraint deciding the economic viability of the flooding project. In fact, significant operational costs must be incurred due to low stability and adsorption loss problems with surfactant-stabilized CO_2-foams.

2.4.6 Low Salinity Waterflooding

In light of economics and concerns over foam requirement to achieve the desired mobility ratio with viscous to heavy oils, an alternative approach to EOR may be needed. Techniques that may yield comparable recoveries to WAG with lower costs may be required for the Alaskan viscous oil deposits. Some experiments done on altering the injection brine salinity in the early-90s opened the door to a new EOR process: low salinity waterflooding (LSWF). From the Alaskan EOR perspective, low salinity waterflooding is a budding technique that has not yet been tested as a pilot for the viscous oil pools. While single well chemical tracer tests (SWCTT) in sandstone reservoirs have shown potential and promise (McGuire et al., 2005a), but its viability as an economically feasible process still remains

under question. These concerns primarily arise due to large upfront capital investments and delayed oil production response of LSWF.

2.4.6.1 Mechanisms of Low Salinity Waterflooding

The main cause of increase in oil recovery due to LSWF is the reduction in residual oil saturation due to an alteration in wettability from an oil-wet to a more water-wet state (Patil et al., 2008b, Mahani et al., 2011, Kasmaei and Rao, 2014). The LSWF process works on the microscopic scale, i.e., multiple ion exchange reactions through a series of aqueous and mineral reactions are the key to low salinity waterflooding (Dang et al., 2015). This happens when water with ion concentration different from that of connate water is injected. This disrupts the chemical equilibrium between the ions in the water and those that sorb on the mineral (clay) surface. In LSWF, there are two typical ion exchange reactions between sodium, calcium, and magnesium.

$$Na^+ + \frac{1}{2}(Ca - X_2) \leftrightarrow (Na - X) + \frac{1}{2}Ca^{2+} \quad (2.1)$$

$$Na^+ + \frac{1}{2}(Mg - X_2) \leftrightarrow (Na - X) + \frac{1}{2}Mg^{2+} \quad (2.2)$$

Here, X denotes the clay mineral on the rock surface. The above reaction is reversible, i.e., during a high salinity waterflood, Na^+ is taken up by the exchanger and calcium and magnesium ions are released. In a low salinity waterflood, the reverse happens. Excess Ca^{2+} and Mg^{2+} are exchanged for release of Na^+. The increase in the concentration of Ca^{2+} and Mg^{2+} reflects a proportionate detachment of positively charged oil particles and organometallic complexes from the clay surface (de Bruin, 2012). Consequently, lower concentration of Ca^{2+} in the produced water as compared to injection and formation water is observed in siliciclastic rocks (Appelo and Postma, 2005, Lager et al., 2007). The decrease in the oleic components from the clay surfaces lowers the residual oil saturation and shifts the wettability from an oil or a mix-wet to a more water-wet state.

LSWF has been effective on carbonates as well. Kasmaei and Rao (2014) observed the contact angle on a Silurian Dolomite decrease from 158° to 113° after diluting a 10.78 g/l brine to one-tenth of its original strength. Like sandstones, injection of low salinity water in carbonate rocks has shown to change the wettability to a more water-wet sate, increasing its spontaneous imbibition capacity and thereby promoting oil recovery (Austad et al., 2008). Diluted sea water injection in carbonate formations has been shown to promote oil recovery by enhancing rock water interactions (Yousef et

al., 2012). Similar LSWF impacts, with dilution of a 194,450 ppm formation water 2 times, 5 times, 10 times, and 100 times with distilled water have shown incremental recoveries up to 5% OOIP in coreflood experiments for core and dead-oil samples retrieved from a carbonate reservoir in Oman (Al Harrasi et al., 2012). Surface active aqueous components in injection water, like Ca^{2+}, Mg^{2+}, and SO_4^{2-}, have been shown to play a significant role in both wettability alteration and rock mechanics. The importance of tuning injection water ions has also been observed. Injecting softened formation water by selectively removing Ca^{2+} and Mg^{2+} has been shown to increase oil recovery. Adding sulfate, borate, and phosphate ions to seawater has shown incremental recoveries up to 20% OOIP for a limestone coreflood experiment using a Middle Eastern light oil (Gupta et al., 2011).

While wettability alteration seems like the main mechanism, the increase in oil recovery seems to be due to a combination of myriad effects. Studies have shown an increase in pH associated with low salinity waterflooding (McGuire et al., 2005a, Austad et al., 2010). McGuire et al. (2005a) observed the pH of BPNS2 (North Sea reservoir crude oil/brine system) coreflood increased from 8 to 10 when a brine of 1,500 ppm salinity flooded a core that had originally 15,000 ppm salinity connate water. They concluded that at elevated pH levels, low salinity waterflooding behaved like alkaline flooding, lowering the interfacial tension between reservoir oil and water. Due to the alkaline nature of the flood, the acidic components of the crude oil were saponified. The in-situ generation of surfactants lowered the interfacial tension that controlled the forces to hold oil in the pores.

2.5 Schrader Bluff Screening for LSWF

The geochemical reactions are the heart and soul of the LSWF process. Therefore, experimental investigation is necessary to evaluate flood performance, determine suitable injection fluid composition, and establish the best injection practice tailored to the rock and fluid system under study. In the absence of experimental data, a preliminary screening study for Alaskan oil fields as suitable LSWF candidates has been performed by Thyne (2016). MPU-Schrader Bluff got the top screening score along with KRU-West Sak and KRU-Kuparuk (Figure 2-2). The criteria comprised several parameters, including reservoir properties, oil and connate water properties, formation temperature, production history, and recovery factor (RF) at estimated ultimate recovery (EUR). Oil recovery from Schrader Bluff currently stands at 17% OOIP with RF at EUR being ~39% OOIP. A review of some of the basic screening parameters is given below.

2.5.1 Permeability

Higher permeability formations are favored candidates for LSWF. This may be true for any type of recovery process and might not be unique to LSWF. Field tests in Alaska conform with this trend (McGuire et al., 2005a, Seccombe et al., 2008). Schrader Bluff is stratified and the permeability varies from 10 mD to over a Darcy in some sections of the reservoir (Strycker and Wang, 2000).

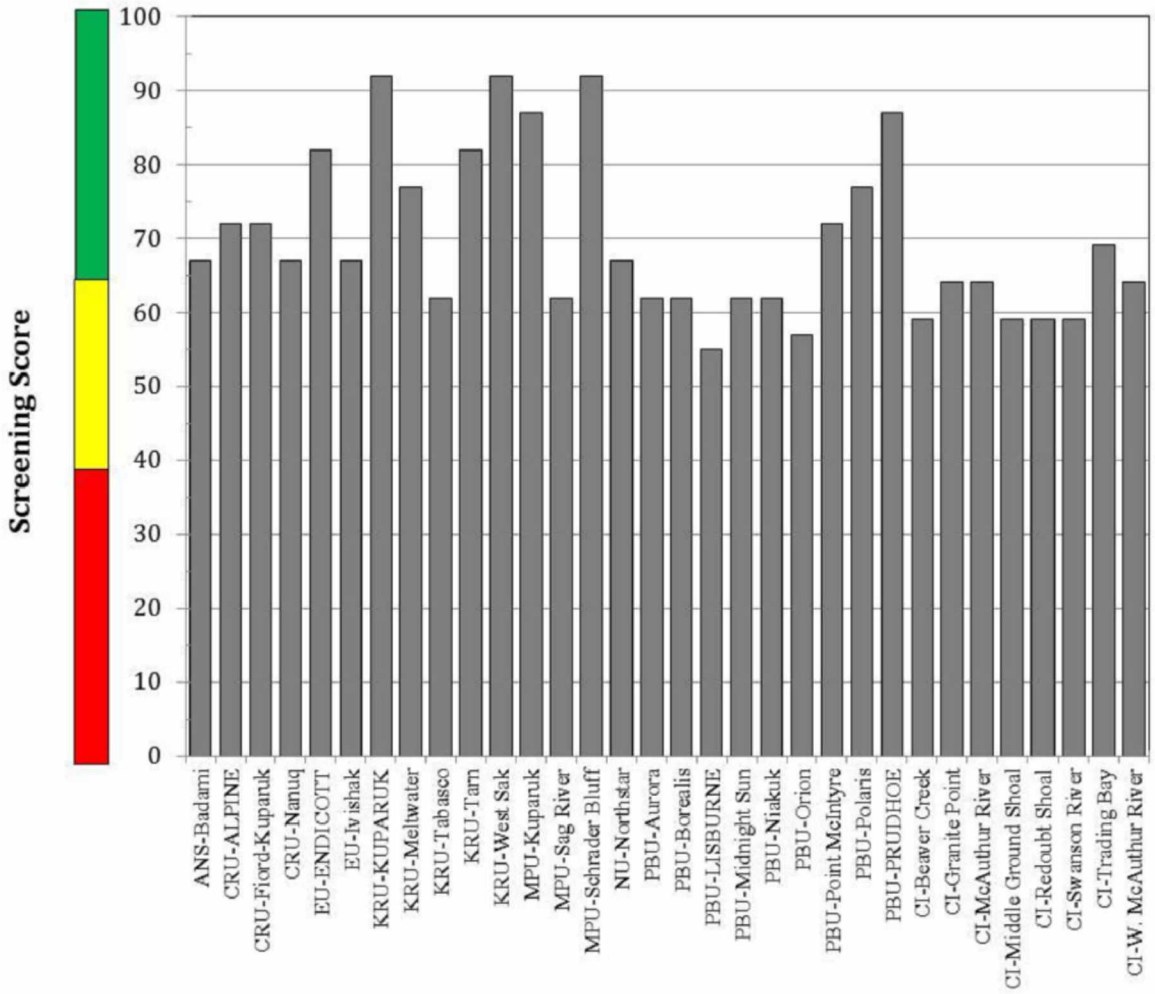

Figure 2-2 Low salinity waterflooding screening score for Alaskan oil fields (Thyne, 2016)

2.5.2 Clay Content

This is perhaps the most important reservoir property that forms a crucial variable of the screening process. Early on, and even during recent times, it was believed that kaolinite should be an integral

component in the detrital clay mix. Much of this belief stemmed from the fact that kaolinite has a low charge imbalance (indicated by a low cation exchange capacity of ~3-10 meq/100g) and thus, holds the acidic and basic components of crude oil weakly as compared to some of its counterparts like montmorillonite (Austad et al., 2010). Thus, desorption of the polar oil components through cation exchange during LSWF is easier on a kaolinite surface. The cation exchange capacity directly affects the multicomponent ion exchange between the adsorbed oil, injection water, and clay site: the most agreed upon mechanism for LSWF. Thyne (2016), however, stated that the incremental recovery is independent of clay *type* and depends only upon the *amount* of clay in the rock matrix. He based his argument on incremental oil production for sandstones vs. clay content observed from a myriad of previous studies done on low salinity waterflooding (Figure 2-3). Schrader Bluff's clay matrix is a medley of kaolinite, chlorite, smectite, and illite (Werner, 1987). The clay distribution is non-uniform and varies from 5% to as high as 30% in some areas, putting the formation in good standing as a LSWF candidate based on this criterion.

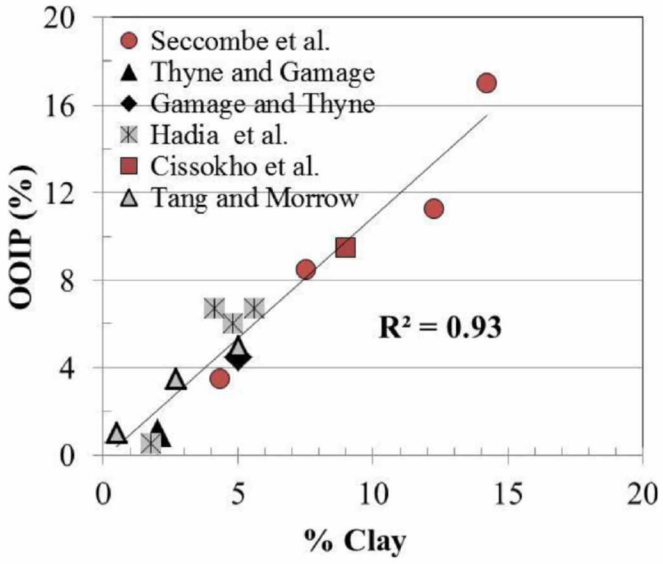

Figure 2-3 Incremental oil recovery vs. clay content in clastics (Thyne, 2016)

2.5.3 Oil Properties

The evidence of polar components in the reservoir oil is a must for the low salinity mechanism to take effect (Austad et al., 2010, Fjelde et al., 2014, Thyne, 2016). The polarity is a direct measurement of

the total acidic and basic strength of the fluid measured in terms of total acid number (TAN) and total base number (TBN), respectively. The acidic components may be carboxylic groups that are part of large molecules, present in the oil asphaltene and resin fractions. These acids are attached to the tail of the hydrocarbon cluster and may be adsorbed onto the negatively charged clay surface through cation exchange, cation bridging, ligand bridging, or water bridging (Lager et al., 2008). The most active basic substance in the crude oil is a pyridine type cyclic nitrogen compound (Austad et al., 2010). These are positively charged and may be directly adsorbed on the negatively charged clay sites. Thus, both acidic and basic components adsorb on the clay surface, rendering the reservoir rock oil-wet in those places. This equilibrium among the aqueous species is disrupted when low salinity water having a much lower ion concentration is injected, leading to desorption of cations, especially Ca^{2+}. Both high TAN and high TBN oils show similar responses to LSWF, i.e., there appears to be no bias to the type of polar compounds present. The response to LSWF is directly proportional to the amount of polar components present (Figure 2-4).

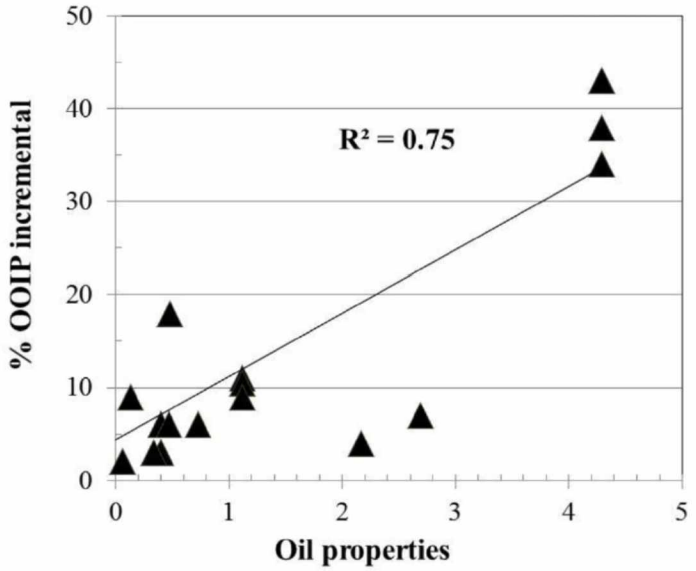

Figure 2-4 Low salinity waterflood response with increasing polar content (Thyne, 2016)

Table 2-2 shows the Total acid and base number for two West Sak crude oil samples. Figure 2-5 shows TAN and TBN values for seven Schrader Bluff wells. The average acid and base numbers for

these wells are about 0.8 and 1.14 respectively, putting Schrader Bluff crude around the 10% incremental recovery mark on Figure 2-4.

Table 2-2 Total acid and base number for two West Sak oil samples (Kovscek et al., 2004)

Oil	TAN	TBN
West Sak A	1.51	2.42
West Sak B	1.05	2.45

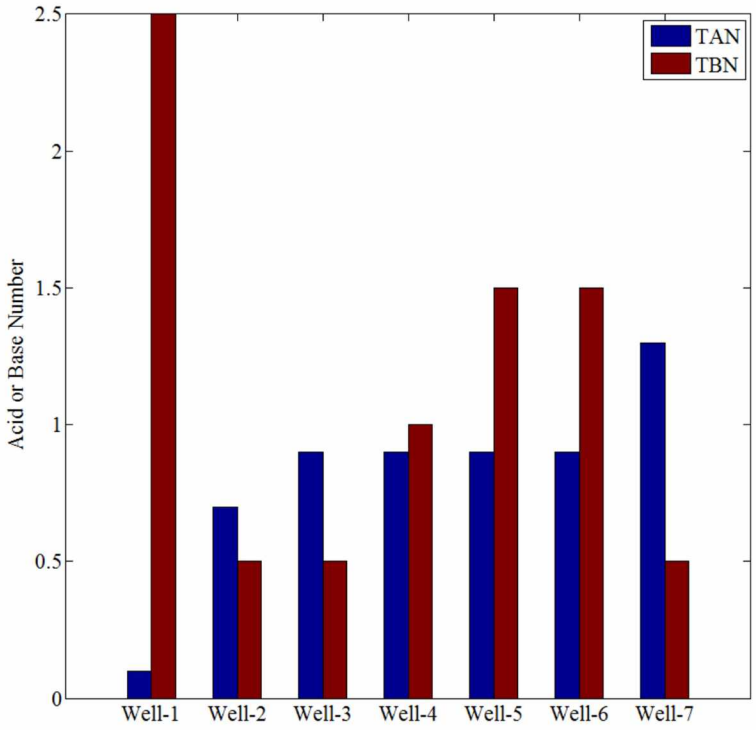

Figure 2-5 Crude oil acid and base numbers for 7 Schrader Bluff Wells (Paskvan et al., 2016)

2.5.4 Formation Water

It is desired that the formation water contains active cations, especially divalents (Ca^{2+}, Mg^{2+} etc.). The success of LSWF depends upon a balanced initial adsorption of cations, protons (H^{+}), and organic material on to the clays (Austad et al., 2010). For a crude oil having high acidic components, formation water containing a high amount of divalents may lead to a higher adsorbed organic content

due to cation bridging at various clay sites. This may render the rock more oil-wet and consequently give better performance when water of sufficiently low cationic strength is injected.

While Ca^{2+} has higher replacing power than Na^{+}, but depending upon the formation water chemistry, the latter may also act as a bridge between acidic oil components and the clay surface. This may be the case where Na^{+} outnumbers Ca^{2+} by a large margin in the formation water mix. In such a scenario, one may expect oil retention to be low when water with sufficiently low Na^{+} disrupts the adsorption equilibrium, leading to improved LSWF performance. Although the formation water ionic breakdown for Schrader Bluff was not available, a general formation water composition for the Alaska North Slope reservoirs (Figure 2-6) shows a large difference between Na^{+} and Ca^{2+}, indicating that Na^{+} may be the dominant bridging material.

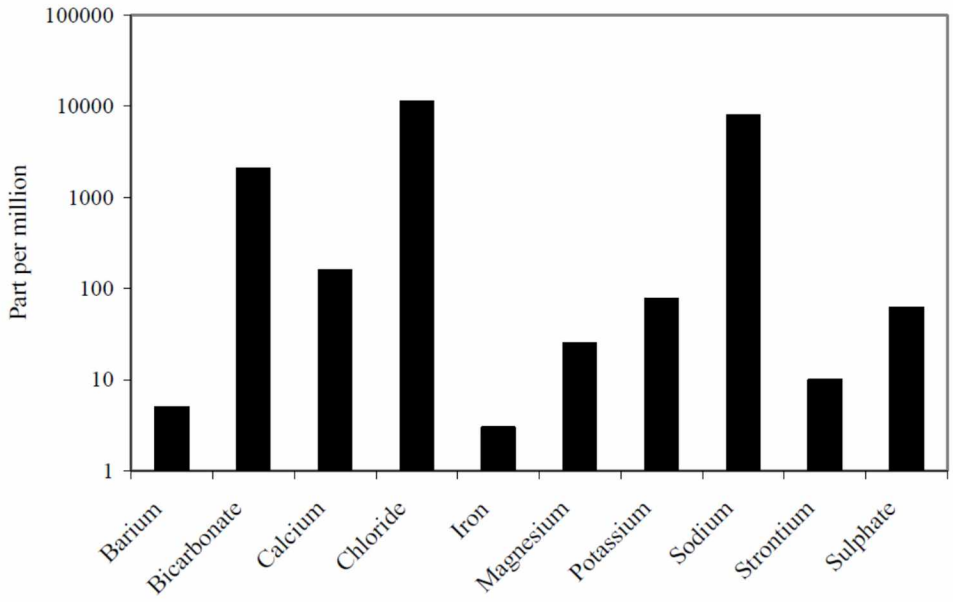

Figure 2-6 Alaska North Slope reservoirs' formation water composition (McGuire et al., 2005a)

The Schrader Bluff reservoir water has a salinity of ~ 27,000 ppm TDS with an average salinity of 20,000 ppm *NaCl* equivalent (Strycker and Wang, 2000). This is similar to the scenario just discussed and may only require injection water of sufficiently low salinity.

2.5.5 Temperature

Low salinity waterflood performance has been observed to decrease with increasing formation temperature (Figure 2-7). At 260°F [126.7°C], there seems to be no low salinity effect. Schrader Bluff is at ~81°F [27.2°C] and meets this criterion as well. Although the LSWF effects for temperatures below 90°F [32.2°C] are not shown in the figure, Austad et al. (2010) reported that below 100°F [37.8°C], temperature wasn't a factor affecting LSWF behavior.

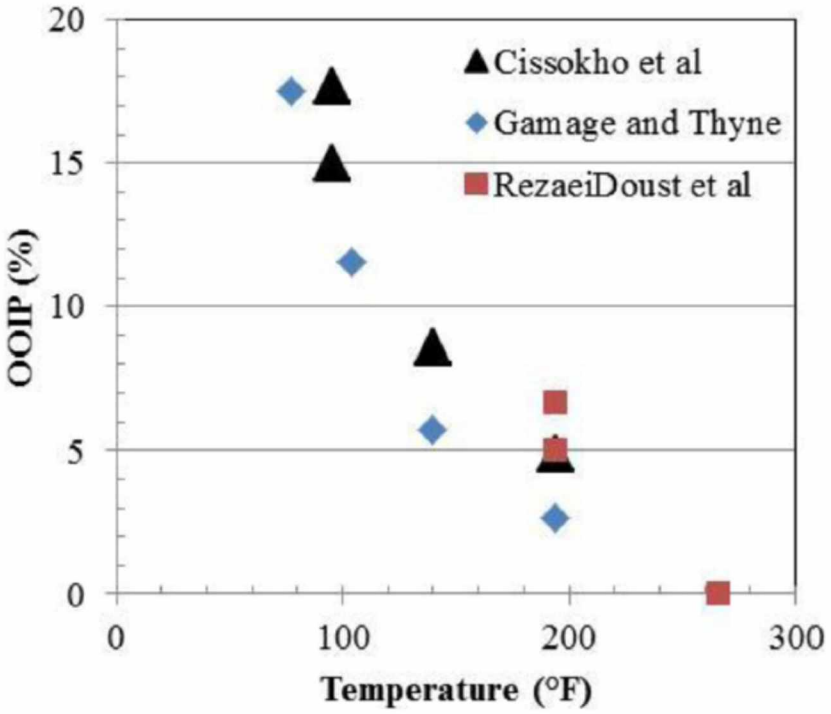

Figure 2-7 Incremental oil due to LSWF vs. temperature (Thyne, 2016)

CHAPTER 3 SCHRADER BLUFF PATTERN MODELING

3.1 Grid Definition

The model used for the study is based on the work done by Ning et al. (2011) for the Schrader Bluff OA sand. As can be seen from Figure 3-1, the sands are highly stratified over a 40 ft [12 m] interval and hence to capture the heterogeneity, a 2 ft [0.6 m] grid size was chosen in the vertical direction, making 20 layers for the model (Figure 3-2). Areally, the grid is spread over 1500 ft x 2500 ft [457 m to 762 m] to accommodate two 2000 ft [610 m] sections of an injector-producer pair aligned along the J-direction. The grid size in both the I- and J-directions is 100 ft [30.5 m]. The depth to the top of the model is 4,000 ft [1,219 m].

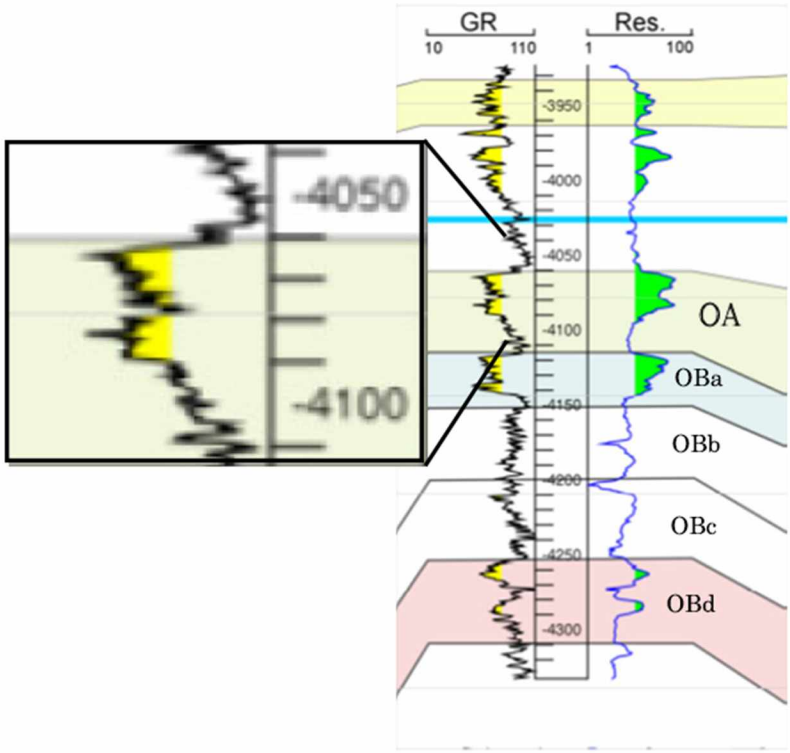

Figure 3-1 Typical Gamma Ray log response of the Schrader Bluff O sands. Modified from (Paskvan et al., 2016)

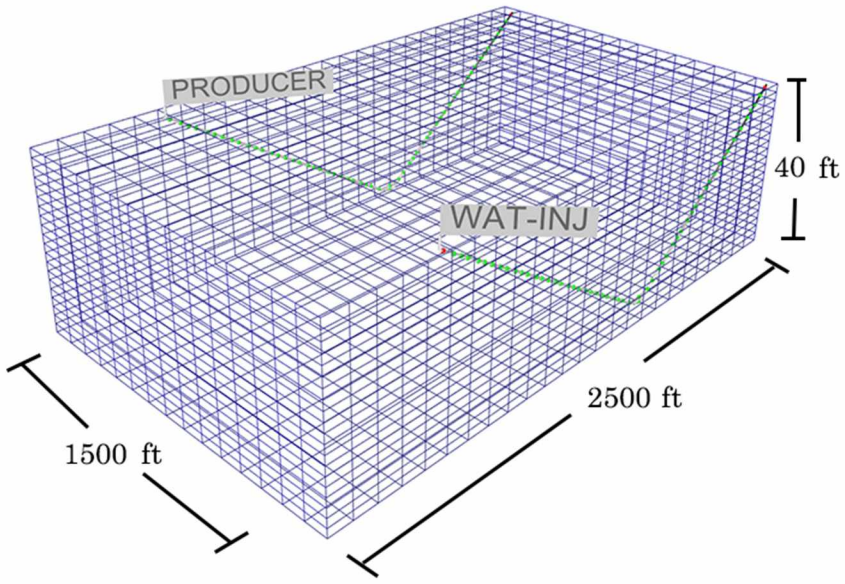

Figure 3-2 Grid structure used for the simulation model. 18x vertical exaggeration

3.2 Petrophysical Property Modeling

3.2.1 Sand Quality

In general, the Schrader Bluff sands are highly unconsolidated and exhibit high porosity and permeability. However, within discrete sand units there are thin, silty sand sequences of relatively low reservoir quality. The blocky gamma ray (GR) signature at the bottom reflects good porosity-permeability sands (Figure 3-1). This lower section overlies a silt sequence that separates the OA and OBa sand units. Within this first section, there is a high permeability zone, as shown by the abrupt peak of the GR log to the left.

The blocky lower OA sands are overlain by a thin section of silty sands (shift of GR response to the right). This section is followed by an upward coarsening sequence that tops off with a sharp erosional contact. OA, being the youngest member of the lower sands, represents a transition from inner-shelf distal deltaic to a river-dominated muddy-marine depositional environment (AOGCC, 2015). The upper sands in this section have better permeability. The porosity and permeability was modeled based on the sand quality, i.e., better quality layers were assigned higher petrophysical values.

3.2.2 Porosity Modeling

The porosity of the OA sands has been given indirectly in the study on VRWAG by Ning et al. (2011). In their study, the authors reported 8,448 MRB [1,343 Mrm^3] of water injected for the waterflood performance. This water injected was equivalent to 1.87% HCPV, which translates to 26% porosity for the reservoir model. MATLAB's Reservoir Simulation Toolbox (MRST) was used to populate porosity in each layer through a Gaussian field (Lie, 2014). The method uses a normal distribution of values between two set bounds with a predefined standard deviation. In MRST, the basic form of this function can be applied as:

$$p = gaussianField(N)$$

This function creates an approximate Gaussian random field with dimensions given by N. The field is generated by convolving a normally distributed random field with a Gaussian filter (Lie, 2014). The idea was to keep the porosity heterogeneous while averaging 26% for the whole model. Therefore, while applying the Gaussian field, the filter size was kept the same in both the I- and J-directions. Furthermore, as stated earlier, the 40 ft [12.2 m] interval is made up of sands of varying quality. Hence, better quality sand layers were given higher minimum and maximum bounds, and vice-versa (Table 3-1).

Table 3-1 Porosity bounds for respective layers

Layer	Min	Max
1	0.01	0.05
2	0.2	0.28
3	0.2	0.3
4-6	0.22	0.35
7-8	0.18	0.28
9-12	0.22	0.32
13-18	0.25	0.35
19	0.2	0.3
20	0.01	0.05

Figure 3-3 shows the porosity for layers 1, 4, 7, and 14 modeled by applying the Gasussian field equally in both the I- and J-directions. A 3D rendering of the porosity model with the histogram is shown in Figure 3-4.

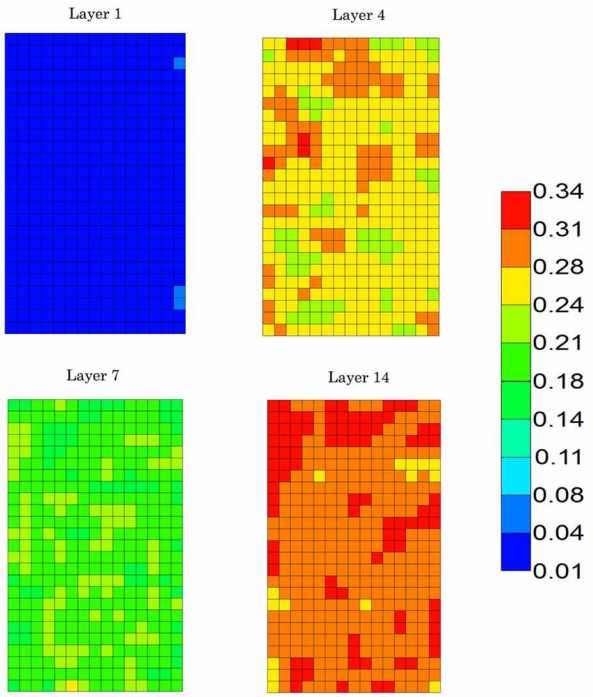

Figure 3-3 Porosity map for layers 1, 4, 7, and 14

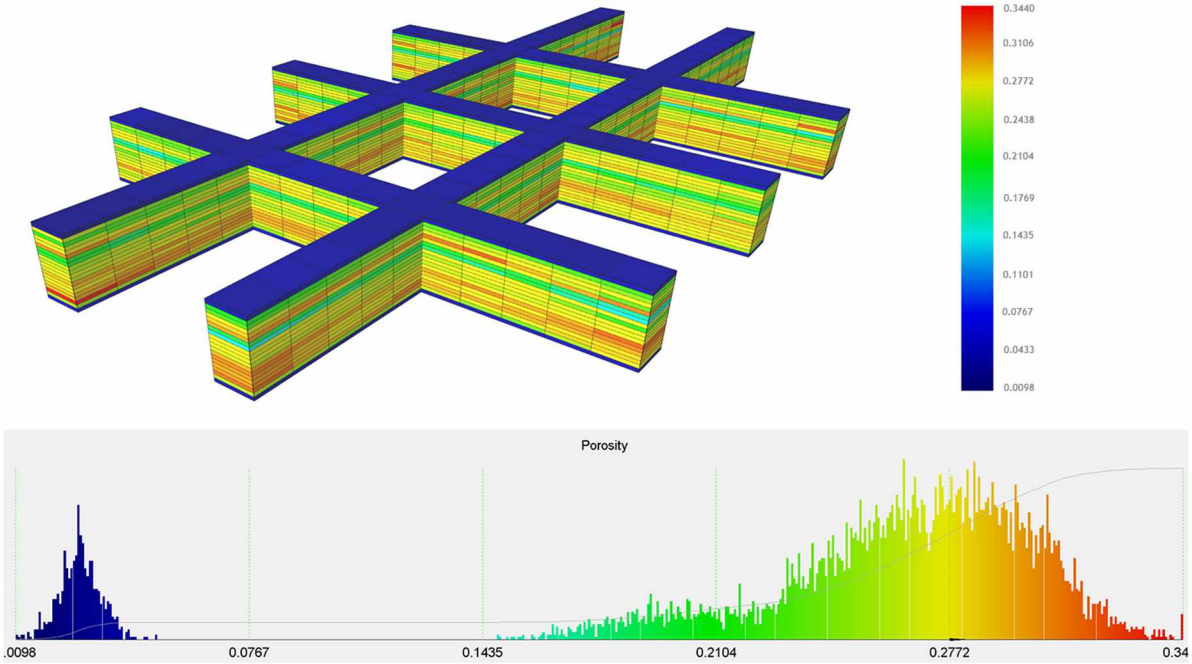

Figure 3-4 Porosity 3D model slabs with histogram

We can see that porosity is bi-modally distributed. This is because of layers 1 and 20, which are mostly silty and hence, have low porosity. The model was initialized to see the total HCPV and required altering the porosity slightly (reduced by a factor of 0.117) to match the initial fluids in place with those of Ning et al. (2011). The total HCPV after the modification was 2.564E+07 ft^3 [7.25E+05 m^3]. The total OOIP was 4.26E+06 STB [6.77E+05 sm^3].

3.2.3 Permeability Modeling

Permeability was modeled by providing typical values for each layer at 4 corners of the model and was gridded for all bocks using a Delaunay triangular based linear interpolation method. It was intended to get a distribution similar to that used by Ning et al. (2011).

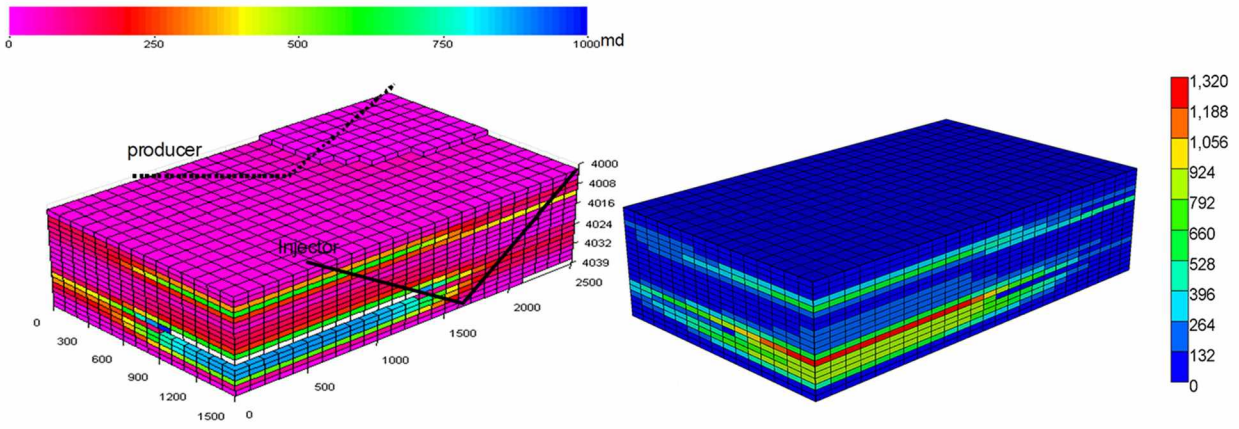

Figure 3-5 Permeability models – Left: Ning et al. (2011); Right: Model used for the study

The permeability values for the 3 visible corners of the illustration provided by Ning et al. (2011) were decoded with the aid of the color bar (Figure 3-5, left) and were used as input to the model under study (Figure 3-5, right). A part of layer 14 was nulled out by the authors. This is probably a high permeability streak, as can be seen from the GR log response (Figure 3-1). However, there was high uncertainty for permeability for all layers for the fourth corner that cannot be seen in the illustration. Permeability of those layers became a tuning parameter for model validation, as discussed in Chapter 5.

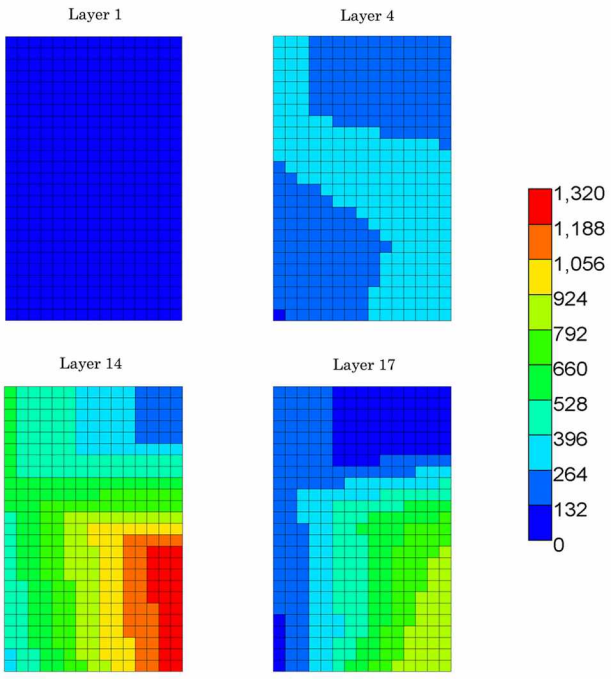

Figure 3-6 Permeability map for layers 1, 4, 14, and 17

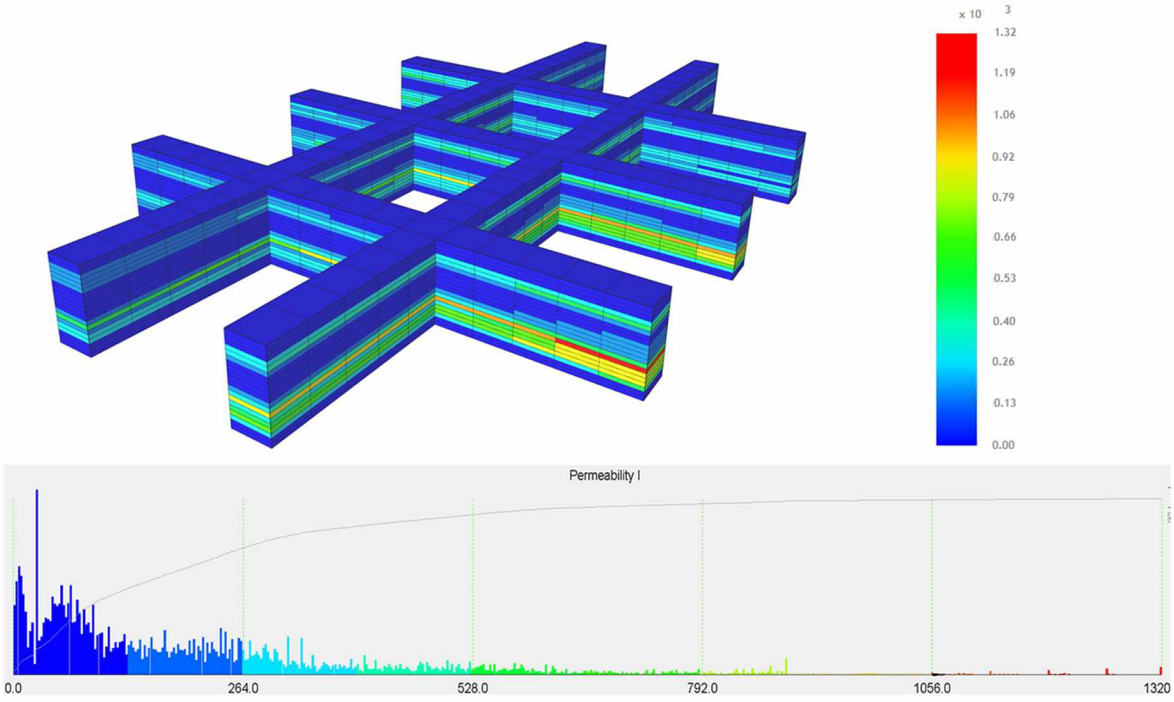

Figure 3-7 Permeability 3D model slabs with histogram

Figure 3-6 shows the permeability in the I-direction for layers 1, 4, 14, and 17. A 3D realization of the permeability distribution with the histogram is shown in Figure 3-7. The histogram shows the lognormal distributon of permeability spread across 20 layers in the model, with the maximum value reaching 1,320 mD.

Permeability in the J-direction was kept the same as that in the I-drection, whereas that in the K-direction was given 10% of the value in the I-direction.

3.2.4 Formation Compressibility

The shallow Schrader Bluff sands have higher compressibility as compared to the deeper, more consolidated formations. A constant value of 50E-06 psi^{-1} was used for all simulations (Taylor and Seamount Jr., 2002). Detailed modeling of compressibility was not performed as the recovery processes, waterflood and WAG, were applied by honoring voidage and keeping the reservoir pressure near its initial value. Hence, the role of formation compressibility in oil recovery was assumed to be negligible.

3.2.5 Relative Permeability

The relative permeability curves were generated using generalized correlations (Honarpour et al., 1986). The initial estimates of endpoint relative permeabilites and saturations were taken from previous studies for the West Sak reservoir (Bakshi, 1991). Figure 3-8 shows the oil-water and gas-liquid relative permeability curves for the West Sak lower sands. Since these sands correlate with the Schrader Bluff O sands, these were the initial relative permeability curves used for the study.

Before predicting performances for the EOR models, it was intended to validate the model's production performance for waterflood and WAG with that published by Ning et al. (2011). Hence, the final set of curves were modified from the original set by tuning endpoint relative permeabilites and saturations. The correlations of Honarpour et al. (1986) were modified slightly in this regard to transform them into generalized correlations (Equations 3.1 through 3.4) to be used for tuning purposes. The tuning parameters are described in detail in Chapter 5.

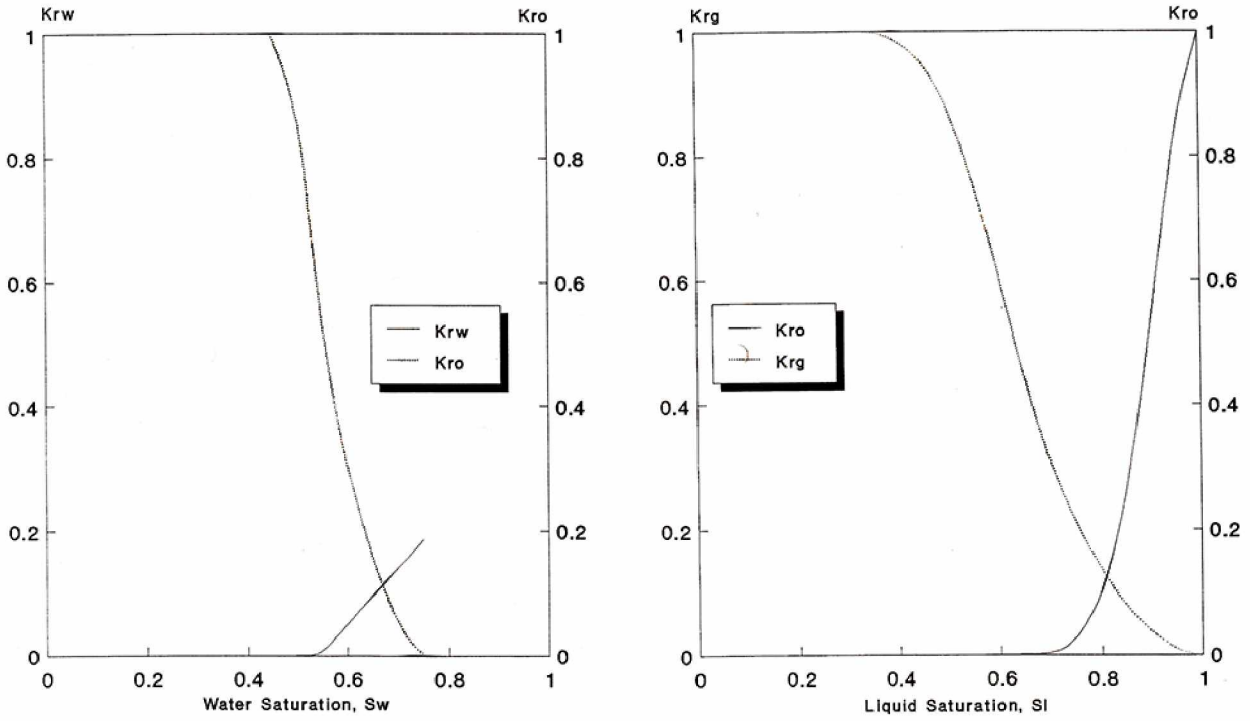

Figure 3-8 Relative permeability curves for the West Sak lower sands (Bakshi, 1991)

$$K_{rw} = K_{rwiro}\left(\frac{S_w - S_{wcrit}}{1 - S_{wcrit} - S_{oirw}}\right)^{N_w} \tag{3.1}$$

$$K_{row} = K_{rocw}\left(\frac{S_o - S_{orw}}{1 - S_{wcon} - S_{orw}}\right)^{N_{ow}} \tag{3.2}$$

$$K_{rog} = K_{rogcg}\left(\frac{S_l - S_{org} - S_{wcon}}{1 - S_{gcon} - S_{org} - S_{wcon}}\right)^{N_{og}} \tag{3.3}$$

$$K_{rg} = K_{rgcl}\left(\frac{S_g - S_{gcrit}}{1 - S_{gcrit} - S_{oirg} - S_{wcon}}\right)^{N_g} \tag{3.4}$$

where K_{rw}, K_{row}, K_{rog}, and K_{rg} are the water, oil (for oil-water), oil (for gas-liquid), and gas relative permeabilities, respectively, at any time. K_{rwiro} is the water relative permeability at irreducible oil saturation, K_{rocw} is the oil relative permeability at connate water saturation, K_{rogcg} is the oil relative permeability at connate gas saturation, and K_{rgcl} is the gas relative permeability at connate liquid

saturation. S_w, S_o, S_l, and S_g are the water, oil, liquid (oil + water), and gas saturations, respectively, at any time instant. S_{wcon} is the connate water saturation, S_{wcrit} is the critical water saturation, S_{orw} is the residual oil saturation to water, S_{org} is the residual oil saturation to gas, S_{gcon} is the connate gas saturation, and S_{gcrit} is the critical gas saturation. N_w, N_{ow}, N_{og}, and N_g are the exponents defining the curvature of the water, oil (for oil-water), oil (for gas-liquid), and gas relative permeability curves.

Even though in some literature the oil relative permeability at connate water saturation is observed to be 1 for the ANS viscous oil (Bakshi, 1991), theory suggests that the relative permeability of a fluid should at most be equal to the saturation of that fluid (Peters, 2012), with the exception of gas. Relative permeability to gas is observed to be 1 even at initial water saturation. This was given due consideration when modifying the curves during model validation. Figure 3-9 shows the oil-water and Figure 3-10 shows the gas-liquid curves used in the simulation model.

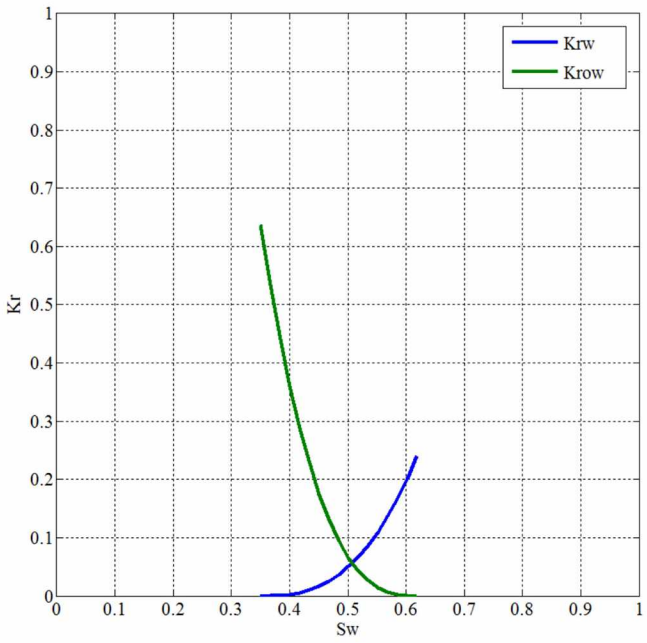

Figure 3-9 Oil-water relative permeability

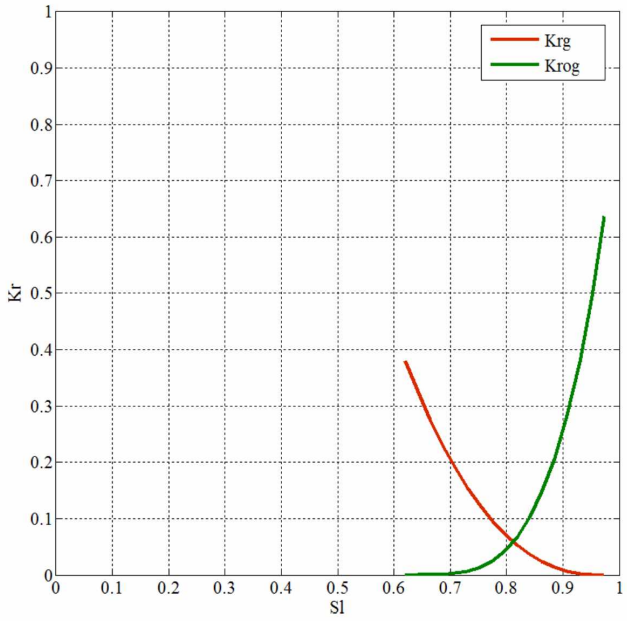

Figure 3-10 Gas-liquid relative permeability

3.3 Well Pattern

The West Sak and Schrader Bluff fields are composed of multilayer reservoirs. Economics have dictated drilling multilateral wells to access two or more reservoirs with a single well (Figure 3-11). In some cases the wells may be undulated to penetrate the pay zone from the top to the bottom and then back up (Targac et al., 2005, Ning et al., 2011). In this way, it may be possible for a single well to contact two pay zones.

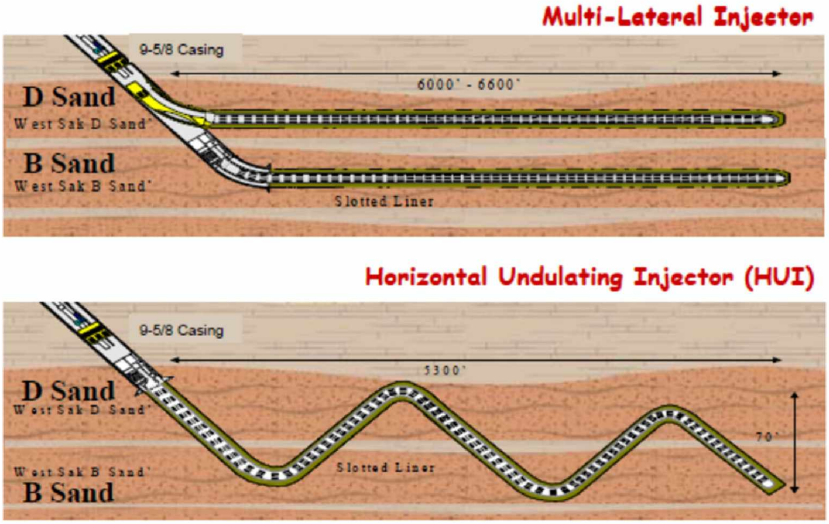

Figure 3-11 Injection well layout schemes for West Sak (Targac et al., 2005)

The well layout is as shown in Figure 3-2. A 2,000 ft [610 m] injector-producer pair was aligned along the J-direction (long side) of the model in a V-shaped trajectory and was completed along the whole 2,000 ft [610 m] length. Since a line drive waterflood pattern is followed for West Sak/Schrader Bluff reservoirs (Targac et al., 2005), the type pattern essentially represents a quarter pattern with 4,000 ft [1,219 m] horizontal wells.

CHAPTER 4 SCHRADER BLUFF OIL EQUATION OF STATE TUNING

Data for the fluid used in this study was taken from Ning et al. (2011) (Table 4-1). It is characterized by 30% C_1, ~3% C_2-C_6, and about 67% C_{7+}. The negligible amounts of intermediates reflects biodegradation and are consistent with observations in literature (Smalley et al., 1997). The detailed compositional analysis is shown in Figure 4-1. The bubble point pressure is 1,490 psia [10,273.19 kPa] at the formation temperature of 75°F [23.89°C] (Ning et al., 2011).

Table 4-1 Initial composition of the Schrader Bluff fluid

	Mol. Frac.	MW	SG
CO_2	0.00027	44.01	0.818
N_2	0.00052	28.01	0.809
C_1	0.30394	16.04	0.3
C_2	0.0019	30.07	0.356
C_3	0.00264	44.1	0.507
i-C_4	0.00221	58.12	0.563
n-C_4	0.00343	58.12	0.584
i-C_5	0.00323	72.15	0.625
n-C_5	0.00257	72.15	0.631
C_6	0.00748	84	0.69
C_{7+}	0.67188	328.297	0.913

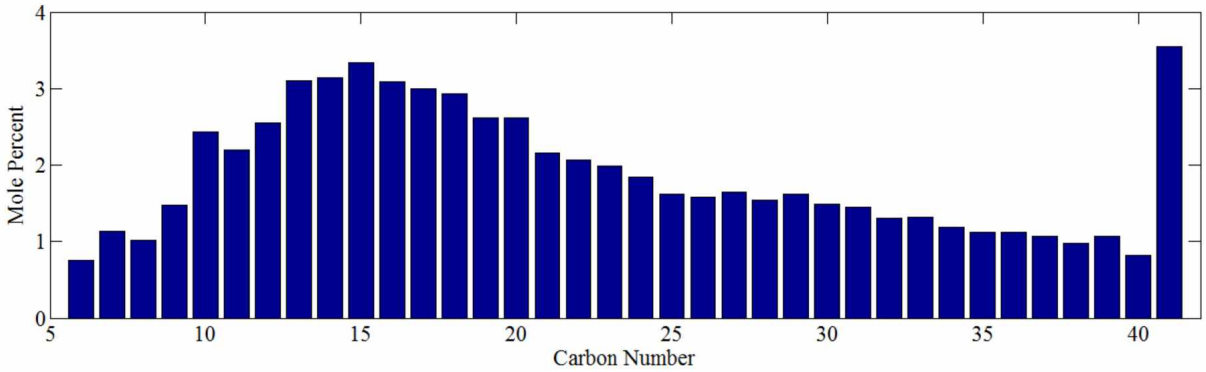

Figure 4-1 Compositional analysis of the Schrader Bluff oil

4.1 C_{7+} Characterization and Component Lumping

The C_{7+} fluid was split into 200 single carbon number (SCN) and lumped into 5 pseudo components using the gamma distribution technique (Whitson et al., 1989). The Peng Robinson Equation of State (Peng and Robinson, 1976) was used to calculate phase boundary and phase equilibrium properties. The component properties were computed using correlations (Twu, 1984). The resulting approach gave a 15-component equation of state (EOS) initial model. N_2 through C_6 were further lumped to get a 9 component EOS model to speed up the simulation runs. Components with similar properties were lumped together: N_2-C_1; C_2-C_3; C_4-C_5-C_6, with the properties of the pseudo components computed using correlations (Lee and Kesler, 1975) and subsequent tuning to match lab data. A trace gas component was also added to the compositional makeup to assist the solubility of vapor phase in water, and hence, obviate anticipated numerical convergence issues during CO_2 flooding (Table 4-2).

Table 4-2 Fluid compositional makeup with properties used for the study

	Mol. Frac.	MW	SG	P_c (psia)	T_c (°F)	Vol. Shift
CO_2	0.000269	44.010	0.8180	1069.862	87.890	-0.09435
N_2-C_1	0.304365	16.060	0.3006	666.910	-116.798	-0.15382
C_2-C_3	0.004538	38.228	0.4449	653.844	160.512	-0.10665
C_4-C_6	0.018914	72.653	0.6403	500.626	384.830	-0.03340
HYP_1	0.029469	104.921	0.7712	448.701	581.597	0.01891
HYP_2	0.185693	171.421	0.8242	302.156	791.624	0.13783
HYP_3	0.266174	297.673	0.8881	191.599	1047.019	0.27264
HYP_4	0.15543	499.477	0.9526	133.226	1297.433	0.30828
HYP_5	0.035046	820.743	1.0189	103.068	1547.183	0.22681
TRACE	1.00E-04	16.060	0.3006	666.910	-116.798	-0.15382

4.2 EOS Tuning to Match Lab Data

The data available to model the EOS was taken from Ning et al. (2011). The tuning was done in the simulator, using a least-squares regression algorithm with dynamic selection of the most meaningful regression parameters from the larger set of selected variables (Agarwal et al., 1990).

4.2.1 Saturation Pressure

The saturation pressure is influenced greatly by the binary interaction coefficients (BICs) between the components. The BIC between two components can be calculated as (WINPROP, 2015):

$$\delta_{ij} = 1 - \left(\frac{2V_{ci}^{1/6} V_{cj}^{1/6}}{V_{ci}^{1/3} + V_{cj}^{1/3}} \right)^{\theta} \tag{4.1}$$

where, V_{ci} is the critical volume of component i and θ is the binary interaction coefficient exponent. It has been found that 1.2 provides a decent match for paraffin-paraffin interaction coefficients (Oellrich et al., 1981).

To match the saturation pressure, the initial value of θ was taken as 1.2. This value was regressed to 1.0527375. The BICs between the trace component and all components were kept 0. The saturation pressure obtained from the EOS was 1,489.85 psia [10,272.89 kPa] at 75°F [23.89°C].

4.2.2 Single Stage Flash

The single stage flash gas-oil ratio was reported to be 180.6 scf/STB [32.32 sm^3/sm^3] and the oil API was given to be 16.9° by Ning et al. (2011). However, the Schrader Bluff oil used by the authors for their simulations had 18°API gravity while having similar volumetric properties. The volume shifts and the critical pressures and temperatures of the C_{7+} pseudo components were slightly altered to match 18°API and GOR for the oil (Table 4-2). In addition to these, the molecular weight of the heaviest C_{7+} pseudo component was also taken as a regression variable. Table 4-3 reports the lab values with those predicted by the EOS.

Table 4-3 Single stage flash test comparison

	Ning et al. (2011)	EOS
GOR (scf/STB)	180.6	176.71
Oil API	18	18

The oil formation volume factor (FVF) is an important volumetric property of any reservoir fluid. This was not given for the fluid dataset used for the study. However, the observed oil FVF at bubble

point pressure from the tuned EOS was 1.07 RB/STB, which resonates with that of the Schrader Bluff fluid (Strycker and Wang, 2000).

4.2.3 Viscosity

Table 4-4 reports the viscosities provided by Ning et al. (2011) in their publication on VRWAG for the fluid composition as specified in Table 4-1. However, for their simulations, they used a slightly different (76 cp viscosity, in tune with 18°API) Schrader Bluff fluid. Since viscosity plays a critical role in fluid flow, and hence recoveries, the EOS was tuned to match 76 cp viscosity at initial reservoir conditions (Table 4-5).

Table 4-4 Oil viscosity provided for the Schrader Bluff fluid (Ning et al., 2011)

Pressure (psia)	Viscosity (cp)
2500	141.1
2000	130
1700	125
1600	122.5
1490	120

Viscosities above the bubble point pressure were varied (from the value at initial conditions) in a way similar to that observed in Table 4-4, while those below the bubble point were computed using a typical viscosity correlation (De Ghetto et al., 1995).

Table 4-5 Viscosity used to model the viscosity parameters of the EOS

Pressure (psia)	Viscosity (cp)
2500	85.79
2000	79.04
1700	76
1600	74.48
1490	72.96
1281	79.23
1078	90.79
800	110.31
625	128.43

The Lohrenz-Bray-Clark method (Lohrenz et al., 1964) of calculating mixture viscosity that incorporated the correlation developed by Jossi-Stiel-Thodos (Jossi et al., 1962) was coupled with the EOS. The Jossi-Stiel-Thodos correlation is as follows:

$$[(\mu - \mu^*)\xi + 10^{-4}]^{0.25} = a_0 + a_1\rho_r + a_2\rho_r^2 + a_3\rho_r^3 + a_4\rho_r^4 \quad (4.2)$$

where:

$$\xi = \frac{T_c^{1/6}}{M^{1/2}P_c^{2/3}} \quad (4.3)$$

Here, μ is the oil or gas viscosity (cp), μ^* is the low-pressure mixture viscosity (cp), and M, T_c, and P_c are the mole fraction weighted molecular weight, critical temperature (K), and critical pressure (atm) of the fluid mixture, respectively. ρ_r is the reduced density of the mixture calculated as:

$$\rho_r = \frac{\rho}{\rho_c} = \frac{V_c}{V} \quad (4.4)$$

where ρ is the fluid density calculated by the EOS, ρ_c and V_c are the critical density and critical volume of the fluid mixture, and a_0 through a_4 are the coefficients of the fourth degree polynomial that was used to fit the viscosity data by Jossi et al. (1962). However, with the default values of the coefficients, this correlation holds true for gases and light oils only. For matching the viscosity, the critical volumes of all C_{7+} pseudo components along with coefficients a_0 through a_4 were regressed (Table 4-6). Figure 4-2 shows the match between the target and that predicted by the EOS.

Table 4-6 Default and final parameters used in the EOS to compute viscosity

Parameter	Default	Regressed	Deviation (%)
a_0	0.1023	0.08184	-20.00
a_1	0.023364	0.018691	-20.00
a_2	0.058533	0.070239	20.00
a_3	-0.040758	-0.032606	-20.00
a_4	0.0093324	0.011198	19.99
V_c, HYP_1	0.40996898	0.49191239	19.99
V_c, HYP_2	0.67731761	0.71808615	6.02
V_c, HYP_3	1.1451827	1.3529553	18.14
V_c, HYP_4	1.6417786	1.8907399	15.16
V_c, HYP_5	2.0346001	2.0772439	2.10

Additionally, a mixing exponent parameter, α, was also set as a tuning parameter and regressed to 0.8 from its default value of 1. α is used to compute the mixture's critical volume:

$$V_c = \left(\sum_{i=1}^{n} x_i V_{ci}^{\alpha} \right)^{1/\alpha} \tag{4.5}$$

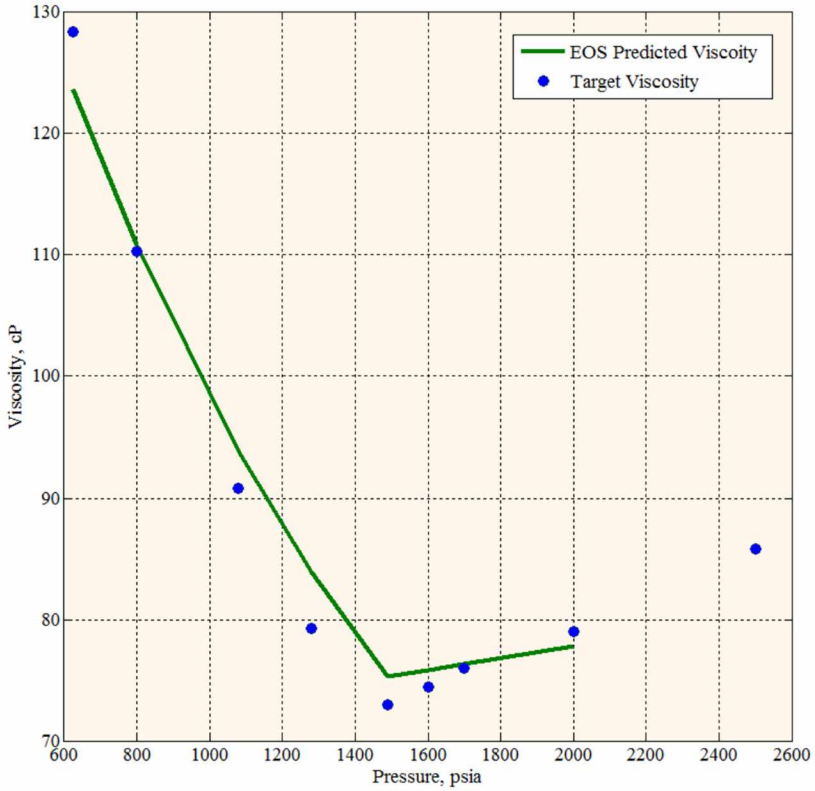

Figure 4-2 Target and EOS predicted oil viscosity

4.3 Modeling CO_2-Oil Interaction

Understanding the CO_2-oil drive mechanism is central for any carbon dioxide EOR flood. The most important properties to model include the saturation pressure, density, and viscosity of the CO_2 contacted reservoir oil. In this regard, the CO_2-hydrocarbon binary interaction coefficients (BICs) play an important role and can be tuned to match swelling factors from a swelling test.

4.3.1 Multicontact Miscibility Test

The PVT simulation of the tuned EOS for multicontact miscibility with pure CO_2 was carried out using the Multiple Mixing-Cell method (Ahmadi and Johns, 2008). The test start pressure was 1,700 psi [11,721.1 kPa] at 75°F. The first contact miscibility (FCM) pressure was computed to be greater than 2,600 psi [17,926.4]. The multiple contact miscibility (MCM) was achieved at 1,718 psi [11,845.2 kPa] after three contacts through the forward contacts vaporizing drive mechanism.

4.3.2 Liquid-Liquid-Vapor (LLV) Behavior

Injection of CO_2 into an oil reservoir at temperatures below 120°F [49°C] can form a second liquid hydrocarbon phase (L_2) rich in CO_2 (Nutakki et al., 1991, Pan et al., 2014). The CO_2-rich hydrocarbon phase and the other two (liquid, L_1 and vapor, V_1) hydrocarbon phases coexist in equilibrium within a certain pressure and CO_2 mole fraction region. The simulator used for this study (and most other commercial ones) could not handle a three-phase flash, and using a two-phase flash caused significant numerical difficulties when a CO_2 mole fraction and the grid block pressure fell in the LLV region. The problem was more pronounced near the producer where grid blocks had lower pressures.

In this scenario, two possible solutions were considered:

1. Keeping the producer BHP high enough to not let grid block pressures fall in the LLV region.
2. Lower the CO_2-C_{7+} fraction BICs to shrink the LLV region (Pan et al., 2014).

The bottomhole pressure of a producer in the OA sand is about 800 psia, so this was not altered. Secondly, the injection pressure could not be raised higher than what was required to keep the voidage replacement ratio (VRR) of one. Therefore, it was not possible to raise the model pressure beyond that dictated by voidage replacement.

In this outlook, the BICs between CO_2 and hydrocarbon fractions were lowered cautiously to shrink the LLV region (Table 4-7). Figure 4-3 shows the three phase hydrocarbon regions for different CO_2-hydroarbon BIC sets. Here, BIN refers to the binary interaction coefficient for CO_2 and the C_{7+} pseudo fractions. The shaded area bounded by the black phase boundary depicts the LLV region with CO_2 for the fluid used in the study.

The shrinkage in the LLV region was not significant but was sufficient to keep specific pattern sections near the producer from facing numerical issues at specific times during a CO_2 cycle (Figure 4-4). Point A in Figure 4-3 corresponds to conditions in the highlighted grid in Figure 4-4 (layer 2) that fell in the middle of the LLV region for the original CO_2 BIC set, but outside it for the tuned BICs.

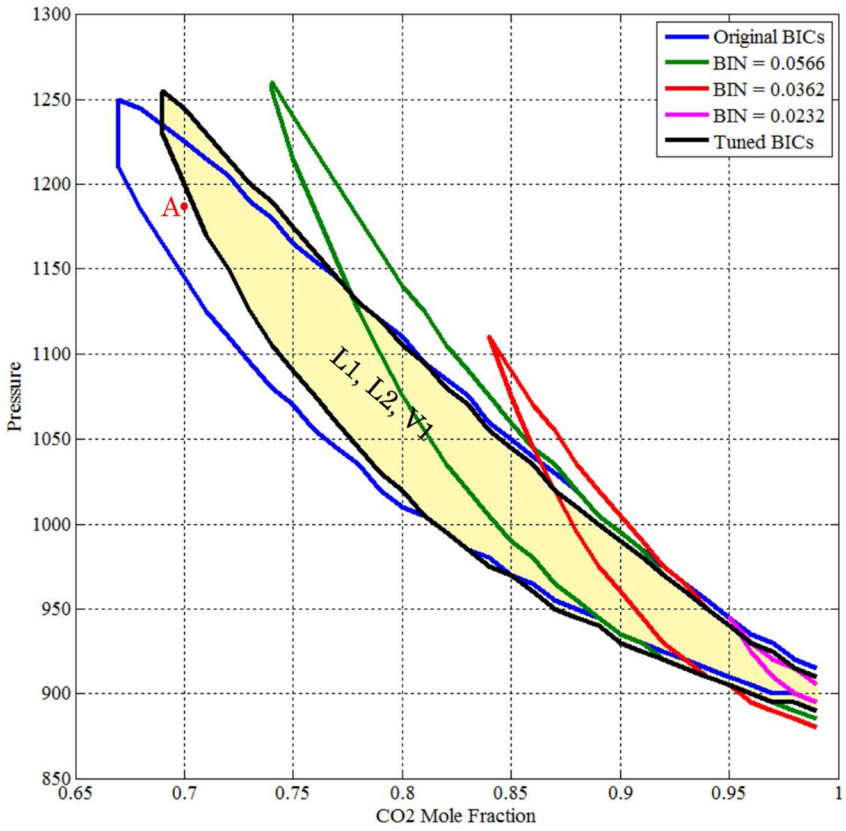

Figure 4-3 LLV regions for varying CO_2-hydrocarbon BICs

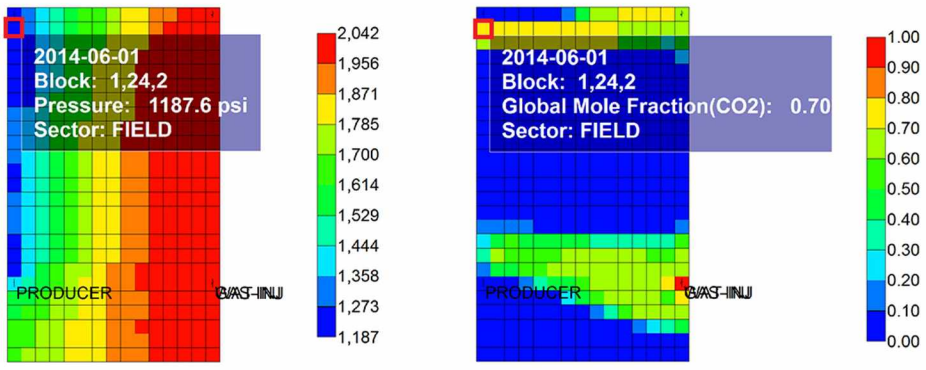

Figure 4-4 Pressure (left) and CO_2 mole fraction (right) map for layer 2 after 0.2 HCPV CO_2 injection

Table 4-7 CO_2-C_{7+} interaction coefficients before and after tuning

	Default	Tuned
HYP_1	0.115	0.0707582
HYP_2	0.09	0.0753357
HYP_3	0.15	0.0870075
HYP_4	0.15	0.0930880
HYP_5	0.15	0.1132597

4.3.3 CO_2-Oil Phase Properties

Alteration in the CO_2-hydrocarbon BICs would affected the phase behavior of the fluid, including important CO_2 contacted oil properties like density, viscosity, and saturation pressure. In the absence of swelling test data, matching the CO_2 contacted oil viscosity was given the highest priority, as it had a direct impact on the fluid flow performance. Ning et al. (2011) observed the Schrader Bluff oil viscosity to decrease from 76 cp to about 15 cp after the end of the last WAG cycle. The interaction parameters between CO_2 and the hydrocarbon were altered in such a manner to get close to 15 cp viscosity for a CO_2-oil mixture having 50% CO_2 for 1,600–2,300 psia [11,032–15,858 kPa] pressures (Figure 4-5).

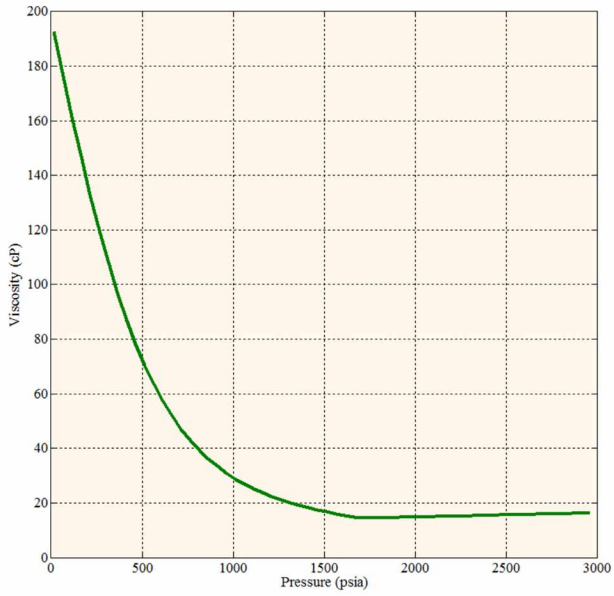

Figure 4-5 Two-phase flash CO_2-oil viscosity results

It was observed that further lowering the CO_2-hyrocarbon BICs to reduce the LLV region had a negative impact on fluid flow properties for CO_2 contacted reservoir oil. The critical volume (V_c), liquid Z-factors, and hence, molar volumes, V_m, decreased drastically for low binary interaction parameters between CO_2 and C_{7+} pseudo fractions, especially at high CO_2 mole fractions. The decrease in the critical volume was more pronounced as compared to the molar volumes. The result was an increase in the reduced molar volume ($V_r = V/V_c$) for low BICs at high CO_2 concentrations. Since the viscosity model of Jossi et al. (1962) is a function of inverse of reduced volume, an increase in its value will result in a decrease in the viscosity of the mixture.

Table 4-8 Liquid phase properties for two CO_2 BIC sets for varying CO_2 mole fractions

CO_2 Mol Frac.	0.3		0.5		0.7		0.85	
	Tuned	0.0241	Tuned	0.0241	Tuned	0.0241	Tuned	0.0241
Z-Factor	0.939	0.938	0.742	0.741	0.693	0.545	0.721	0.401
V_m (m^3/kmol)	0.191	0.190	0.151	0.150	0.141	0.111	0.146	0.081
V_c (m^3/Kmol)	0.531	0.531	0.393	0.393	0.359	0.264	0.376	0.175
$(V_r)^{-1}$	2.787	2.789	2.608	2.613	2.554	2.387	2.569	2.149
Viscosity (cp)	33.205	33.493	14.456	14.779	11.494	4.753	13.074	1.405

Table 4-8 shows the Z-factor, volumes, and viscosity at 1,765 psia [12,169 kPa] and 75°F [23.89°C] for the tuned model and for CO_2-C_{7+} interaction coefficients set to 0.0241 for CO_2 mole fractions of 0.3, 0.5, 0.7, and 0.85. The viscosities match well for CO_2 mole fractions up to 0.5, above which the deviation among the properties increases. Viscosity, being a critical flow property, reduces to abnormally low values at high CO_2 concentrations (>= 0.85) (Figure 4-6). Near the injection well where CO_2 mole fraction would be above 0.9, the observed viscosity would have been below 0.5 cp when the CO_2-C_{7+} interaction coefficients were set to 0.0241, something unphysical for the fluid under study.

The swelling characteristics of CO_2 were also observed through the increase in bubblepoint pressure with increasing amounts of CO_2. From an initial value of 1,489 psia [10,266 kPa], the saturation pressure increased to 6,448 psia [44.457 kPa] at 65 mole percent CO_2 (Figure 4-7). The increase was sharp after 60% CO_2 in the mixture.

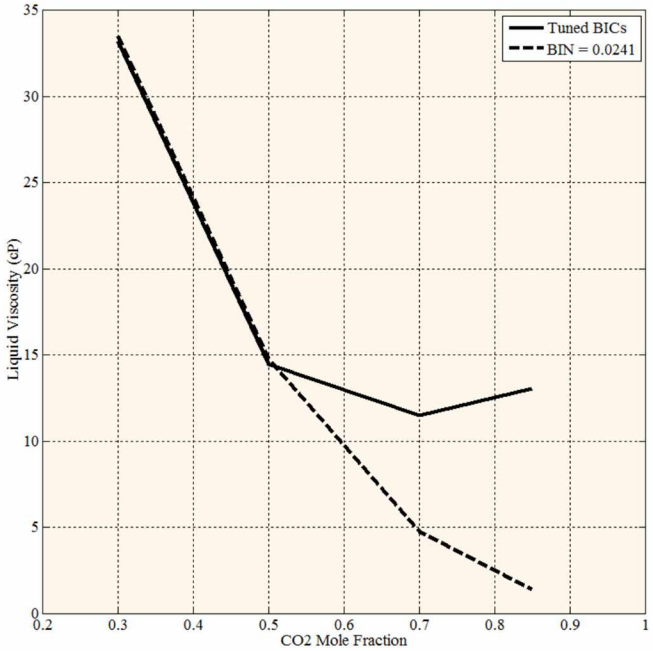

Figure 4-6 Liquid viscosities for the tuned and reduced BIC set from a CO_2-oil two-phase flash at 1765 psia and 75°F

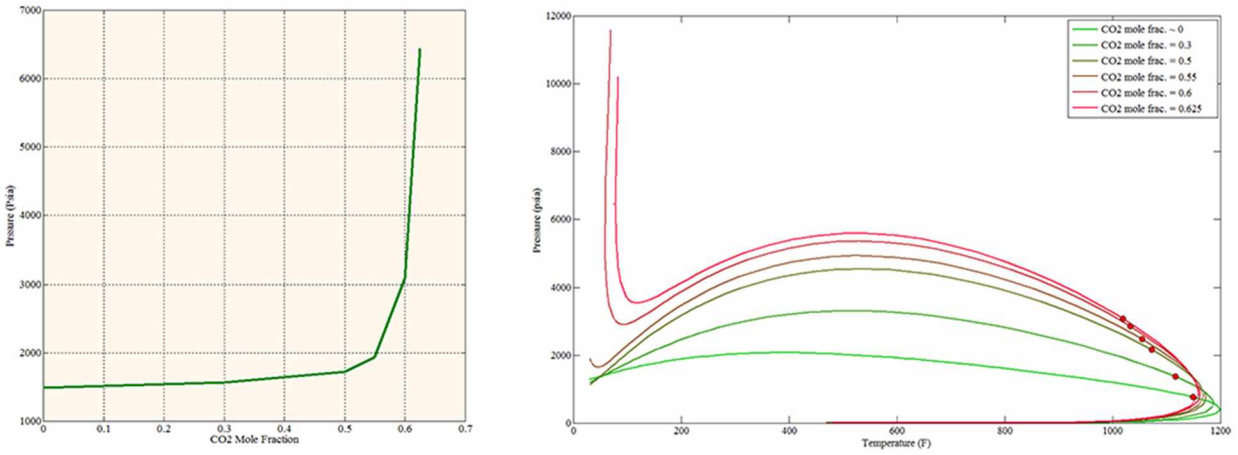

Figure 4-7 Saturation pressure (left) and phase envelope (right) for the EOS predicted fluid model for varying CO_2 mole fractions

CHAPTER 5 VALIDATION OF SIMULATION MODEL

Reservoir simulation is a tool for assessing reservoir performance from flow simulations on a reservoir model. The main use here is to identify the best possible approach to develop the field for the given market conditions. This requires the mathematical model to represent subsurface physics as closely as possible. Unfortunately, there is uncertainty inherent in every model. This can arise from (1) data measurements; (2) data interpretation; (3) geophysical and geologic modeling; (4) transmissibility calculation; and (5) flow simulation. Most commonly, uncertainty lies in porosity distribution, permeability distribution and rock and fluid property calculations (relative permeability, adsorption, etc.). Therefore, it becomes imperative to validate the model by matching past production performance to establish its representativeness for accurate future production forecasts.

As previously stated, this study is an extension of the work done by Ning et al. (2011) and the petrophysical and fluid models have been adapted from their study. However, as remarked in Chapter 3, there was uncertainty regarding permeability at the fourth corner of the reservoir model for all 20 layers (Figure 3-5). This rendered 20 permeability uncertainty values at those points. Furthermore, the relative permeability data was also unavailable. Therefore, 10 relative permeability parameters were also added to the tuning set of variables that, in combination with the absolute permeability parameters, required tuning to match the production performance observed by Ning et al. (2011). These rock and fluid parameters included: oil, water, and gas relative permeability endpoints; residual oil saturation to water; residual oil saturation to gas; connate gas saturation; relative permeability exponents for oil in oil-water and gas-liquid tables; and water and gas relative permeability exponents, respectively. The following assumptions made while generating oil-water and liquid-gas relative permeabilities should be noted:

i. Critical water saturation was set equal to connate water saturation
ii. Irreducible oil saturation was set equal to residual oil saturation for both oil-water and liquid-gas systems
iii. Critical gas saturation was kept same as connate gas saturation.

The model was validated by matching the waterflood and CO_2-WAG production rates and cumulative recoveries from Ning et al. (2011) while maintaining bottomhole conditions similar to those observed in the OA sand.

5.1 Waterflood Performance

A manual history matching approach was taken by changing the previously mentioned absolute permeability and oil-water relative permeability parameters. The initial set of relative permeability and saturation endpoints were taken from Bakshi (1991) and the scanning curves were generated by using the relative permeability model of Honarpour et al. (1986).

5.1.1 Manual History Match Procedure

i. During each trial, the absolute permeabilities at the fourth corner were altered for each layer. Data from various logs from the O sand were taken to help maintain the permeability trend with depth. Initially, all 20 layers were modified. However, with subsequent runs, layers 4 through 6 and 12 through 17 were identified as more sensitive to shifts in production profiles, especially oil rates. Layer 14, being the high permeability zone, influenced the water breakthrough time.

ii. Once the permeability values at the four corners for all layers were obtained, the same were exported to MATLAB. Here, permeability throughout the grid structure was populated using a Delaunay triangular linear interpolation algorithm that was applied on each layer separately. The permeability in the J-direction was kept the same as that in the I-direction, while the vertical permeability was kept a tenth of the horizontal permeability.

iii. The simulation was run and the match between the predicted and observed profiles was analyzed. In case the discrepancy between oil rate and recovery was large, step two was repeated. Ultimate oil recovery was matched by modifying the residual oil saturation to water (S_{orw}).

iv. Once the error between the observed and predicted profiles became moderate, the relative permeability parameters were also modified, in addition to absolute permeability, to fine tune the model. In this regard, the waterflood oil rate can be subdivided into three distinct regions: early, middle, and late times (represented by regions 1, 2, and 3, respectively, in Figure 5-1).

v. The oil relative permeability at connate water (K_{rocw}) had a considerable impact on the oil rate profile during early times. The water relative permeability end point (K_{rwiro}) as well as the water relative permeability exponent (N_w) were seen to influence the water breakthrough time (point A in Figure 5-1). These were modified in conjunction with the permeability of layer 14.

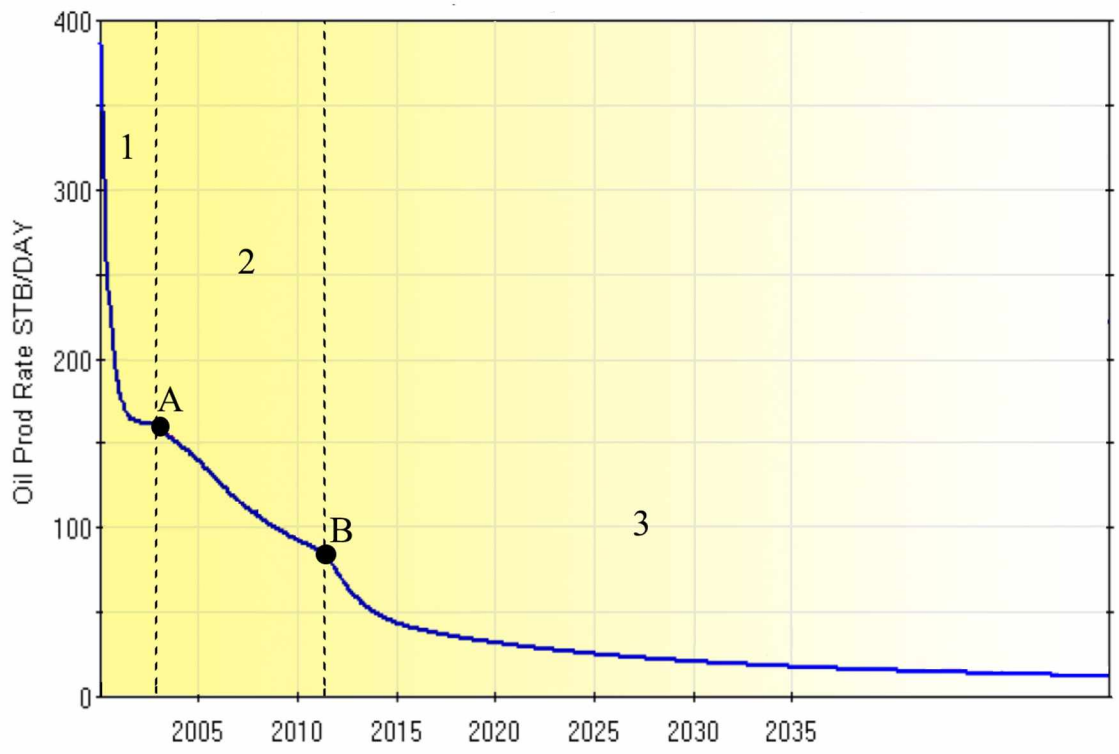

Figure 5-1 Waterflood oil rate. Modified from Ning et al. (2011)

vi. Once the early time oil rate was matched, the middle region was in tune with the observed data from Ning et al. (2011). However, the slope following the water breakthrough as well as attainment of the maximum allowable bottomhole fluid (BHF) rate for the producer (point B in Figure 5-1) were matched. The oil and water relative permeability exponents (N_{ow} and N_w) and the water relative permeability endpoint (K_{rwiro}) had an impact on the time taken to achieve this BHF limit. Given the match for the oil rate, point B occurred quickly with a decrease in N_w.

vii. The late time profile was affected by the oil relative permeability exponent (N_{ow}) and the residual oil saturation to water (S_{orw}). It was observed that S_{orw} had an impact on the sudden break in slope (and its steepness) past point B. Figure 5-2 shows the flowchart to match the waterflood performance.

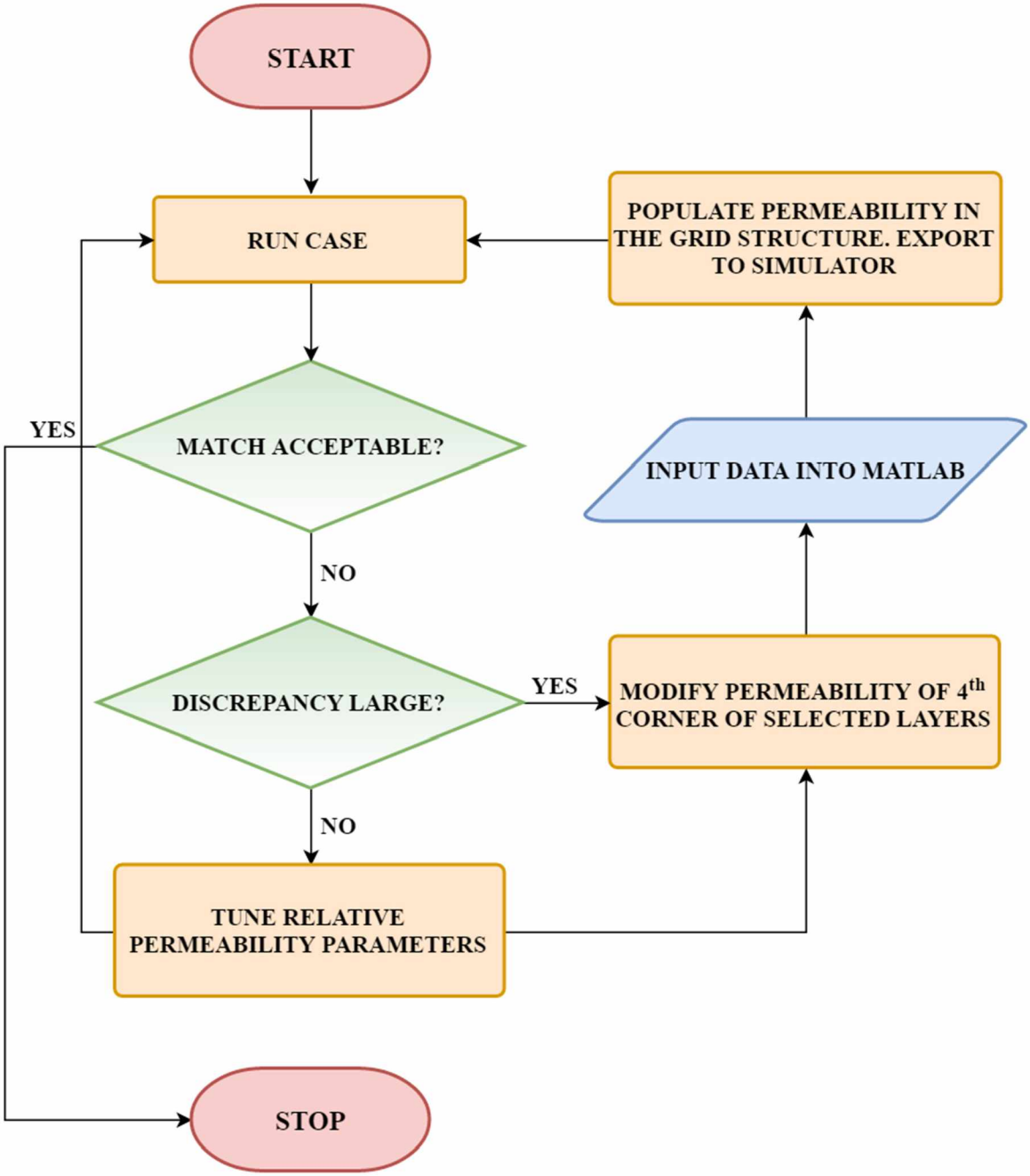

Figure 5-2 Workflow to match the waterflood performance

Besides the geological and reservoir parameters, operational constraints also have a significant impact on flow performance, especially production rates. The waterflood was run for 50 years (2000-2050) at a constant producer bottomhole pressure of 800 psia [5,516 kPa]. The annual reservoir depletion was maintained at 4% HCPV by constraining the producer's total bottomhole fluid rate (oil + gas + water) at 500 RB/day [79.5 rm^3/day]. This resonates with the 1,000–2,000 RB/day [159–318 rm^3/day] bottomhole fluid rate observed for a whole well in the OA sand.

The injection well rate was altered to honor reservoir voidage and keep the reservoir pressure near its initial value of 1,785 psia [12,307 kPa] (Figure 5-3).

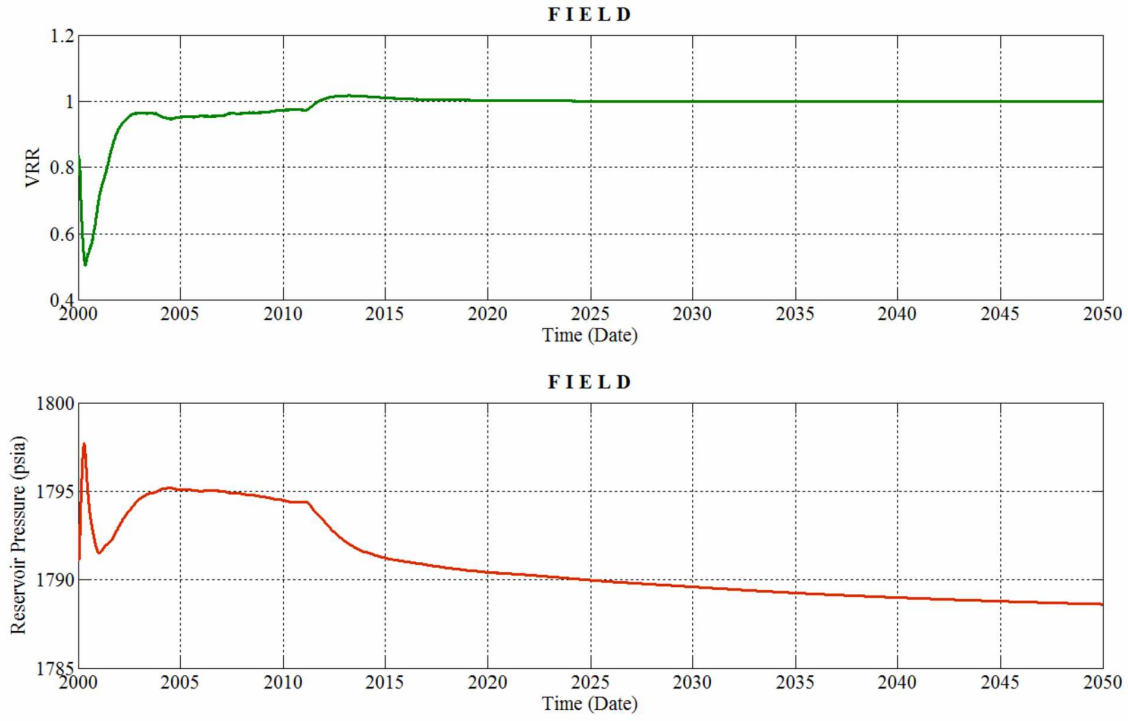

Figure 5-3 Voidage rate replacement (VRR) (top) and average reservoir pressure (bottom) profiles for the field during waterflood

5.1.2 Results

After several trials and tuning, a good match for the production profiles was finally seen (Figure 5-4). The matching process was complex, as it required alternating between WAG and waterflood simulations. The permeability of layers 3-6 and 12-16, along with the oil and water relative permeability and saturation endpoints, was key in matching the waterflood production profiles. It was

observed that changing the absolute and oil-water relative permeability parameters to obtain an adequate match for the WAG model often deteriorated the waterflood performance fit, and vice-versa. It was also noticed that modifying the liquid-gas relative permeability parameters had negligible impact on the waterflood performance. This may be because the Schrader Bluff oil has very little dissolved gas (FVF ~ 1.07 RB/STB) and the reservoir was undersaturated throughout the model runs.

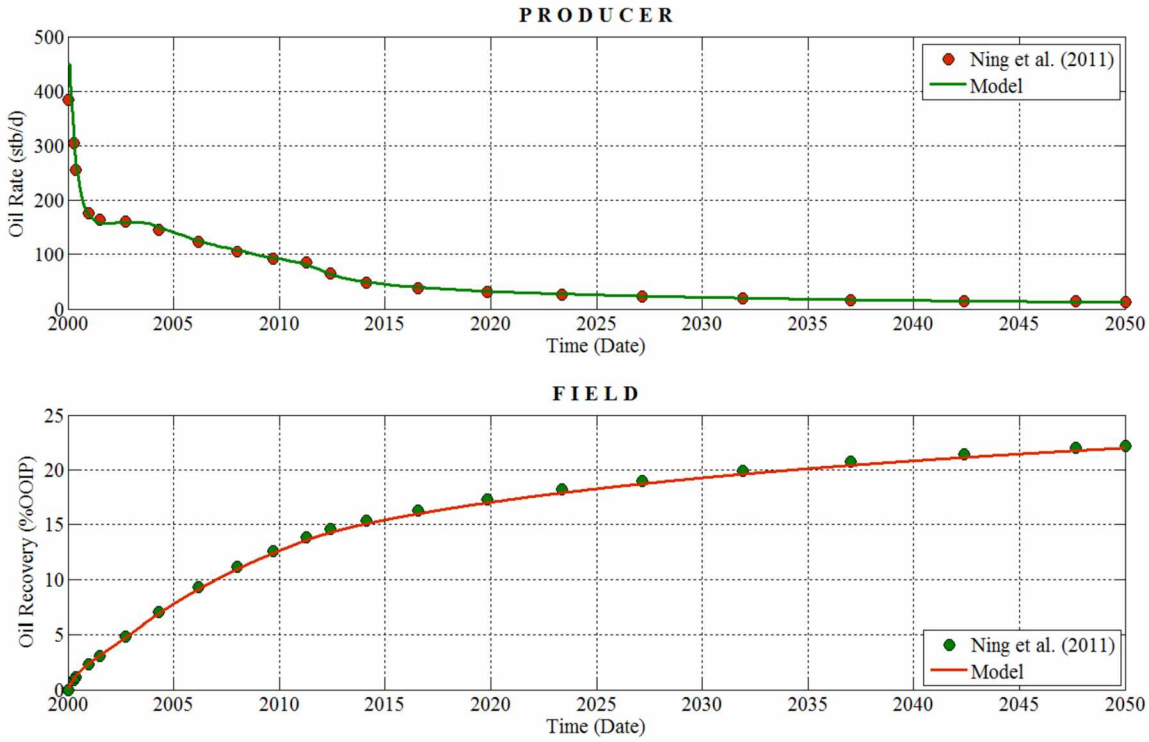

Figure 5-4 Oil rate and oil recovery performance match for waterflood validation test

Table 5-1 shows the match between total cumulative oil produced, cumulative water injected, and the field recovery factor after 50 years.

Table 5-1 Comparison of other waterflood performance parameters

	Ning et al. (2011)	Model
Oil Produced (MSTB)	934	946
Water Injected (MRB)	8449	8281
Recovery Factor (%)	22.2	22.2

5.2 CO_2 WAG Performance

Calibrating the reservoir model for CO_2-WAG was more complicated than doing so for waterflood, as now the gas-liquid relative permeability parameters also had a significant impact on the flow performance. This was because injection gas drive also dominated the reservoir drive mechanism, in addition to water drive, due to CO_2 half-cycles. As previously stated, the validation runs were alternated between waterflood and WAG simulations to ensure model calibration for both processes. Due to the addition of gas-liquid relative permeability variables, the tuning set of variables became very large. Hence, a combination of automatic and manual history matching approaches were taken to match the oil rates and recoveries for CO_2-WAG as observed by Ning et al. (2011). The manual approach was similar to that described in Figure 5-2 and hence, will not be discussed in this section.

5.2.1 Parameterization

Once a good match for waterflood was achieved, the absolute permeability was not altered any further and only relative permeability parameters were selected as tuning variables in the automatic history matching workflow (Table 5-2). The oil-water relative permeability parameter limits were chosen based on the observations during the calibration of the waterflood model to keep practical bounds. The gas relative permeability endpoint upper limit was selected so as to not exceed $S_{org} + S_{wcon}$ at any time during flow simulation (Honarpour et al., 1986). Exponents' bounds were taken on the basis of observed values used for the Schrader Bluff fluid in a previous study (Strycker and Wang, 2000).

Table 5-2 Tuning set of variables for CO_2-WAG model calibration

Parameter	Lower Limit	Upper Limit
K_{ro} End Point	0.57	0.65
K_{rw} End Point	0.19	0.40
K_{rg} End Point	0.30	0.45
S_{gcon}	0.02	0.05
S_{org}	0.20	0.28
S_{orw}	0.30	0.45
N_w	2	3.5
N_{ow}	2.4	4
N_g	2.2	3
N_{og}	2.6	4

In addition to these, the following conditions were further imposed on three additional saturation endpoints.

$$S_{oirw} = S_{orw} \tag{5.1}$$

$$S_{oirg} = S_{org} \tag{5.2}$$

$$S_{gcrit} = S_{gcon} \tag{5.3}$$

5.2.2 History Match Error

The simulator's inbuilt history match error objective function was used to evaluate the history match quality. The error function measures the relative differences between the simulated results and the measured data for each objective function (CMOST, 2015) (Equation 5.4). Generally, a field may have multiple wells, with each well having multiple types of production data to match. In such a case, each well has a separate objective function defined for it. In our case, we just had one well with two types of data to match: oil rate and oil recovery. Hence, one objective function sufficed. Furthermore, the objective function defined in the simulator is one of a weighted type, i.e., different types of production data can be weighted separately depending on the level of trust in the measured data. However, for our problem, the data to match was taken from Ning et al. (2011) who predicted the WAG performance on a mechanistic type pattern model (TPM). Hence, there was no bias towards either type of data and both were equally weighted.

$$Q_i = \frac{1}{\sum_{j=1}^{N(i)} tw_{i,j}} \times \sum_{j=1}^{N(i)} \frac{\sqrt{\frac{\sum_{t=1}^{T(i,j)} (Y_{i,j,t}^{s} - Y_{i,j,t}^{m})^2}{NT(i,j)}}}{Scale_{i,j}} \times 100\% \times tw_{i,j} \tag{5.4}$$

where:

i,j,t	Subscripts representing, well, type of production data, and time
N(i)	Total number of production data types for well *i*
NT(i,j)	Total number of measured data points
$Y^{s}_{i,j,t}$	Simulated results

$Y^{m}_{i,j,t}$ Measured results

$tw_{i,j}$ Term weight

$Scale_{i,j}$ Normalization scale.

The normalization scale is the maximum of the following:

$$\Delta Y^{m}_{i,j} + 4\times Merr_{i,j} \tag{5.5a}$$

$$0.5\times\min(|\max(Y^{m}_{i,j,t})|, |\min(Y^{m}_{i,j,t})|) + 4\times Merr_{i,j} \tag{5.5b}$$

$$0.25\times\min(|\max(Y^{m}_{i,j,t})|, |\min(Y^{m}_{i,j,t})|) + 4\times Merr_{i,j} \tag{5.5c}$$

where:

$\Delta Y^{m}_{i,j,t}$ Maximum measured change for i^{th} well and j^{th} production data

$Merr_{i,j}$ Measurement error (ME).

The measurement error accounts for error terms with different units and essentially normalizes the error function. It is half the absolute error range, i.e., it represents 1 standard deviation from the mean. Multiplying it by 4 is used to include 2 standard deviations on each side of the mean (95% confidence). Therefore, if the simulated result is between *historical value* ± *ME*, the match is satisfactory. If the simulation results are the same as the measured results, the history match error is 0%. History match error up to 5% is generally considered acceptable (CMOST, 2015). In the case of more than one well, the global history match error is computed as a weighted average of all independent objective functions:

$$Q_{global} = \frac{1}{\sum_{i=1}^{NW} w_i} \sum_{i=1}^{NW} w_i Q_i \tag{5.6}$$

where:

Q_{global} Global objective function

Q_i	Objective function for well *i*
NW	Total number of wells
w_i	Weight of Q_i in the calculation of Q_{global}.

Since the production data was matched for just one well, equation 5.4 essentially becomes independent of *i*.

$$Q = \frac{1}{\sum_{j=1}^{N} tw_j} \times \sum_{j=1}^{N} \frac{\sqrt{\frac{\sum_{t=1}^{T(j)} (Y_{j,t}^{s} - Y_{j,t}^{m})^2}{NT(j)}}}{Scale_j} \times 100\% \times tw_j \tag{5.7}$$

where:

$$N = 2 \qquad tw_1 = tw_2 = 1 \qquad NT(1) = NT(2) = 53$$

And the global objective function simplifies to:

$$Q_{global} = Q \tag{5.8}$$

5.2.3 Optimizer

CMOST's DECE™ (Designed Exploration and Controlled Evolution) optimizer was selected for the automatic history matching approach. This optimization method has been applied successfully to various real-world reservoir simulation studies, including black oil, heavy oil, and thermal processes (CMOST, 2015). The DECE™ optimizer uses an iterative approach in which a designed exploration stage is followed by a controlled evolution stage. In the exploration stage, the goal is to explore the search space in a designed random manner such that maximum information about the solution space can be gathered. Here, parameter values are selected using experimental design and Tabu search (Glover, 1986) techniques to create representative simulation datasets. Statistical analysis is then applied on the simulation results of the designed exploration stage. The DECE™ algorithm

scrutinizes each candidate value of all parameters and determines if rejecting (banning) certain values from being picked might improve the solution quality, i.e., minimize the objective function (Equation 5.6). These candidate values are remembered and are not picked in the next controlled evolution stage. However, the algorithm checks the rejected values periodically to test the validity of previous rejections, thereby minimizing the possibility of getting trapped in a local minima. In the event a previous rejection is found to be invalid, the corresponding candidate value is picked up again in the pool of "potential solution set" and is used again in subsequent evolutionary stages.

5.2.4 Numerical Issues

Modeling the CO_2-WAG process had an added challenge of overcoming the numerical instability due to formation of the three-phase hydrocarbon region in different sections of the reservoir during flow simulations (Figures 4-3 and 4-4). As described in the previous chapter, this was not handled well by the simulator and there was only a narrow margin for reducing the CO_2-hydrocarbon interaction coefficients. It often happened that for a specific combination of absolute and relative permeability, the simulator experienced frequent formation of significant second hydrocarbon (solvent-rich) liquid phases. Attempting a two-phase flash in the three-phase liquid-liquid-vapor (LLV) region caused discontinuities in both phase equilibrium and phase boundary calculations. This caused the simulator to converge the second liquid phase sometimes to the primary liquid and sometimes to the vapor phase, often during alternate time steps. This phase switching led to large oscillations in density (and hence, pressure) in regions where this phase condition was encountered (Figure 5-5). Consequently, this caused convergence failures during flash calculations leading to time step cuts and, in more adverse circumstances, premature termination of simulations. Selecting the right combination of the tuning variables that would give a representative waterflood and CO_2-WAG performance while giving clean simulation runs without significant numerical problems was challenging.

G E M T I M E S T E P S U M M A R Y

Time Step			Time		Maximum Changes						Mat Bal	Cum time	Solver		Convergence Flags (0=conv; 1=unconv)			
	Size	Newton			Pressure		Saturation		Composition		Err	step	Iter/	Cum				
No.	days	cycls	Days	Date	Block	psia	Block	Fraction	Block	Fraction	%	cuts	Cycl	Fail	var	res	wel	cer	gmc
2681	1.0e-6	1	4093	2011.03.16	1,9,3	-105	1,9,3	-81e-3(o)	1,9,3	-10e-5(1)	75e-4	25	1.0	0	0	1		0	
2682	1.0e-6	1	4093	2011.03.16	1,9,3	104.8	1,9,3	8.1e-2(o)	1,9,3	1.0e-4(1)	75e-4	25	1.0	0	0	1		0	
2683	1.0e-6	1	4093	2011.03.16	1,9,3	-105	1,9,3	-81e-3(o)	1,9,3	-10e-5(1)	75e-4	25	1.0	0	0	1		0	
2684	1.0e-6	1	4093	2011.03.16	1,9,3	104.8	1,9,3	8.1e-2(o)	1,9,3	1.0e-4(1)	75e-4	25	1.0	0	0	1		0	
2685	1.0e-6	1	4093	2011.03.16	1,9,3	-105	1,9,3	-81e-3(o)	1,9,3	-10e-5(1)	75e-4	25	1.0	0	0	1		0	
2686	1.0e-6	1	4093	2011.03.16	1,9,3	104.8	1,9,3	8.1e-2(o)	1,9,3	1.0e-4(1)	75e-4	25	1.0	0	0	1		0	
2687	1.0e-6	1	4093	2011.03.16	1,9,3	-105	1,9,3	-81e-3(o)	1,9,3	-10e-5(1)	75e-4	25	1.0	0	0	1		0	
2688	1.0e-6	1	4093	2011.03.16	1,9,3	104.8	1,9,3	8.1e-2(o)	1,9,3	1.0e-4(1)	75e-4	25	1.0	0	0	1		0	

Figure 5-5 Numerical convergence problems due to phase switching

5.2.5 Results

Figure 5-6 shows the oil rates and oil rate errors for 134 cases. The errors should typically follow a constant decreasing trend as the optimization process filters out unfit parameter sets. The base error was ~10.2% (base case) and decreased to ~7.3% over 134 trials. The automatic history matching performance is usually better than this, however, there were several cases where the simulator experienced LLV regions and sometimes got stuck in them infinitely, as shown in Figure 5-5. This resulted in the scheduler terminating the cases, which exceeded the maximum allotted time per simulation. Due to premature termination, the whole time span of simulation was never achieved and the convergence between the oil rates was bad. These cases gave high oil rate errors and prevented a rapid decrease in the error. Some of these cases stand out in the error plot (red circles). The tapering off of the errors after the 85th case may be attributed to this.

The abnormally terminated cases are clearly visible in the cumulative oil profiles as well (Figure 5-7). These are mostly around the year 2020. The error outliers for such cases also stand out, similar to those in oil rate. Because the cumulative oil profile is a smooth curve (unlike oil rate, which was undulating due to CO_2-contacted oil rate peaks), the model predicted profiles conformed to the history. Hence, the absolute error itself was low (~1.9% for the base case) and the decrease was only slight, to ~1.3%. Since both oil rates and cumulative oil were weighted equally (Equation 5.7), the global error was a mean of the oil rate and the cumulative oil errors (Figure 5-8). The error trend was the same as that observed in Figures 5-6 and 5-7, and the decrease was also a mean, from ~6% to ~4.3%.

The operational constraints were kept the same as those in waterflood and injection rates were altered to keep average field pressure near its initial value by roughly maintaining a VRR of one (Figure 5-9). The injection schedule was set as 30% HCPV CO_2 spread across 10 WAG cycles (3% HCPV CO_2 per cycle), keeping a WAG ratio of 1:1. This is the same injection plan that was used by Ning et al. (2011) in their study. By following the pressure maintenance scheme, the water and gas injection rates conformed decently to those reported by the authors (Figure 5-10). The relative permeability parameters obtained from the automatic history match process were altered slightly to keep the waterflood match intact. An acceptable match for oil rates and recovery performance was finally obtained (Figure 5-11).

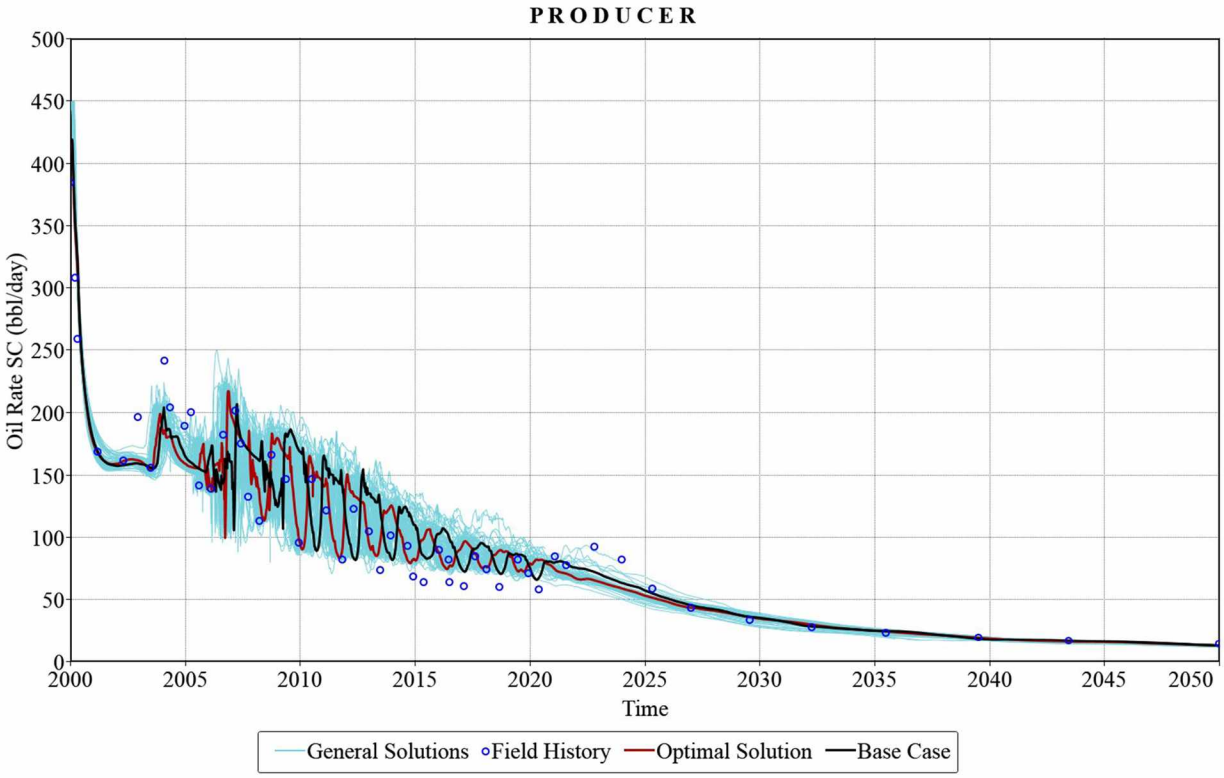

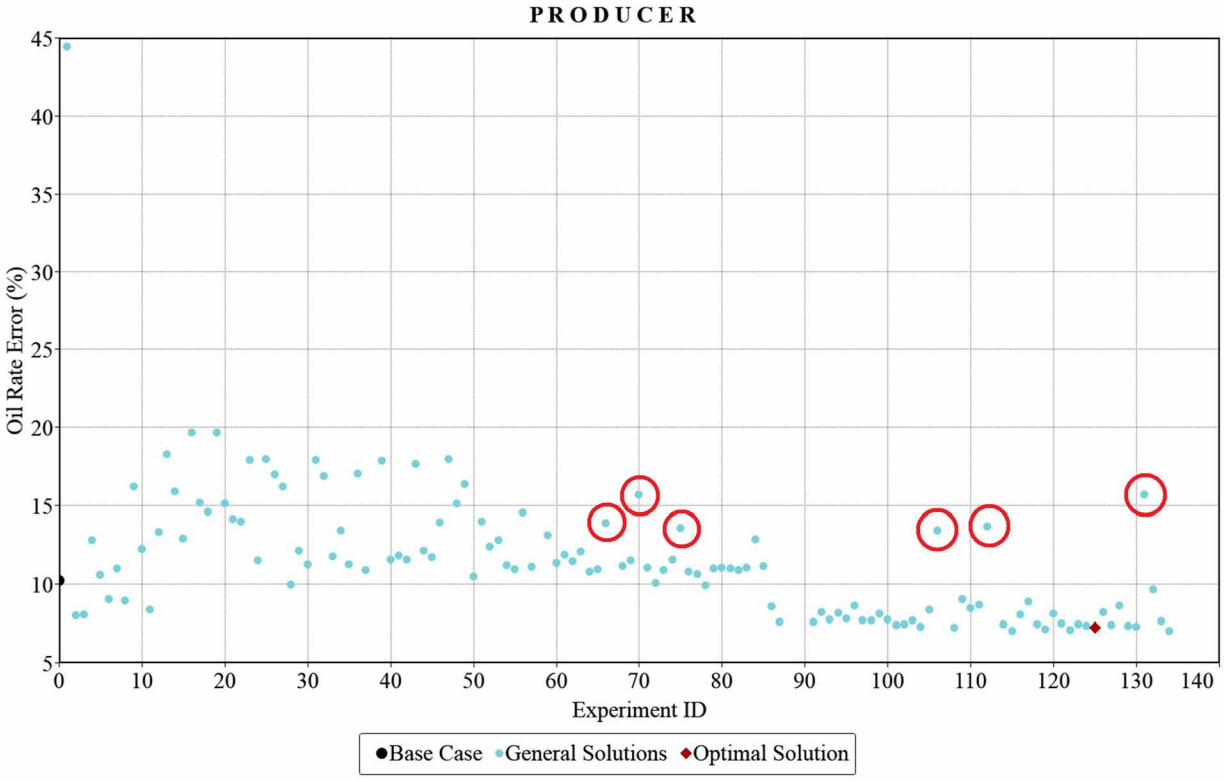

Figure 5-6 Oil rate profiles (above) and errors (below) during automatic history matching

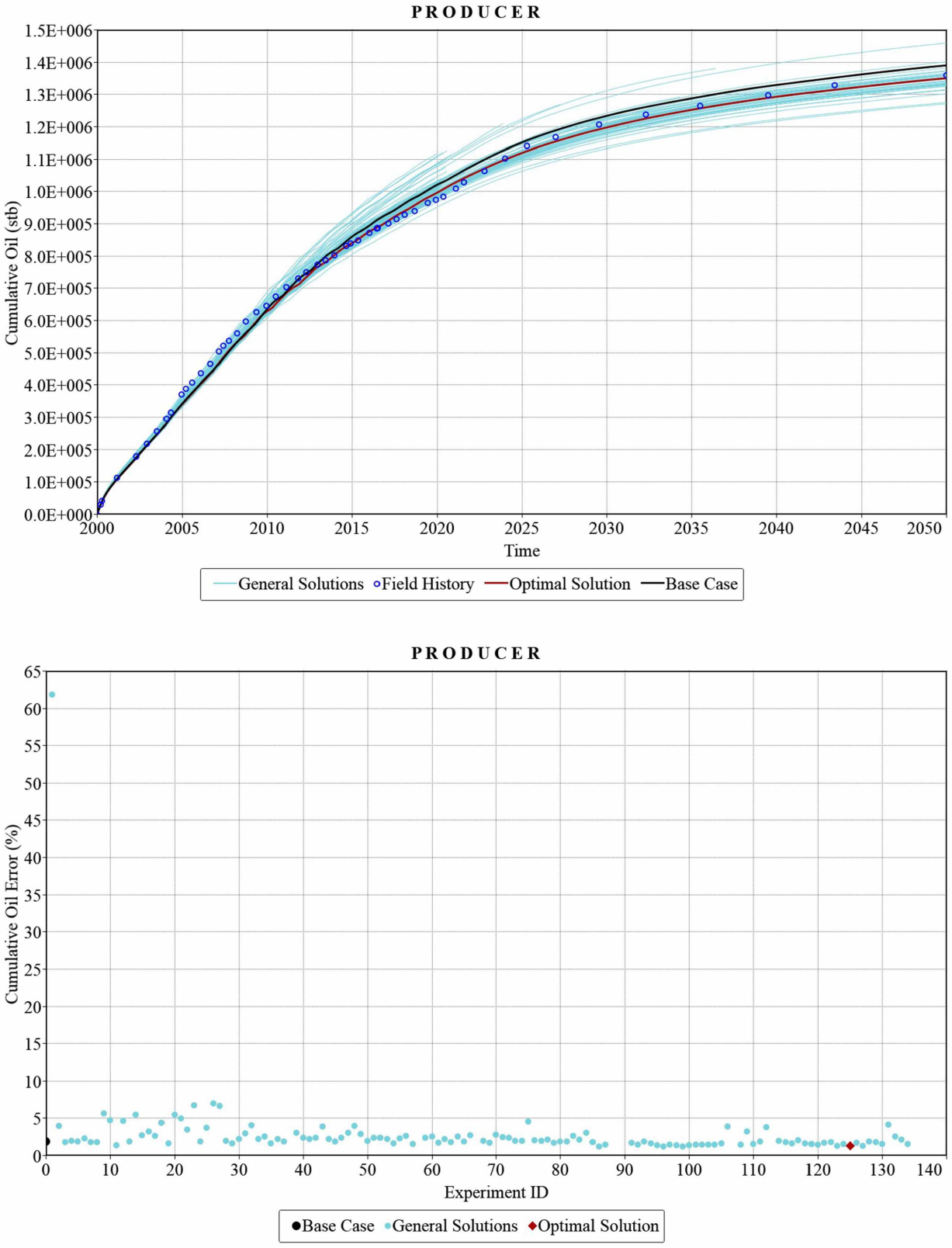

Figure 5-7 Cumulative oil profiles (above) and errors (below) during automatic history matching

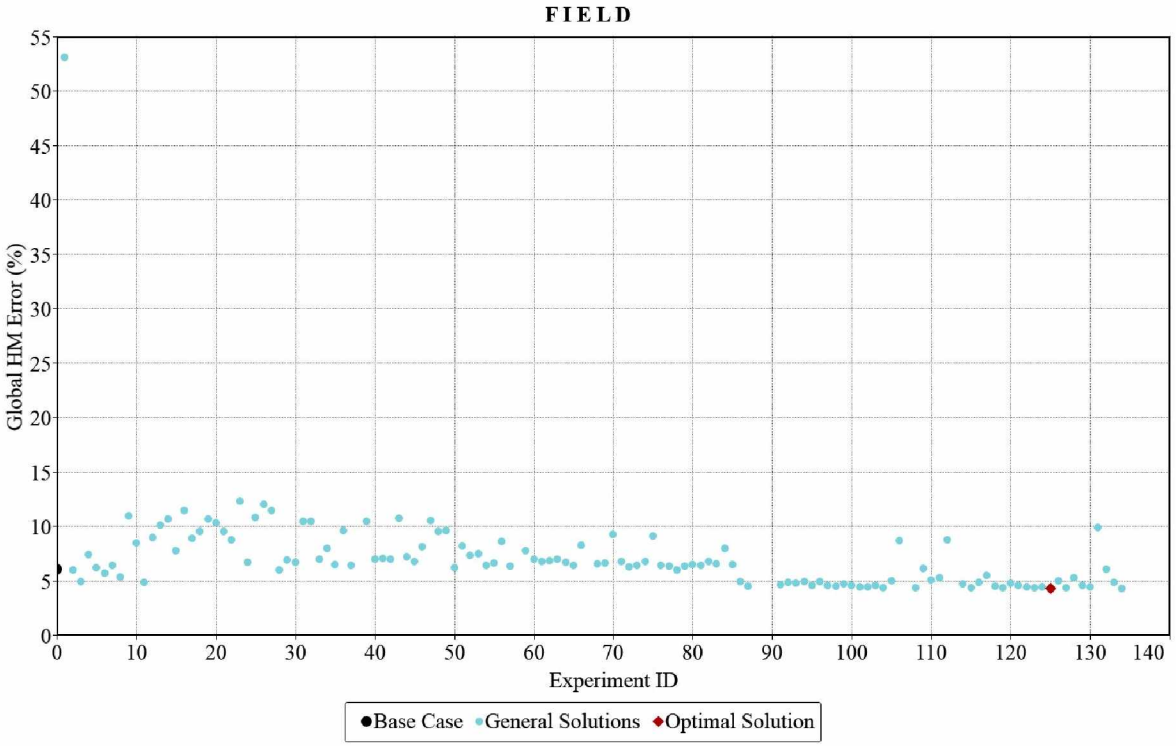

Figure 5-8 Global history match error for different parameter cases

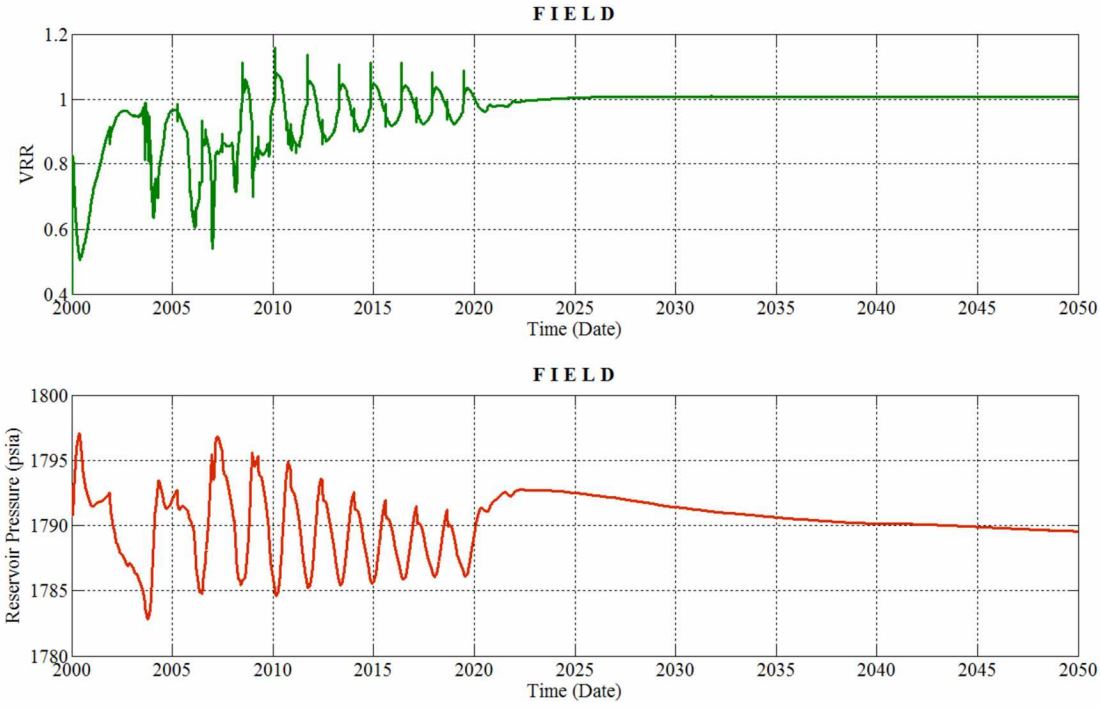

Figure 5-9 Voidage rate ratio (VRR) (top) and average reservoir pressure (bottom) profiles for the field during CO_2-WAG

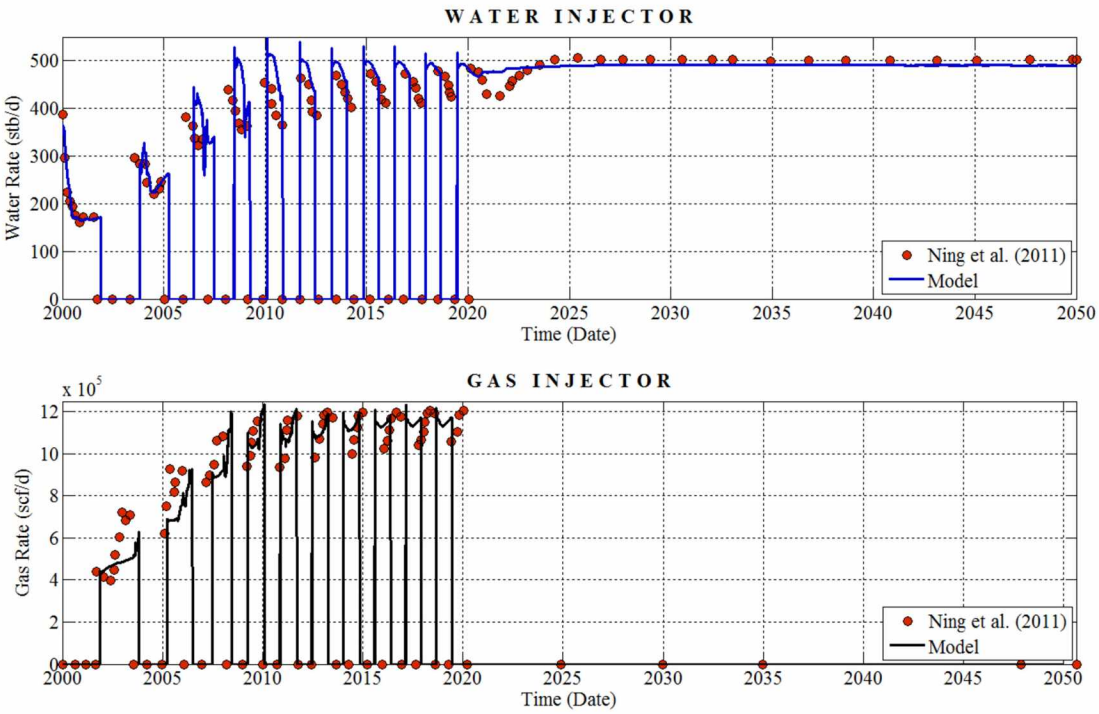

Figure 5-10 CO_2-WAG validation test water (above) and gas (below) injection rates comparison with those reported by Ning et al. (2011)

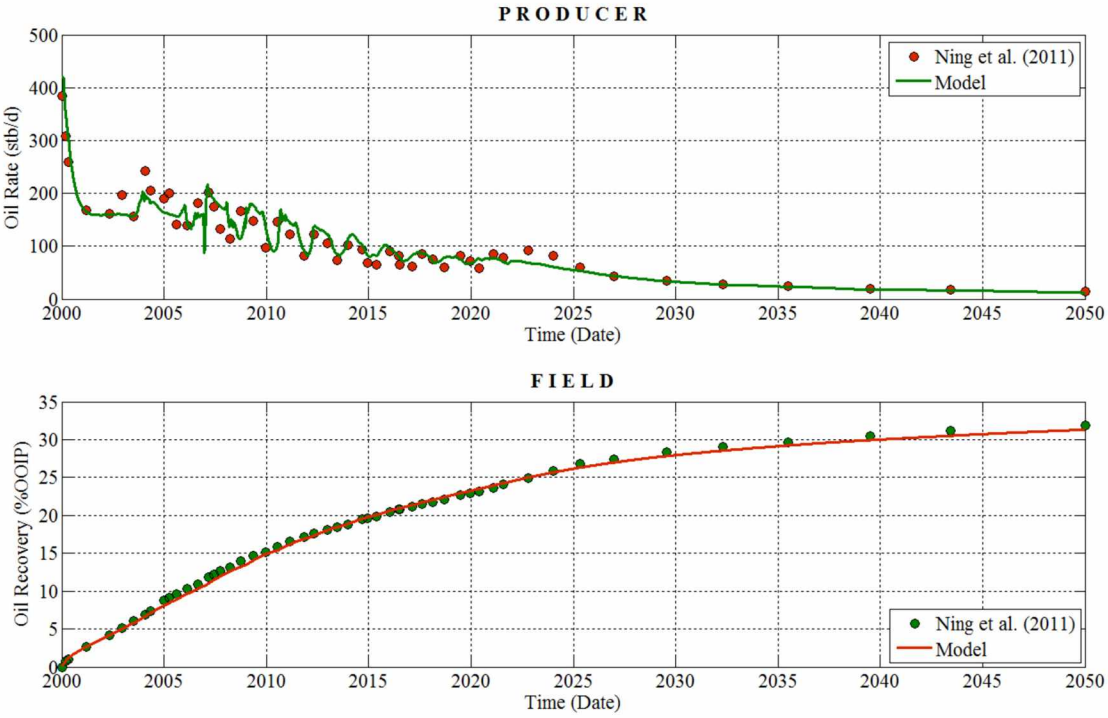

Figure 5-11 CO_2-WAG oil rates and recovery performance for the validation test

The final values of the tuning variables are shown in Table 5-3 and the permeability-I map at the producer plane is shown in Figure 5-12. The 4th corner of the simulation model (corner of uncertainty) is marked within the red bounding box.

Table 5-3 Final value of relative permeability parameters used in the reservoir model

Parameter	Final Value
K_{ro} End Point	0.637
K_{rw} End Point	0.238
K_{rg} End Point	0.379
S_{gcon}	0.026
S_{org}	0.27
S_{orw}	0.38
N_w	2.40
N_{ow}	2.68
N_g	2.50
N_{og}	3.89

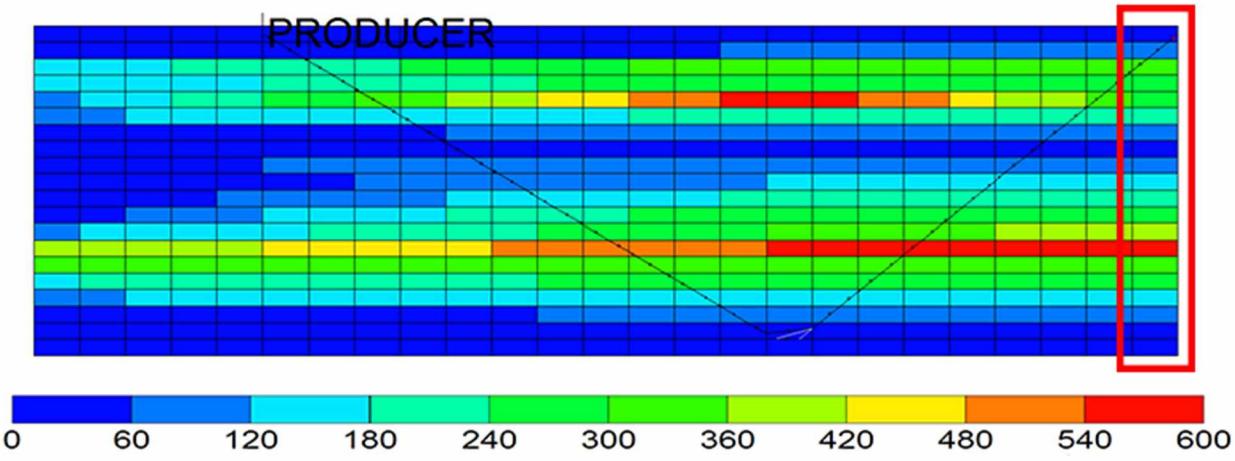

Figure 5-12 Permeability-I map at the producer plane of the model

CHAPTER 6 LOW SALINITY ENHANCED OIL RECOVERY

Low salinity waterflooding (LSWF), also known as LoSal® (trademark of BP p.l.c.), SmartWater (Yousef et al., 2010, Yousef et al., 2012), Smart Water (RezaeiDoust et al., 2009, Austad et al., 2010), Advanced Ion Management (service mark of ExxonMobil), and Designer Waterflooding (trademark of Shell), enhanced oil recovery (EOR) increases oil recovery by altering the formation wettability towards a more water-wet state. This is the dominant mechanism that causes a release of oil droplets adsorbed on the pore walls, thereby lowering the residual oil saturation after the waterflood (Figure 6-1). This happens through a series of geochemical reactions at the microscopic level. This process was modeled compositionally and the change in wettability was represented qualitatively by a shift in the relative permeability curves based on the reservoir salinity conditions at the pore scale.

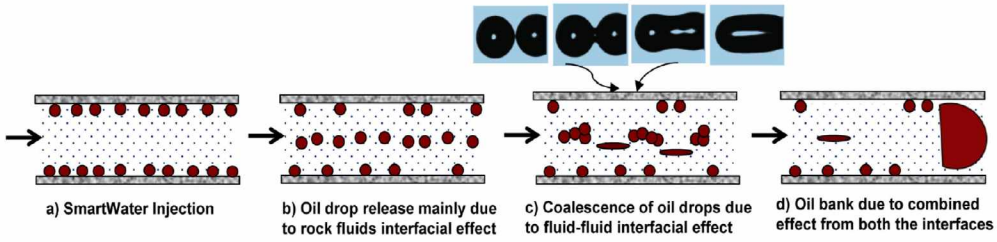

Figure 6-1 Low salinity waterflood schematic showing release of oil droplets (Ayirala et al., 2016)

6.1 Aqueous Species

The injection water chemistry plays a pivotal role in determining the success of an LSWF project. The ionic mix for the low salinity water should ideally be *tuned* depending on the formation water, in-situ oil, and reservoir mineralogical architecture to achieve best results. However, tuning injection water for the desired concentration of cationic and anionic species can be expensive, as it may require huge upfront investments for a water treatment plant. Depending upon the anticipated daily throughput of injection water and expected flood performance, the plant design and sizing may become cost prohibitive. Therefore, dilution of the formation water or gathering injection water from a nearby low salinity water source become practical options for LSWF implementation.

In a lot of cases, seawater is diluted directly and used for low salinity waterflooding. Seawater is popular because it is cheaply available for offshore projects or near-shore drill pads. Seawater has shown some success for low salinity waterflood projects on carbonates (Austad et al., 2008, Emadi et al., 2011). Where seawater is inaccessible, low salinity water from nearby aquifers may be used. It is usually located at shallow depths where the formation has access to surface water mixing, keeping the salinity low. The Schrader Bluff formation has this advantage. The Prince Creek formation sits on top of the Schrader Bluff formation (Werner, 1987) and has formation water of very low salinity (McGuire et al., 2005a), ideal for LSWF operations. Table 6-1 shows the compositional makeup of the reservoir and low salinity water used in the simulation model. Because data for formation water was not available, the following guidelines were obeyed to determine the ionic concentrations:

1. The *NaCl* equivalent salinity is about 22,000 ppm (Strycker and Wang, 2000)
2. The ratio of divalents to Cl^- is approximately the same as that observed in nearby formations (Patil et al., 2008b)
3. The pH is kept roughly the same as that in nearby formations (McGuire et al., 2005a).

Table 6-1 Breakup (ppm) of prominent aqueous species in the formation and injection water

Species	Formation Water	Injection Water
H^+	5.00E-05	2.187E-05
Ca^{2+}	183	120
Na^+	9,280	957
Cl^-	13,062	1,550
OH^-	6.295E-03	4.922E-03
HCO_3^-	565	131
pH	7.4	7.73
TDS	23,095	2,780

The injection water makeup corresponds to the water sample tested in well MPU F-77 from the Prince Creek aquifer (McGuire et al., 2005a). There were four primary aqueous species – H^+, Ca^{2+}, Na^+,

and Cl^- and four secondary aqueous species: OH^-, HCO_3^-, $CaHCO_3^+$, and $NaHCO_3$. The distinction between them is made in the way the simulator initialized the geochemical model: the concentrations of the primary species were entered and the secondary aqueous components were calculated internally by solving chemical-equilibrium equations, described in the next section. It is important to note that since HCO_3^- was a secondary aqueous component, its concentration was calculated internally by the simulator based on the molalities of the primary components including CO_2, and a limited set of geochemical reactions coupled with the simulation model. The formation water bicarbonate (HCO_3^-) concentration calculated by the simulator seems to be four or five times lower than that expected in Schrader Bluff. This premise can be drawn from the bicarbonate alkalinity seen in the surrounding fields on the North Slope (Figure 6-2).

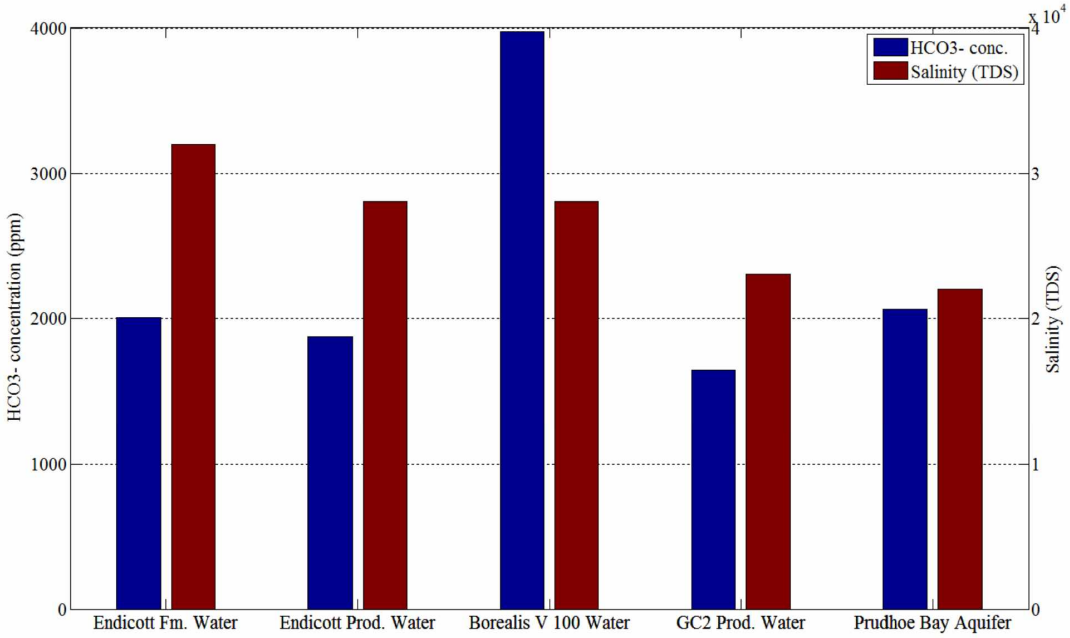

Figure 6-2 Formation and produced water bicarbonate alkalinity for ANS fields (McGuire et al., 2005a)

A realistic concentration of HCO_3^- could have been brute-forced into the simulator by providing the molalities of each aqueous component (primary + secondary) explicitly. However, with this mode of input, the specified concentrations might not have been in equilibrium during initialization. In such a scenario, the respective aqueous components would have started reacting with each other based on

the set of geochemical equations provided, causing significant changes in pressure during the start of the simulation and the associated numerical instability. The only alternative to this was to provide a comprehensive list of reactions that would have enabled the simulator to gauge the bicarbonate alkalinity more accurately, however, at the expense of considerable computation time.

6.2 Geochemical Reaction Modeling

Although a myriad of mechanisms may take place during a LSWF (McGuire et al., 2005a, Austad et al., 2010), given the simulator's capabilities and limitations, only additional oil recovery due to wettability alteration through cation exchange was modeled. In reality, there are numerous types of reactions possible within the formation water itself and between the formation water and the rock. The rock mineral architecture may itself be extremely complex, being composed of several types of silicate, micaceous, feldspars, and carbonates. The formation water may have compounds of chlorides, carbonates, bicarbonates, hydroxides, etc., with each cation. Encompassing all the possible reactions would have been be time- and resource-prohibitive. Furthermore, it has been observed that only a few sets of reactions are at the forefront in driving the low salinity ion exchange mechanism (Dang et al., 2014, Dang et al., 2015). The geochemical reactions are key to the low salinity waterflood process and can be subdivided into three broad categories: (1) intra-aqueous reactions; (2) mineral reactions and; (3) ion exchange reactions.

6.2.1 Intra-Aqueous Reactions

Since the WAG process used CO_2 as a solvent, an important aqueous reaction was one concerning CO_2 and water. Furthermore, the reservoir crude also had some CO_2 present.

$$CO_2\,(aq) + H_2O \rightleftharpoons H^+ + HCO_3^- \tag{6.1}$$

The intra-aqueous reactions proceed at their own pace. Some are fast, some are slow. The above reaction is very fast and reversible, and is governed by a chemical equilibrium constant defined as:

$$Keq_1 = \frac{\alpha_i(H^+)\alpha_i(HCO_3^-)}{\alpha_i(CO_2(aq))} = 10^{-6.4} \tag{6.2}$$

where $\alpha_i(.)$ is the activity of the species and is related to the activity coefficient (γ_i) through

$$\alpha_i = \gamma_i m_i \tag{6.3}$$

where m_i is the molality of the component i. The activity of CO_2 in Equation 6.2 is equal to its molality. Another reaction concerns the dissociation of water to provide H^+ ions:

$$H^+ + OH^- \rightleftharpoons H_2O \tag{6.4}$$

This reaction is also extremely fast, reversible, but weighs heavily towards the formation of water.

$$Keq_2 = \frac{1}{\alpha_i(H^+)\alpha_i(OH^-)} = 10^{14.03} \tag{6.5}$$

For the given reservoir brine composition and the planned low salinity water and low salinity CO_2-WAG flood, there were four types of possibilities for the formation of complexes, each with Na^+ and Ca^{2+}: chlorides, hydroxides, carbonates, and bicarbonates. The concentration of CO_2 in the grid blocks was anticipated to increase sharply during the WAG flood, therefore, the reactions with either carbonates or bicarbonates, or both were given due consideration. To get a clearer perspective on the reaction path modeling and associated concentration of the species, the formation water was equilibrated with 0.02 moles of an exchanger surface (clay) using a reaction batch modeling package, PHREEQC (Parkhurst and Appelo, 1999), linked to an exhaustive list of aqueous, mineral, and ion exchange reactions from the LLNL database (Wolery, 1992). The exchanger was added to see the equivalent fractions of Na^+ and Ca^{2+} attached to the clay surface. This would give some insight into the dominant bridging cation between the polar components of the oil and the clay sites for the given water chemistry.

It was observed that the concentration of $CaHCO_3^+$ was about 7 times that of $CaCO_3$ while the strength of $NaHCO_3$ was 257 times that of $NaCO_3^-$ during initialization (see Appendix). It was therefore decided to include the dissociation reactions for $CaHCO_3^+$ and $NaHCO_3$ (Equations 6.6

through 6.9) while excluding the ones for their carbonate counterparts in the geochemical model, a tradeoff in favor of simulation run time over model detail. Furthermore, HCO_3^- plays a key role in the dissolution of calcite, a very important reaction for LSWF. Therefore, it was deemed necessary to track the changes in its concentration as accurately as possible.

$$CaHCO_3^+ \rightleftharpoons Ca^{2+} + HCO_3^- \tag{6.6}$$

$$Keq_3 = \frac{\alpha_i(Ca^{2+})\alpha_i(HCO_3^-)}{\alpha_i(CaHCO_3^+)} = 10^{-1.2} \tag{6.7}$$

$$NaHCO_3 \rightleftharpoons Na^+ + HCO_3^- \tag{6.8}$$

$$Keq_4 = \frac{\alpha_i(Na^+)\alpha_i(HCO_3^-)}{\alpha_i(NaHCO_3)} = 10^{-1.4} \tag{6.9}$$

The equilibrium constant (Keq) for these reactions is a function of temperature and is calculated as a fourth order polynomial, i.e., $log_{10}(Keq) = a_0 + a_1T + a_2T^2 + a_3T^3 + a_4T^4$. The coefficients a_0 through a_4 are given in Table 6-2.

Table 6-2 Coefficients a_0 through a_4 to calculate Keq as a function of temperature

	a_0	a_1	a_2	a_3	a_4
log(Keq_1)	-6.5492E+00	9.0017E-03	-1.0212E-04	2.7619E-07	-3.5614E-10
log(Keq_2)	1.4928E+01	-4.1876E-02	1.9736E-04	-5.5495E-07	7.5811E-10
log(Keq_3)	-1.1873E+00	1.6494E-03	-1.1886E-04	8.5789E-07	-2.0430E-09
log(Keq_4)	-3.5165E-01	9.4890E-03	-3.5316E-05	2.1980E-07	-4.1635E-10

The activity coefficients (γ_i) for the ions were calculated using a modified version of the Debye-Hückle model (Truesdell and Jones, 1974):

$$\log(\gamma_i) = -\frac{Az_i^2\sqrt{I}}{1 + Ba_i\sqrt{I}} + b_iI \tag{6.10}$$

where A = 0.5085 and B = 0.3285E+10 m^{-1} are constants at 77°F [25°C] and vary only slightly between 41-95°F [5-35°C]. That is, they hold good for the Schrader Bluff reservoir temperature range. a_i and b_i are fit parameters specific to different ions (Table 6-3).

Table 6-3 Truesdell-Jones model parameters (Truesdell and Jones, 1974, Parkhurst, 1990)

Species	a_i (Å)	b_i
H^+	4.78	0.24
Ca^{2+}	4.86	0.15
Na^+	4.32	0.06
Cl^-	3.71	0.01
OH^-	10.65	0.21
HCO_3^-	5.4	0

I in Equation 6.10 is the ionic strength that describes the number of electrical charges in the solution (Appelo and Postma, 2005). Numerically,

$$I = {}^1/_2 \sum m_i z_i^2 \tag{6.11}$$

When the formation water was initialized in PHREEQC, the concentration of *NaCl* was found to be significant (see Appendix). However, the reaction of dissociation of *NaCl* into Na^+ and Cl^- had no impact on the LSWF performance and was eventually omitted from the geochemical model.

6.2.2 Mineral Reactions

Rock mineralogy identification is an important aspect of geochemical studies. The West Sak/Schrader Bluff sands are quartz dominant with some feldspars, mica, and traces of glauconite (Werner, 1987). The clay is composed of kaolinite, illite, chlorite, and smectite. The goal here is to model the geochemical process as accurately as possible. Therefore, tracking the dissolution and precipitation for each independent mineral and its impact on the reservoir architecture may be of some interest. Consider the following dissolution reactions for anorthite, K-feldspar, kaolinite, and illite:

$$Anorthite + 8H^+ \rightleftharpoons 4H_2O + Ca^{2+} + 2Al^{3+} + 2SiO_2(aq) \quad (6.12)$$

$$K - feldspar + 4H^+ \rightleftharpoons 2H_2O + K^+ + Al^{3+} + 3SiO_2(aq) \quad (6.13)$$

$$Kaolinite + 6H^+ \rightleftharpoons 5H_2O + 2Al^{3+} + 2SiO_2(aq) \quad (6.14)$$

$$Illite + 8H^+ \rightleftharpoons 5H_2O + 0.6K^+ + 0.25Mg^{2+} + 2.3Al^{3+} + 3.5SiO_2(aq) \quad (6.15)$$

To date, there has been evidence of mostly Ca^{2+} and, to a lesser extent, H^+, as bridging elements between the crude oil polar components and the clay surface (Austad et al., 2010). Na^+, even though is less competitive than Ca^{2+} or H^+, may in some cases be the dominant bridging cation due to its sheer abundance in the formation brine and a high Na^+/Ca^{2+} ratio. Since wettability alteration is being modeled through ion exchange only, from an optimal modeling approach, the aqueous species released from these reactions should have a part to play in the cation exchange process. That is, they should either be part of the group of cations replacing the bridging components or the bridged cations themselves. Each new mineral reaction should either contribute to the ion exchange process directly, or at least support it in a non-trivial way to justify the burden of additional transport equations for the mineral species and any new aqueous components that may be generated from them.

Ca^{2+}, Al^{3+}, K^+, and Mg^{2+} collectively form the set of cations for Equations 6.12 through 6.15. While Mg^{2+} and K^+ may be present in the Schrader Bluff formation water, the presence of Al^{3+} is uncertain, as it was not detected in formations from nearby areas (McGuire et al., 2005a). Even though Al^{3+} is higher up in the lyotropic series, the lack of knowledge of its concentration in the formation water did not justify the addition of Equations 6.2 through 6.15 with regards to computation efficiency. The lytropic series for cation exchange is as follows:

$$Li^+ < Na^+ < K^+ \leq NH_4^+ < Mg^{2+} < Ca^{2+} < Al^{3+} < H^+$$

Furthermore, K^+ is a weak cation and in the presence of a large Na^+ concentration, it would neither act as the adsorbing bridge, nor play a significant role in replacing the adsorbed cations due to the presence of stronger cations like Ca^{2+} and Mg^{2+}. For these reasons, the above-listed mineral reactions (Equations 6.12 through 6.15) were not added to the simulator.

The only mineral reaction that was added to the geochemical model was the dissolution of calcite. This and the dissolution of Magnesite have been recognized as the most significant reactions affecting the LSWF performance (Dang et al., 2015, GEM, 2015). About 2% calcite by volume was added to the model to represent the calcite cementation observed in the Schrader Bluff formation.

$$Calcite + H^+ \rightleftharpoons Ca^{2+} + HCO_3^- \tag{6.16}$$

This reaction is initiated by the localized decrease in pH around the mineral surface due to the formation of a weak carbonic acid when CO_2 at high pressure comes in contact with the reservoir brine (Equation 6.1). The above reaction is slower than the intra-aqueous reactions and is governed by a reaction rate, r_m, (Bethke, 1996):

$$r_m = \hat{A}_m k_m \left(1 - \frac{Q_m}{K_{eq,m}}\right) \tag{6.17}$$

where:

$\hat{A}_m$	Reactive surface area for mineral *m*, m^2/m^3
k_m	Rate constant for mineral reaction *m*, $mol/(m^2\text{-}s)$
Q_m	Activity product for mineral reaction *m*
$K_{eq,m}$	Chemical equilibrium constant for mineral reaction *m*.

The rate constant (k_m) is a temperature dependent parameter that varies with temperature as:

$$k_m = k_{0,m}\left[-\frac{E_{a,m}}{R}\left(\frac{1}{T} - \frac{1}{T_0}\right)\right] \tag{6.18}$$

where:

$E_{a,m}$	Activation energy for reaction *m*, J/mol
R	Universal gas constant
T	Temperature of interest, °C
T_0	Reference temperature, °C

$k_{0,m}$ Rate constant for reaction m at temperature T_0.

The LSWF was carried out under isothermal conditions and hence, the rate constant was kept constant for each reaction. The geochemical reaction parameters for Equation 6.16 are given in Table 6-4.

Table 6-4 Geochemical rate parameters for the calcite dissolution mineral reaction

$\hat{A}_m$ (m^2/m^3)	k_m (mol/m^2-s)	K_{eq}	E_a (J/mol)
200	$10^{-8.79}$	$10^{1.7}$	41,870

During a low waterflooding, rock minerals can either dissolve or even precipitate depending on the concentration of respective ions in the brine. Usually, a LSWF proceeds through calcite dissolution and releasing Ca^{2+}. However, an excess of HCO_3^- in any point in the reservoir can also cause calcite precipitation. Therefore, it is desired to have very low bicarbonate alkalinity in the low salinity water. In either case, the porosity is affected as follows:

$$\hat{\phi}^* = \phi^* - \sum_{m=1}^{n_m} \left(\frac{N_m}{\rho_m} - \frac{N_m^0}{\rho_m} \right) \tag{6.19}$$

$$\phi = \hat{\phi}^* [1 + c_r (p - p^*)] \tag{6.20}$$

where φ is the porosity after mineral dissolution/precipitation at pressure p, φ^* is the reference porosity before the mineral dissolution/precipitation, $\hat{\varphi}^*$ is the reference porosity incorporating the mineral dissolution/precipitation effect, N_m and N_m^0 are the moles of mineral m per bulk volume of rock at current time and at time 0, respectively, and c_r and p^* are the rock compressibility and reference pressure, respectively.

In Equation 6.17, the ratio $Q_m/K_{eq,m}$ is called the saturation index of the mineral. The equilibrium constant for the dissolution of calcite is 1.726 at 75°F. If $Q_m/K_{eq,m} > 1$, i.e., $Q_m > 1.726$, dissolution occurs and porosity increases. If $Q_m < 1.726$, precipitation occurs and porosity decreases. Since Q_m is the activity product of the mineral reaction, for dissolution to occur, the activity product of Ca^{2+} and HCO_3^- should be greater than 1.726 times the activity of H^+.

The absolute permeability in the reservoir is also affected by the change in porosity due to mineral dissolution/precipitation and was modeled using the Carman-Kozeny equation (GEM, 2015):

$$\frac{k}{k^0} = \left(\frac{\phi}{\phi^0}\right)^3 \left(\frac{1-\phi^0}{1-\phi}\right)^2 \tag{6.21}$$

where k^0 is the absolute permeability at φ^0.

6.2.3 Ion Exchange Reactions

As previously mentioned, there is equilibrium between the ions in the reservoir brine and those that sorb on the clay surface. Injection of low salinity water disrupts this equilibrium and causes a net desorption of the adsorbed ions and their subsequent replacement by multivalent ions. The abundance and the relative strength of adsorption of ions determine the dominant ion holding the resins and asphaltenes to the clay site. For our rock and fluid system, the dominant bridging ion was Na^+. This was observed from the initialization of the simulation model which was in close agreement with the geochemical model equilibrated in PHREEQC (Appendix) (Table 6-5).

Table 6-5 Equivalent fractions of Na^+ and Ca^{2+} attached to the clay surface

Equivalent Fraction	GEM	PHREEQC
Na-X	0.913	0.869
Ca-X	0.087	0.131

Al^{3+} can also be adsorbed in significant quantities, as it is higher up in the lyotropic series, but its presence in the Schrader Bluff formation water is speculative in the absence of data. Mg^{2+} and H^+ are other ionic species that may form a fraction of ions attached to the clays sites. However, they were not modeled due to their very low concentration as compared to Ca^{2+}, the second-most dominant aqueous species after Na^+. The ion exchange reaction between Ca^{2+} and Na^+ was therefore modeled:

$$Na^+ + \frac{1}{2}CaX_2 \rightleftharpoons NaX + \frac{1}{2}Ca^{2+} \tag{6.22}$$

where X denotes the exchanger (clay sites). In a LSWF, the reaction takes place in the reverse direction. Ca^{2+} that is obtained from the dissolution of calcite replaces Na^{+} sorbed on the clay. In the process of Na^{+} desorption, the organic polar components and organometallic complexes in the crude oil are released from the clay sites, causing a shift in the wettability towards a more water-wet state. Like the chemical equilibrium constant in an aqueous reaction, the ion exchange reactions are governed by a selectivity coefficient defined as:

$$K'_{Na/Ca} = \frac{\zeta(NaX)[m(Ca^{2+})]^{0.5}}{[\zeta CaX_2]^{0.5}[m(Na^{+})]} \times \frac{[\gamma(Ca^{2+})]^{0.5}}{\gamma(Na^{+})} = 0.4 \qquad (6.23)$$

where $\zeta(NaX)$ and $\zeta(CaX_2)$ are the equivalent fractions of Na^{+} and Ca^{2+} sorbed on to the clay surface. The activity coefficient $\gamma(.)$ was calculated from Equation 6.10. The name selectivity coefficient comes from the fact that the natural exchangers show different *selectivity* for different cations. The selectivity coefficients, like equilibrium constants, are dependent on temperature, but for the process modeled, were kept constant as the LSWF process was carried out isothermally. It should be noted that selectivity coefficients are operational variables and not thermodynamic variables like equilibrium constants, i.e., their value is determined empirically (Appelo and Postma, 2005).

6.3 Clay Modeling

The modeling of clay distribution is perhaps most crucial to model a low salinity waterflood. The type of clay most suitable for LSWF is kaolinite as it has a low cation exchange capacity (CEC) (Law et al., 2015) (Table 6-6). CEC is the moles of cation an exchanger can adsorb on its surface. Thus, higher CEC corresponds to larger amounts of cations being retained on the clay surface during a LSWF, thereby causing lower performance.

Table 6-6 CEC values for some common clay types (Law et al., 2015)

Clay Type	CEC (meq/100g)
Kaolinite	3-15
Illite	10-40
Montmorillonite	80-150
Chlorite	10-40

In the simulator, this was fed in terms of eq/m^3 where, eq/m^3 = (mol/m^3) x (charge of ion). Numerically,

$$N_{NaX} + 2N_{CaX_2} = \phi CEC \tag{6.24}$$

where N_{NaX} and N_{CaX2} are the moles of Na^+ and Ca^{2+} adsorbed on to the clay surface. Therefore, the equivalent fractions in Equation 6.23 are:

$$\zeta(NaX) = \frac{N_{NaX}}{N_{NaX} + 2N_{CaX_2}} \tag{6.25}$$

$$\zeta(CaX_2) = \frac{2N_{CaX_2}}{N_{NaX} + 2N_{CaX_2}} \tag{6.26}$$

The clay type and distribution, like other LSWF parameters, are found through rock matrix analysis. Such data for Schrader Bluff was unfortunately not available. Therefore, the clay distribution was modeled from the porosity distribution in the reservoir model. Since the amount of clay varies from 5-30% (Werner, 1987), going by the gamma ray log concept, the cleanest sands having highest porosity were given the lowest limit, while the dirtiest sands having lowest porosity were given the highest limit for clay content. All intermediate values of CEC were calculated through interpolation between these two extremes following a direct inverse relationship with porosity. This also qualitatively follows from the fact that dispersed clays replace sand grains and reduce the clean sandstone porosity (φ_{max}) to an effective reservoir porosity (φ) (Dang et al., 2015):

$$\phi = \phi_{max} - V_{cl}$$

where V_{cl} is volume of dispersed clay. Once the clay distribution was obtained, the CEC (eq/m^3) distribution was calculated from Dang et al.'s (2015) model:

$$CEC = \left[\frac{\rho_r(1-\phi)}{1000\phi}\right] \times [628.58 \times (clay\ fraction) + 48.863] \tag{6.27}$$

where ρ_r is the rock matrix density (2,650 kg/m^3). Figure 6-3 shows a 3D rendering of porosity distribution and the resulting CEC distribution computed from it. The inverse relationship of CEC with porosity is clearly visible, with higher porosity grids having lower CEC and vice-versa. The CEC model is a linear regression fit to the values of 15 rock samples that had clay content from 18-50%. This may define the lower and upper limit of clay content on the applicability of this equation. However, since the primary objective was to establish a framework to model the low salinity waterflood for Schrader Bluff and get a preliminary perspective on its response to viscous oil, Equation 6.27 was used for CEC calculation, even for clay content less than 0.18. In the absence of clay distribution data, there is uncertainty inherent in the performance results obtained through LSWF modeling.

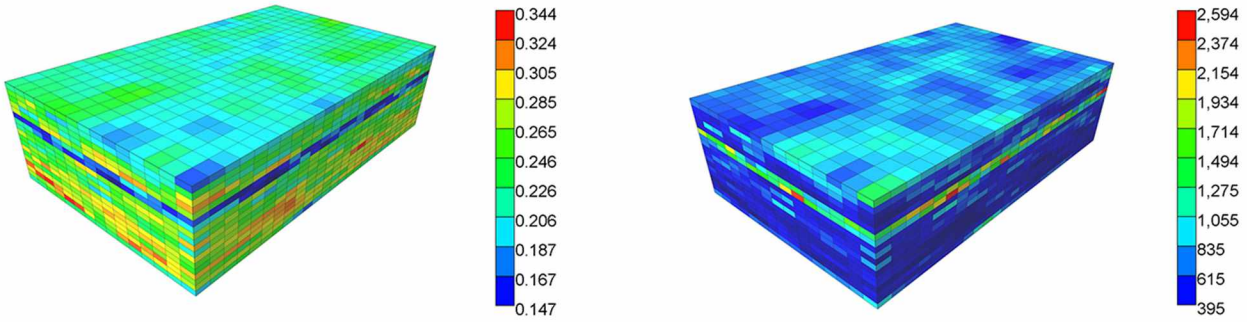

Figure 6-3 3D rendering of porosity distribution (left) and CEC (eq/m^3) distribution (right).

6.4 Wettability Alteration

The shift in wettability was modeled using two sets of relative permeability curves: high salinity and low salinity curves. The high salinity curves were the taken from the history matched model. Usually a series of low salinity waterflood lab tests are done to see the shift in oil-water relative permeability parameters like oil relative permeability endpoint (K_{rocw}), water relative permeability endpoint (K_{rwiro}) and most importantly, the change in residual oil saturation to water (S_{orw}). In the absence of test data, typical values for these parameters representing a shift in the wettability were used (Table 6-7). Additionally, the curvatures for the oil-water curves (N_w and N_{ow}) were also modified to qualitatively represent the ease of oil flow and the resistance to water flow in the pore throats.

Table 6-7 High salinity and low salinity waterflood oil-water relative permeability parameters

Regime	NaX	K_{row}	K_{rw}	S_{orw}	N_w	N_{ow}
HS	0.9	0.64	0.24	0.38	2.4	2.68
LS	0.2	0.74	0.16	0.27	3	2.08

The relative permeability interpolant was the fraction of Na^+ attached to the clay surface ($\zeta(NaX)$). Initially at 0.91 $\zeta(NaX)$, the history matched curve set was used to compute the oil-water relative permeability in the grid blocks, while all $\zeta(NaX)$ values below 0.2 enforced the low salinity curve set.

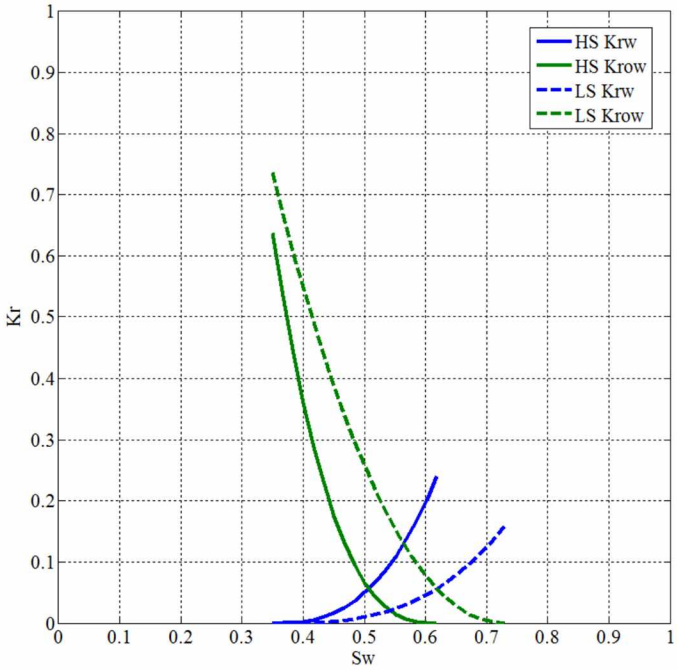

Figure 6-4 High and low salinity oil-water relative permeability

6.5 Numerical Dispersion Control

To get a good resolution of the grid properties at the shock front, low salinity waterflooding modeling often requires grid blocks of very small sizes when using the usual upstream weighted flux calculation regime. At larger block sizes, the upstream scheme smears out block properties due to excessive numerical dispersion of flood fronts. Hence, higher order schemes are required to get a good resolution for modeling reservoirs with practical block sizes (Sammon et al., 2001).

In this consideration, a two point flux scheme was applied that blended usual upstream weighted fluxes with higher order, averaged, two-point weighting scheme under the control of a Total Variation Limiting (TVD) flux limiter (GEM, 2015). This scheme used higher order flux calculation in smooth regions away from the shock fronts where various component, phase saturation, and phase velocities were smoothly varying while reverting to the more stable upstream mobility weighing scheme near frontal regions where compositional variables and saturations were changing most rapidly.

The TVD limiter ensured that overall numerical scheme maintained stability and eliminated over- and undershoots in calculations. The main idea behind using flux limiters was to limit the spatial derivatives to realistic values, thereby guaranteeing that computing properties remain within their physical limits. The limiters were applied to the intercell flows in each component's conservation equation to control throughput and ensure overall stability of the numerical scheme.

CHAPTER 7 LOW SALINITY EOR PERFORMANCE EVALUATION

One of the core objective of this study was to answer the question of achieving 35%+ recovery from the Schrader Bluff viscous oilfield. After validating the reservoir model to a benchmarked waterflood and CO_2-WAG performance by Ning et al. (2011), performance forecasts were done and compared for different recovery processes following 36 years of high salinity waterflood starting in 1981. The recovery processes compared were:

1. Continued high salinity waterflooding
2. Low salinity waterflooding (LSWF)
3. CO_2-WAG
4. Low salinity CO_2-WAG (LSWAG).

For high salinity waterflood, the injection water composition was the same as that of the formation water. The low salinity injection water data was obtained from the water analysis of Well F-77 on the F-pad in Milne Point, Alaska North Slope. This data corresponds to the formation water tested from the Prince Creek aquifer, which has water of very low salinity (2,000-3,000 ppm) (McGuire et al., 2005a). Starting in 2017, the above-mentioned processes were simulated to see the effect on oil rates and recoveries. Other parameters such as water cut, gas-oil ratio, and producer fluid pH were also analyzed. Corrosion due to increasing amounts of CO_2 in the producer well stream was also anticipated for the CO_2-WAG processes for current production facilities on the Alaska North Slope (ANS).

7.1 Injection Schedule

The water injection rates were altered to compensate for reservoir withdrawal to keep the reservoir pressure near its initial limit during all floods by achieving a voidage rate ratio of one (Figures 7-1 and 7-2). For the WAG processes, the ultimate slug size of CO_2 was set as 30% HCPV in 2017 and was spread equally over 10 WAG cycles (3% CO_2 per half-cycle). The WAG ratio was kept 1:1. The bottomhole gas rates were also varied to maintain reservoir pressure. The gas and water rates' alteration in response to the drawdown from the producer spread the WAG cycles across 11 years and 10 months (Figure 7-1).

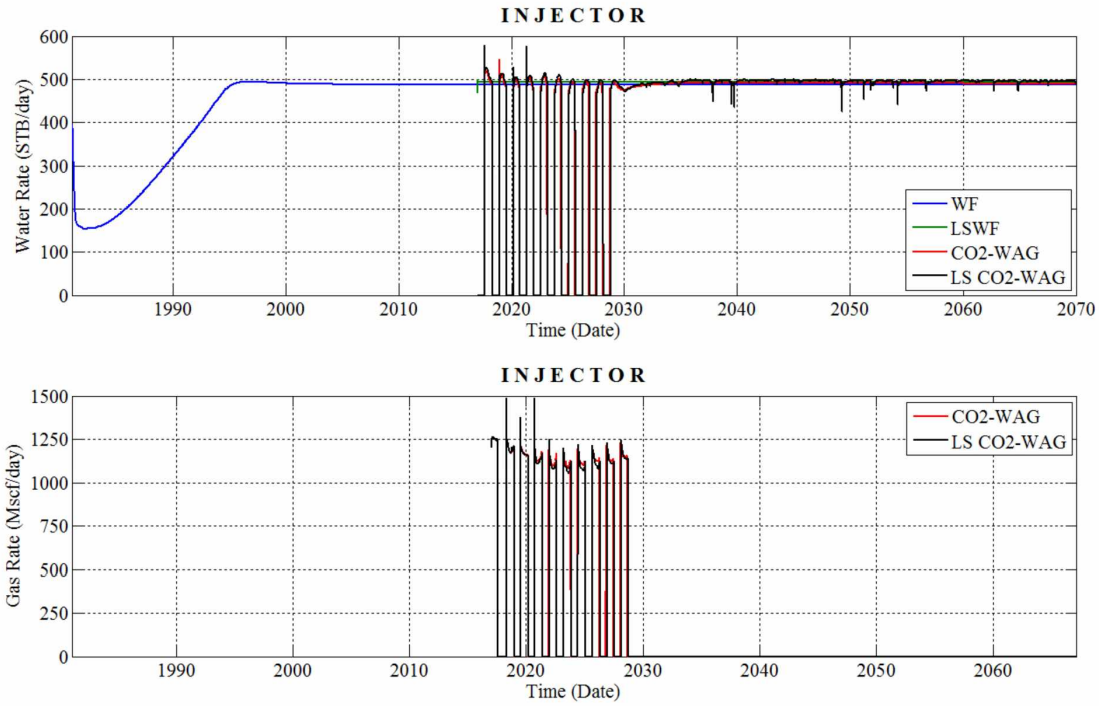

Figure 7-1 Water (above) and gas (below) injection rates during performance forecasts

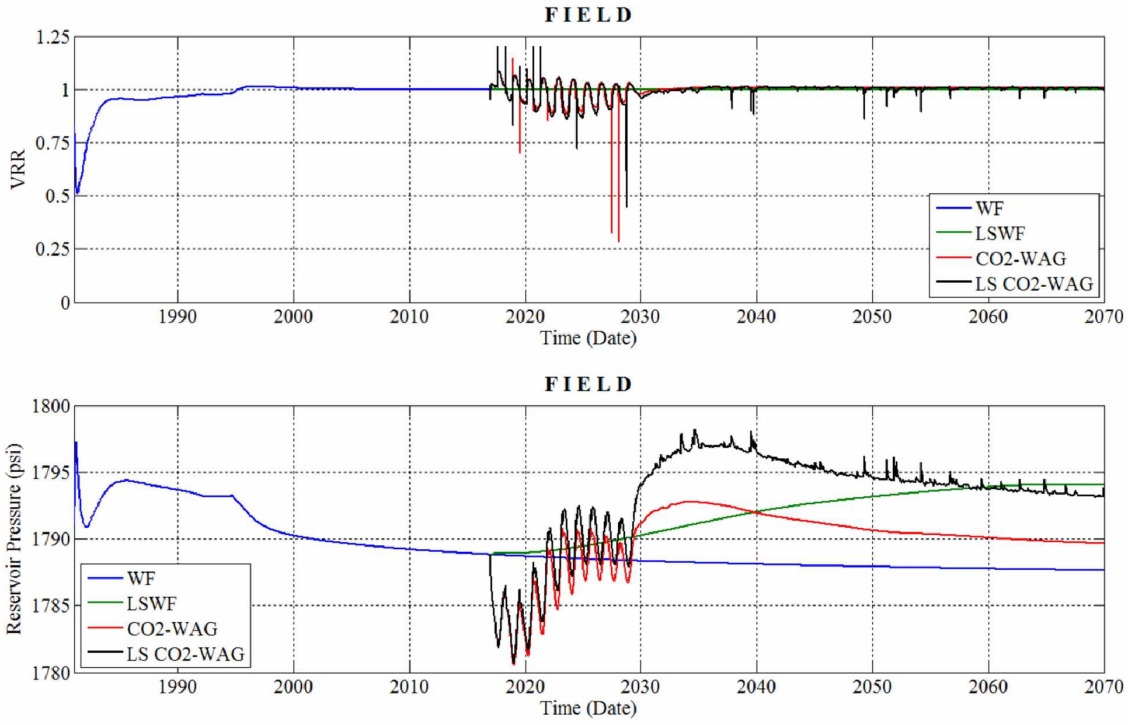

Figure 7-2 Voidage rate ratio (above) and reservoir pressure (below) for the four models

7.2 Production Constraints

The production constraints were set the same as those described in Chapter 5 for validation. This is because producer bottomhole conditions affect the well performance. The well fluid rates are sensitive to bottomhole pressure (BHP). Thus, it was desired to predict the reservoir deliverability based on the downhole conditions that were used to calibrate the reservoir model to get an unbiased perspective on flow performance. For the sake of convenience, these are stated once again:

i. Producer BHP: 800 psi [5,515.8 kPa]
ii. Maximum fluid rate 500 RB/day [79.5 rm^3/day], corresponding to a 4% HCPV annual reservoir voidage.

These are also the operating conditions observed for a typical well in the OA sand.

7.3 EOR Performance Comparison

Figure 7-3 shows the comparison between producer oil rates and field recoveries for continued high salinity waterflooding, low salinity waterflooding (LSWF), CO2-WAG and low salinity CO_2-WAG. The forecast was predicted for 53 years starting from 2017. The ion exchange capability in the simulator was turned off for high salinity waterflood and CO_2-WAG models to prevent ion exchange reactions.

7.3.1 Waterflood Models

Waterflood recovery at the end of the prediction period was 24.65% OOIP, which is only 4.6% OOIP incremental over the value in 2017. Low salinity waterflood recovery was ~27.9% OOIP, a 3.25% OOIP additional over waterflood. This recovery from LSWF is very low compared to the tests done at coreflood and SWCTT levels (McGuire et al., 2005a, Patil et al., 2008b, Sánchez-Rodríguez et al., 2015). Although extreme reservoir stratification could be a possible justification for this, the main reason for the low performance could be the high oil viscosity:

1. Waterflood recovery in general decreases with increasing oil viscosity (Beliveau, 2009) (Figure 7-4). Furthermore, LSWF is a slow response mechanism and the response is slower for viscous and heavy oils.
2. Recovery from low salinity waterflooding takes effect from myriad mechanisms. However, as discussed in Chapter 6, only cation exchange was modeled. The geochemical reactions,

especially the mineral dissolution and precipitation reactions, are slow, and it may take a long time at the field/pilot scale for sufficient contact of low salinity water with the reservoir to dissolve enough calcite and cause sufficient ion exchange reactions.

3. Clay data was also not available and hence, the cation exchange capacity (CEC) was modeled based on a simple linear regression model. It could be possible that the values obtained from the model could be too high. It is desirable to have low CEC clays (like kaolinite) and their distribution plays a vital role in modeling LSWF.

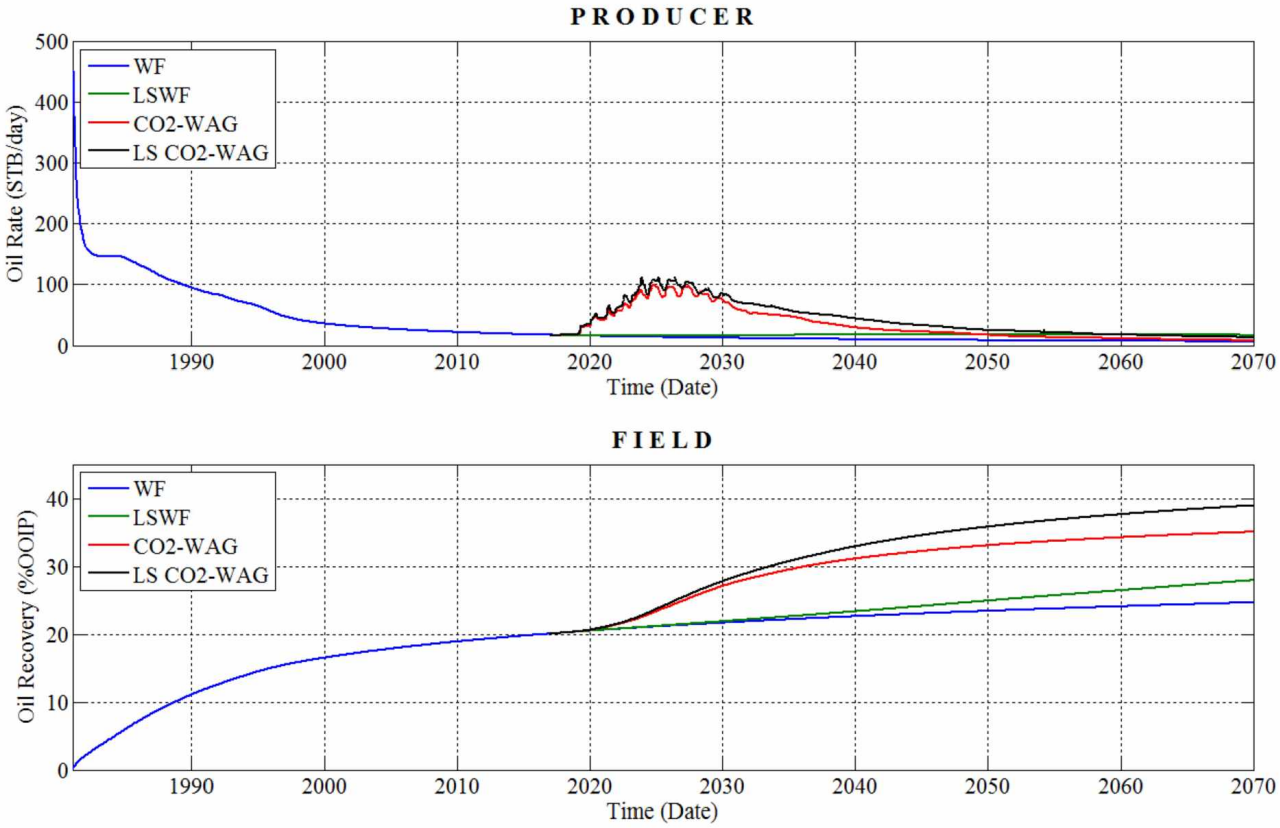

Figure 7-3 Oil rates (above) and field recoveries (below) for the different EOR models

Although the incremental recovery over waterflood from LSWF is not large, it should be noted that the ultimate oil recovery (UOR) would be in tune with the relative permeability of the low salinity EOR model (Table 6-7). The decrease in residual oil saturation (S_{orw}) to waterflood was kept at 11%. While this is consistent with the observations from both light and heavy oil corefloods (Patil et al., 2008b, Sánchez-Rodríguez et al., 2015), the response of LSWF at the core scale can be best assessed

only through experiments. In any case, incremental recovery is expected to correspond to the difference between residual oil saturation for high and low salinity waterfloods. Figure 7-5 gives a clearer perspective on this claim. In 2070, LSWF oil rates are highest (and oil recovery is sharply increasing) as compared to the other three models, even though oil recovery is lower than that for WAG and LSWAG (Figure 7-3). This indicates that LSWF can sustain commercial oil rates even after 2070 until the field recovery close to the UOR is obtained. However, from a business standpoint, such a time may never be reached, as the late response of LSWF would reflect bad project economics in the first place, making it an unattractive as an EOR choice for viscous oil on the ANS.

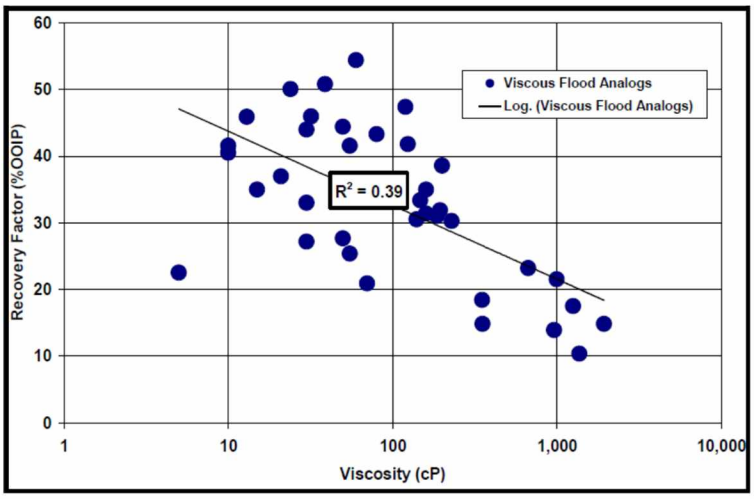

Figure 7-4 Waterflood recovery versus oil viscosity (Beliveau, 2009)

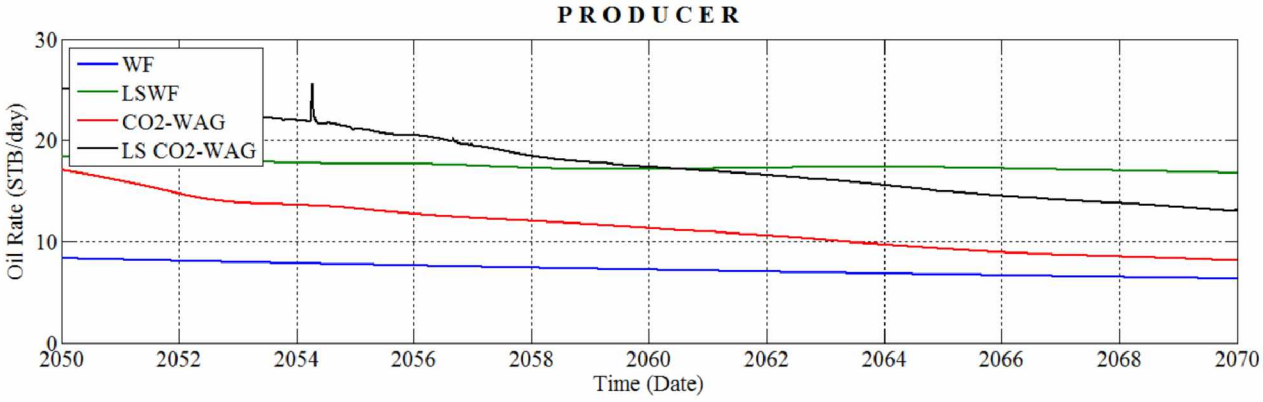

Figure 7-5 Oil rates for the period 2050-2070. The spike in LSWAG profile is due a variation in grid properties caused by minor numerical issues and looks significant because of image magnification

7.3.2 WAG Models

The conventional CO_2-WAG recovers about 35% OOIP by 2070 (Figure 7-3) which is about 10.3% OOIP incremental over waterflood and about 7% OOIP incremental over LSWF. The main recovery mechanism attributed to the additional recovery is the oil viscosity reduction from 76 cp to about 15 cp, which was also observed by Ning et al. (2011). Figure 7-6 shows the oil viscosity profiles after 10%, 50%, and 100% of the total CO_2 slug injection into the reservoir. Clearly, after all the CO_2 had been injected, oil viscosity in 50% of the reservoir dropped to ~15 cp from its initial value. This is the reason for the sharp increase in oil production rate that was associated with the CO_2 breakthrough in the producer. This is consistent with McKean et al.'s (1999) observed doubling of production rates around the well at the time of breakthrough of the miscible injectant (MI).

Alternating CO_2 with low salinity water (LSWAG) recovered most oil: ~39% OOIP. This is a 15% OOIP incremental over waterflood and 4% OOIP incremental over high salinity CO_2-WAG. This model synthesized the benefits of both CO_2-WAG and LSWF. Apart from oil viscosity reduction, additional low salinity benefits were also reaped once the WAG cycles finished. As observed from Figure 7-5 the late time oil rate is higher than conventional WAG. Table 7-1 shows the incremental recoveries over waterflood for the three EOR models.

Table 7-1 Incremental oil recovery and CO_2 utilization efficiency

	1981-2017	2017-2070			
	WF	WF	LSWF	WAG	LSWAG
Total Water Injection (MRB)	5512.7	9674.3	9668.3	8596.3	8561.3
Cum. Water Injected (HCPV)	1.21	2.12	2.12	1.88	1.87
Solvent Injected (MMscf)	-	-	-	2664.2	2670.6
Cum. Oil Produced (MSTB)	845.34	1039.5	1177.7	1478.1	1642.2
Recovery Factor (%OOIP)	20.04	24.65	27.92	35.05	38.95
Add. Oil Prod. Since 2017 (MSTB)	-	194.16	332.36	632.76	796.86
Add. Rec. Since 2017 (%OOIP)	-	4.61	7.88	15.01	18.91
Incremental WF Rec. (%OOIP)	-	-	3.27	10.4	14.3
Improvement Over WF (%)	-	-	13.27	42.2	58.0
Solvent Utilization (Mscf/STB)	-	-	-	6.07	4.43

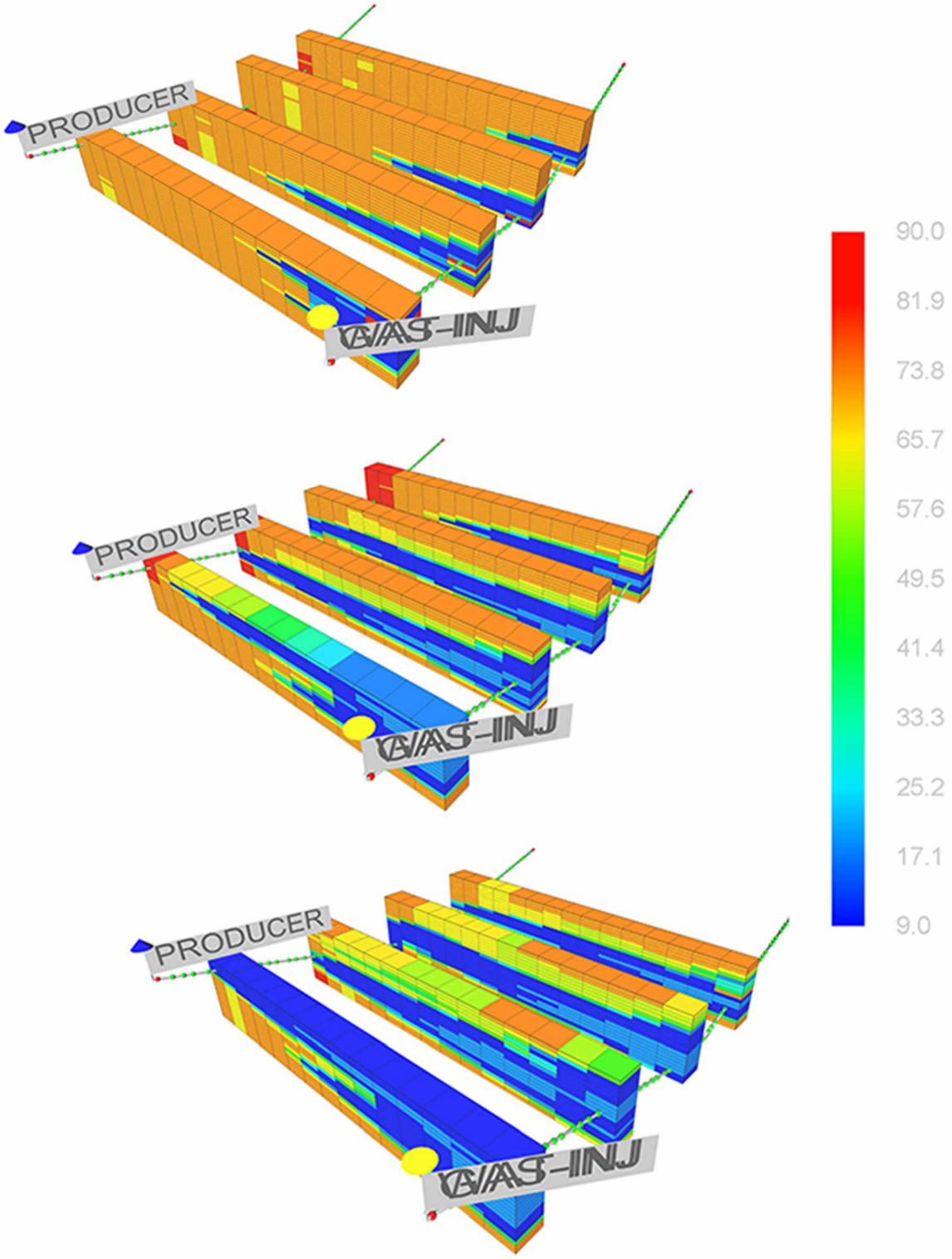

Figure 7-6 Oil viscosity (cp) at 10% (top), 50% (middle), and 100% (bottom) of CO_2 injection

Another performance evaluation parameter for the WAG process is the solvent utilization which is defined as the solvent used to recover an additional stock tank barrel of oil over waterflood (in Mscf/STB). For the WAG and LSWAG models, these came out to be 6.07 and 4.43 Mscf/STB [1.08 and 0.79 Msm^3/sm^3], respectively. These are typical values observed for miscible injection for light oils on the North Slope (Ning et al., 2011). As a matter of fact, these values are a lot lower than those observed for some of the CO_2 EOR projects in the U.S (Lopez, 2012) (Table 7-2).

Table 7-2 CO_2 utilization for few field scale and pilot CO_2 EOR projects in the U.S.

Project	State	Year	Perm. (mD)	Oil API	Viscosity (cp)	CO_2 Utilization (Mscf/STB)
Field Scale Projects						
East Vacuum	NM	1985	11	38	1.0	11.1
Ford Geraldine	TX	1981	64	40	1.4	9.0
Means	TX	1983	20	29	6.0	15.2
North Cross	TX	1972	5	44	0.4	18
Northeast Purdy	OK	1982	44	35	1.5	6.5
Rangely	CO	1986	5-50	32	1.6	9.2
SACROC (17 pattern)	TX	1972	3	41	0.4	9.7
SACROC (14 pattern)	TX	1981	3	41	0.4	9.5
Twofreds	TX	1974	33.4	36	1.4	15.6
Wertz	WY	1986	16	35	1.3	13.0
Pilot Projects						
Little Creek	MS	1975	75	39	0.4	27.0
Maljamar	NM	1983	11.2	36	0.8	8.1
North Coles Levee	CA	1981	9	36	0.5	7.4
Slaughter Estate	TX	1976	8	32	2.0	16.7
Weeks Island	LA	1978	1200	33	0.3	7.9
West Sussex	WY	1982	28.5	39	1.4	8.9

7.4 Gas-Oil Ratio Behavior

The producing gas-oil ratio (GOR) is another important parameter factored in the WAG design. Usually a WAG ratio of 1:1 may lead to high producing GOR during later life of the WAG, often requiring a tapered WAG design for the last few cycles. However, this may not be an issue for the Schrader Bluff oil as it has very little dissolved gas and therefore, poses few high producing GOR related issues. The producing GOR for the type pattern model (TPM) showed a cyclical trend during CO_2 injection cycles and peaked at 9,800 scf/STB [1,745.45 sm^3/sm^3] for WAG and around 9,200 scf/STB [1,638.5 sm^3/sm^3] for LSWAG (Figure 2-1). It should be noted that the increase in producing GOR during the later life of the flood is attributed to hydrocarbon gases, not CO_2 (Figure 7-8).

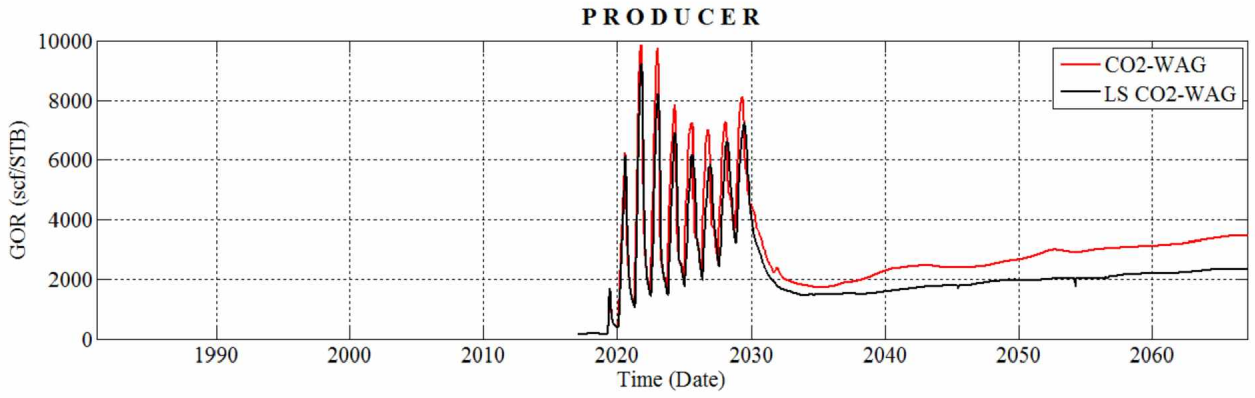

Figure 7-7 Predicted GOR for the WAG and LSWAG type pattern models

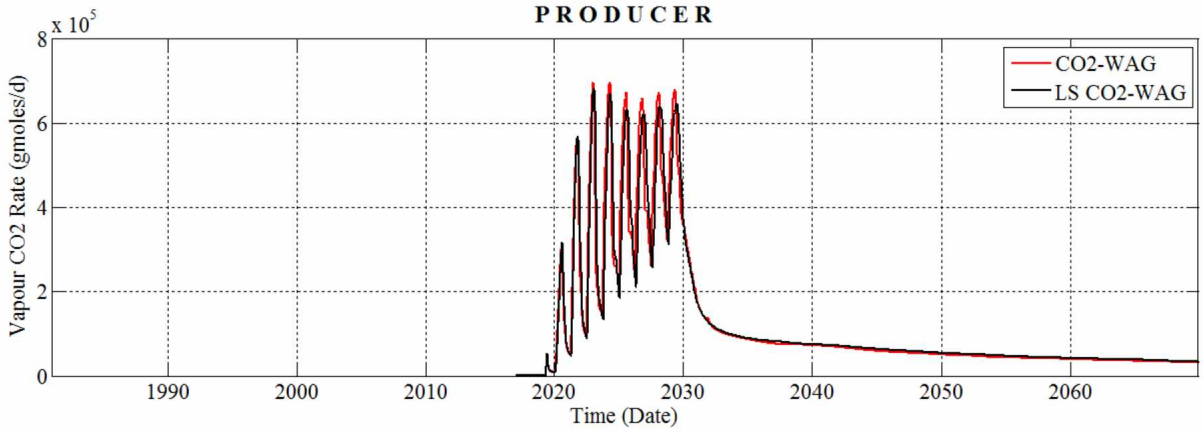

Figure 7-8 Produced CO_2 rate in the gas phase

7.5 Water-Cut Behavior

Water-cut issues must be addressed to ensure the longevity of the reservoir. While the water-cut for waterflood models increased continually, WAG models showed a decrease in water cut during the WAG cycles. This was because gaseous CO_2, along with increased oil flow, made the bulk of the 500 RB/day [79.5 rm^3/day] bottomhole fluid limit set to achieve a 4% annual reservoir depletion rate. After the WAG cycles, the water cut increased steadily.

The utility of low salinity EOR during the later life of the project also came to the fore when observing the water-cut behavior of the well. It was seen that an economic water cut limit of 98% was never reached for LSWF and LSWAG, whereas, the high salinity waterflood and WAG models attained this limit in January, 2041 and May, 2064, respectively. The oil recoveries at these times were 22.7% and 34.6% OOIP for the WF and WAG models, respectively.

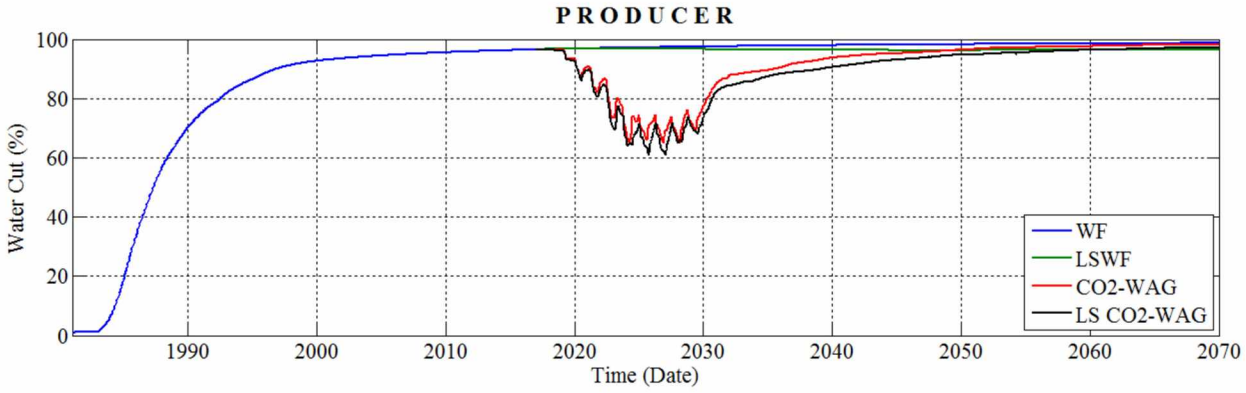

Figure 7-9 Predicted water-cut for the type pattern model

7.6 Field-Wide Aqueous Species Activity

Since all the geochemical reactions were happening simultaneously, the increase/decrease of an aqueous component in the reservoir was dependent on its reaction equilibrium with another aqueous component and also on the equilibrium of other species in the solution. Figure 7-10 shows the plots for field concentrations of Na^+, Ca^{2+}, HCO_3^-, $NaHCO_3$, $CaHCO_3^+$, and aqueous CO_2.

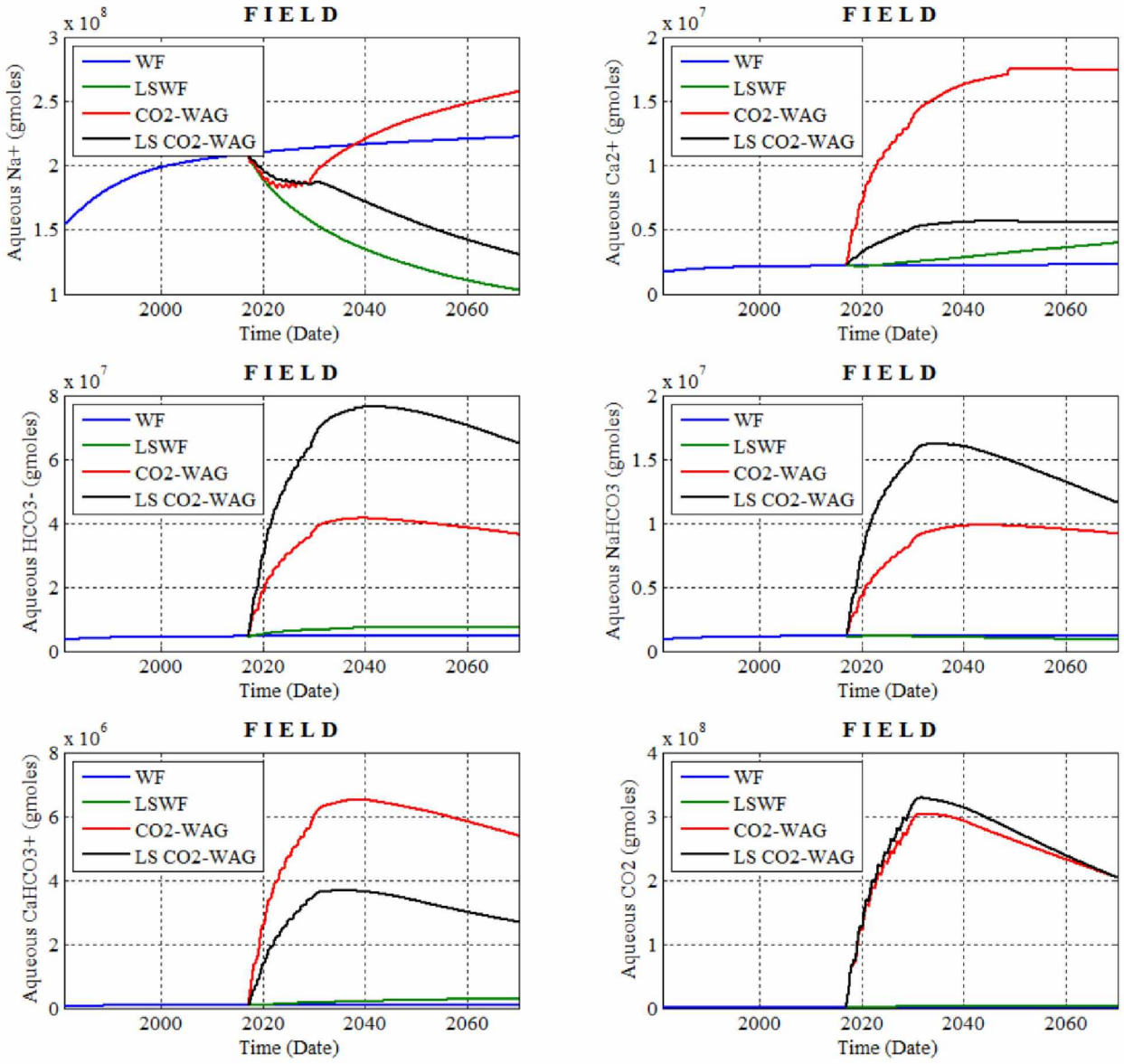

Figure 7-10 Field concentrations of aqueous species during simulation

For high salinity waterflooding, the injection water composition was the same as that of formation water. Hence, one may expect the concentration of the aqueous species to not change with time. The Na^+ concentration appeared to increase from 1981-2017 for the high salinity waterflood, which is in contradiction to this (Figure 7-10). However, on closer examination, it was found that the molalities of Na^+ in 1981 and 2017 were almost identical (Figure 7-11). A slight variation (increase) in the amounts of $NaHCO_3$ and $CaHCO_3^+$ in the injection water compared to the formation water could

provide an explanation for this. Both $NaHCO_3$ and $CaHCO_3^+$ were secondary aqueous species and during formation water initialization were calculated based on the molalities of the primary species (H^+, Na^+, Ca^+, and Cl^-) entered in the simulator. Therefore, their molalities might have been slightly different from their counterparts' in the injection water, triggering the formation of Na^+ and HCO_3^- as per Equations 6.6 and 6.8, respectively. A similar reasoning follows for the slight increase in Ca^{2+} and HCO_3^- concentrations for high salinity waterflooding.

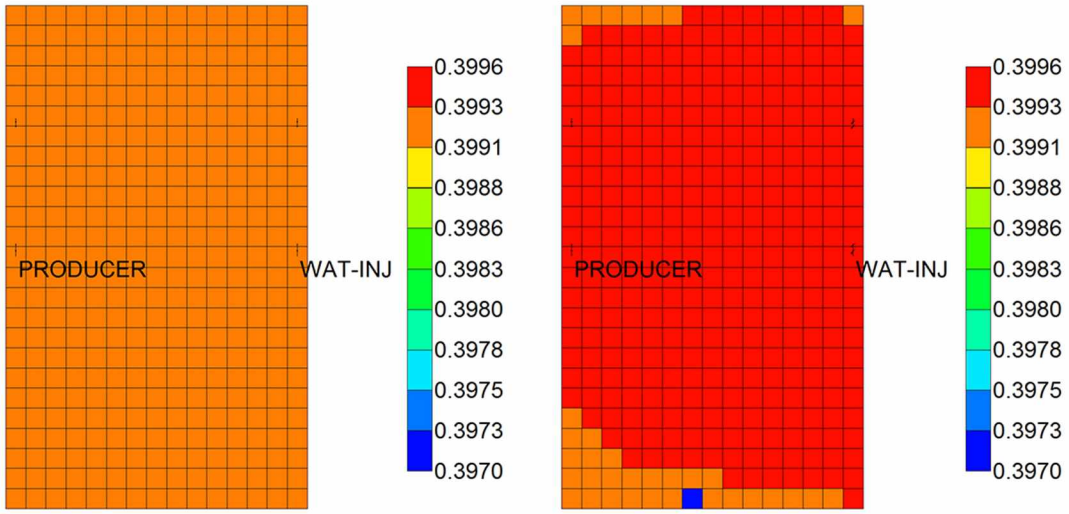

Figure 7-11 Layer 14 Na^+ molality during at 1981 (left) and 2017 (right) for waterflood

For low salinity waterflooding, the amount of Na^+ in the field decreased substantially, as expected, whereas, Ca^{2+} increased (Figure 7-11) due to dissolution of calcite (Figure 7-12). This also increased the reservoir porosity proportionally in the areas affected by mineral dissolution.

During high salinity CO_2-WAG, the amount of HCO_3^- in the formation water increased causing increased concentrations of both $NaHCO_3$ and $CaHCO_3^+$ (Figure 7-10). The increased concentration of the bicarbonate salts subsequently increased the sodium and calcium concentrations as governed by the chemical equilibrium constants for those reactions. The CO_2 in the aqueous phase also caused acidity (release of H^+) and a net dissolution of calcite leading to increased porosity in those affected regions (Figure 7-12).

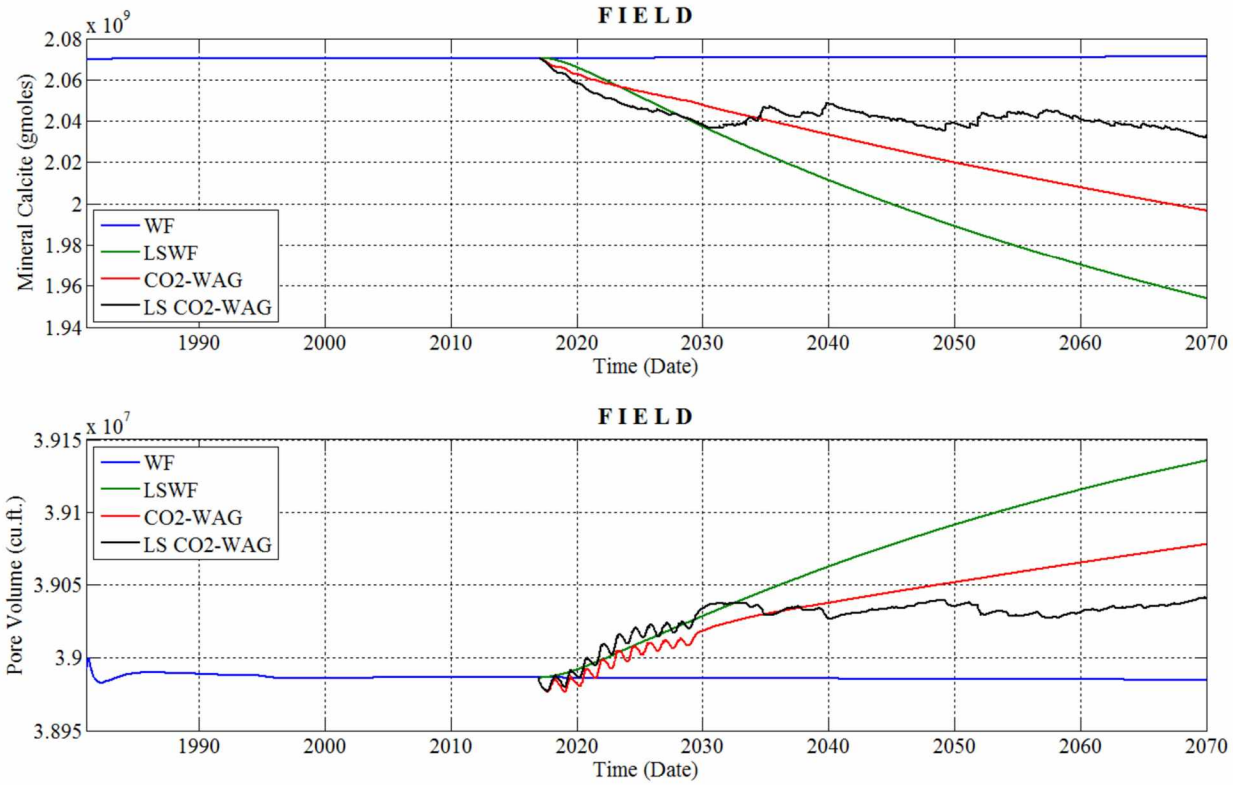

Figure 7-12 Changes in calcite (above) and pore volume (below) in the reservoir

The low salinity WAG showed similar trends for aqueous ionic species except for one difference: the lower Na^+ concentration in solution due to the low salinity water (Figure 7-10). However, the amounts of $NaHCO_3$ were quite higher than those for high salinity WAG, while observed field-wide $CaHCO_3^+$ was lower than that for conventional WAG.

Table 7-3 Equivalent fraction of Na^+ on the clay surface

Year	LSWF	LSWAG
1981	0.913	0.913
2017	0.913	0.913
2042	0.742	0.723
2070	0.617	0.601

Table 7-3 shows the fraction of sodium attached on the exchanger surface. The decrease in Na^+ from the exchanger surface due to replacement with Ca^{2+} made them available to participate in the intra-aqueous reactions to form their bicarbonate species. By the same logic, the deficiency of Ca^{2+} due to increased adsorption on the clay sites explains low $CaHCO_3^+$ amounts during LSWAG as compared to conventional WAG. Even though in 2070, there still seem to be a good amount of NaX in the pattern, it should be noted that some (higher permeability) layers were preferentially flooded. Hence, these layers saw a sharper decrease in NaX, as compared to others (Figure 7-13).

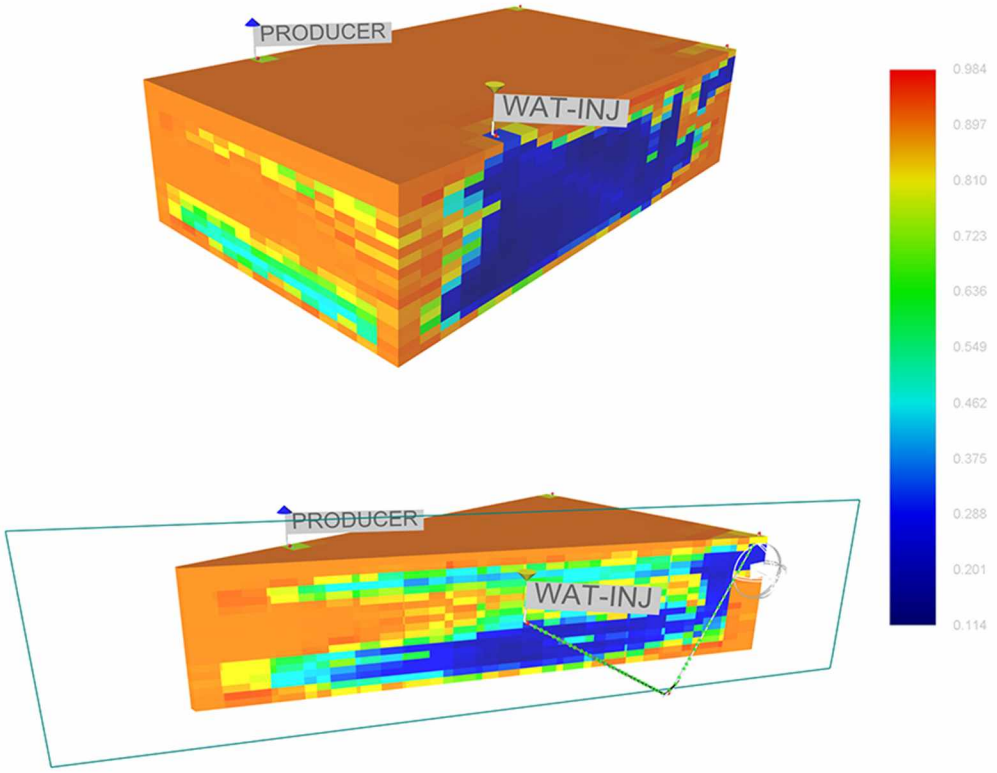

Figure 7-13 Fraction of Na^+ attached to the exchanger surface at 2070. Full and cross-sectional view across the diagonal

7.7 Effluent pH Monitoring and Corrosion

Low salinity waterflooding increases the pH through the dissolution of calcite. This was also observed from the LSWG simulations (Figure 7-14). However, the CO_2-WAG and LSWAG showed a substantial decrease in pH due to the formation of the bicarbonate acid in-situ (Equation 6.1).

Apparently, the localized increase in pH due to calcite dissolution was not enough to counteract the acidity caused by the dissociation of CO_2 in water. Even once the WAG cycles were over, there was still enough CO_2 in the reservoir to keep the pH low.

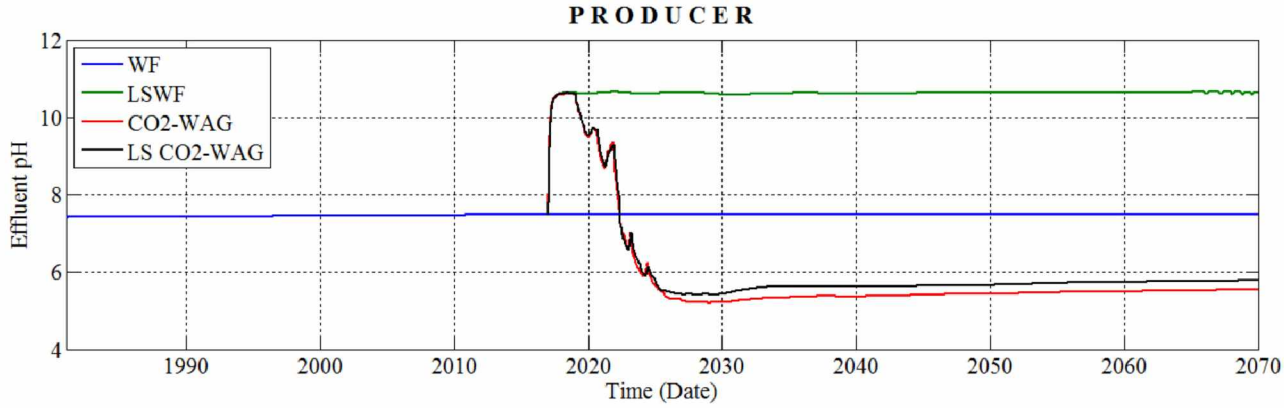

Figure 7-14 Effluent pH for the EOR models

Low pH can be indicative of severe corrosion problems that may arise in the well and flowline tubulars used on the North Slope. It has been observed that operations can be carried out safely using corrosion inhibitors as long as the effluent CO_2 mole fraction is below 25%. However, the WAG and LSWAG simulations show that once CO_2 breakthrough occurs, the CO_2 mole fraction is around 80%. This can have operational implications for brown fields like Schrader Bluff that do not use corrosion resistant tubulars for wells and surface facilities.

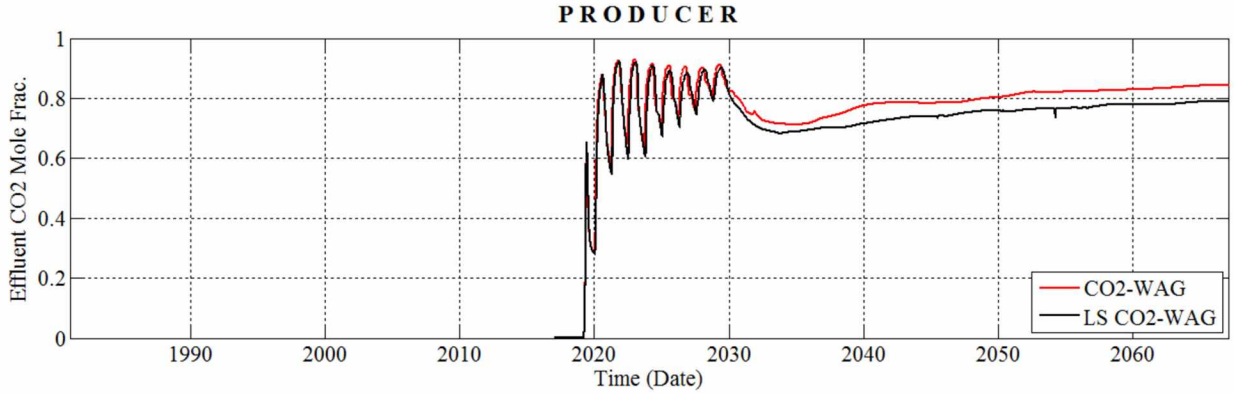

Figure 7-15 Effluent CO2 mole fraction

7.8 Possible Solution

It was thought to raise the pH of the injection water as a possible solution to tackle the corrosion challenge, since replacing the well equipment on the ANS might be cost-prohibitive. It was intended to inject alkaline water so that it would react with the acid formed in-situ due to CO_2 flooding and neutralize it. Hence, to test this concept, an exhaustive list of intra-aqueous reactions was incorporated in the simulator (Table 7-4). The mineral and ion exchange reactions, on the other hand were kept the same as those in the pattern flood model.

Table 7-4 Intra-aqueous reactions for the coreflood simulation

Reaction	K_{eq} at 75°F
$H^+ + OH^- \rightleftharpoons H_2O$	$10^{14.03}$
$CO_2\,(aq) + H_2O \rightleftharpoons H^+ + HCO_3^-$	$10^{-6.38}$
$CO_3 + H^+ \rightleftharpoons +HCO_3^-$	$10^{10.36}$
$CaCO_3 + H^+ \rightleftharpoons Ca^{2+} + HCO_3^-$	$10^{7.16}$
$CaHCO_3^+ \rightleftharpoons Ca^{2+} + HCO_3^-$	$10^{-1.2}$
$CaCl^+ \rightleftharpoons Ca^{2+} + Cl^-$	$10^{-0.713}$
$CaOH^+ + H^+ \rightleftharpoons Ca^{2+} + H_2O$	$10^{12.73}$
$NaCO_3^- + H^+ \rightleftharpoons Na^+ + HCO_3^-$	$10^{9.85}$
$NaHCO_3 \rightleftharpoons Na^+ + HCO_3^-$	$10^{-0.142}$
$NaCl \rightleftharpoons Na^+ + Cl^-$	$10^{1.61}$
$NaOH + H^+ \rightleftharpoons Na^+ + H_2O$	$10^{14.23}$

Due to the added list of equilibrium reactions, it was not possible to carry out simulations at the pattern scale due to increased computational load and time constraints. Therefore, a 1-D coreflood model was constructed having typical properties of the Schrader Bluff formation. These properties are listed in Table 7-5.

Table 7-5 Core properties for the 1-D low salinity floods

Parameter	Value
No. of grid blocks	50
Length, ft	2.86
Diameter, inches	1.3
Porosity	0.26
Permeability, mD	200
Rock Compressibility, psi^{-1}	50E-06

The rock and fluid properties were kept the same as in the pattern simulation model for both high salinity and low salinity conditions. The pH of the injection water was raised to 11.27 by mixing quicklime (CaO) through the following steps:

1. Initially, CaO was equilibrated with fresh water (pH 7) to achieve a saturation index (SI) of -10.5. This level of dissolution corresponds to a pH increase to 12.74.
2. The fresh water + CaO was mixed with the Prince Creek water (Table 7-6) in the ratio 1:9.

Table 7-6 Composition (ppm) of fresh water, intermediate, and high pH water for 1-D floods

Species	Fresh Water	Fresh Water + CaO	High pH Inj. Water
H^+	1.064E-04	2.138E-10	6.325E-09
Ca^{2+}	2.4	474.15	123.93
Na^+	64	63.77	864.42
Cl^-	105	104.91	1,403.23
OH^-	1E-04	4.946E+02	16.86
HCO_3^-	0.946	0.001	5.105
pH	7.0	12.74	11.27

The simulations were carried out for low salinity waterflooding, low salinity CO_2-WAG and high pH CO_2-WAG. The coreflood was simulated under Schrader Bluff conditions. An overburden on 1,785

psi [12,307 kPa] was modeled. The downstream pressure was kept the same as the overburden pressure. Both gas and water injection was carried out at 10 cc/hr constant fluid rate. For the WAG models the ultimate CO_2 slug size was kept at 50% PV. Equal volumes of gas and water were injected during the WAG cycles, followed by chase water injection. The high pH LSWAG simulations were further subdivided into two scenarios: for the first case, once the WAG cycles concluded, the chase water resorted to the Prince Creek water (pH 7.73). In the second case, the chase water was the same high pH water (pH 11.27). The total simulation time was 7 days.

The WAG cycles ended in a little over five days. Expected results in pH were not seen as the pH still stayed low even for high pH injection floods (Figure 7-16). The pH did recover for the low salinity WAG models after six days, indicating that with the current WAG design, the pH will stay low during the WAG cycles and for some time during chase water injection as well, if the high pH LSWAG models are expanded to pattern scale. Therefore, corrosion cannot be prevented using this scheme. Perhaps an alteration in the WAG design might offer a solution.

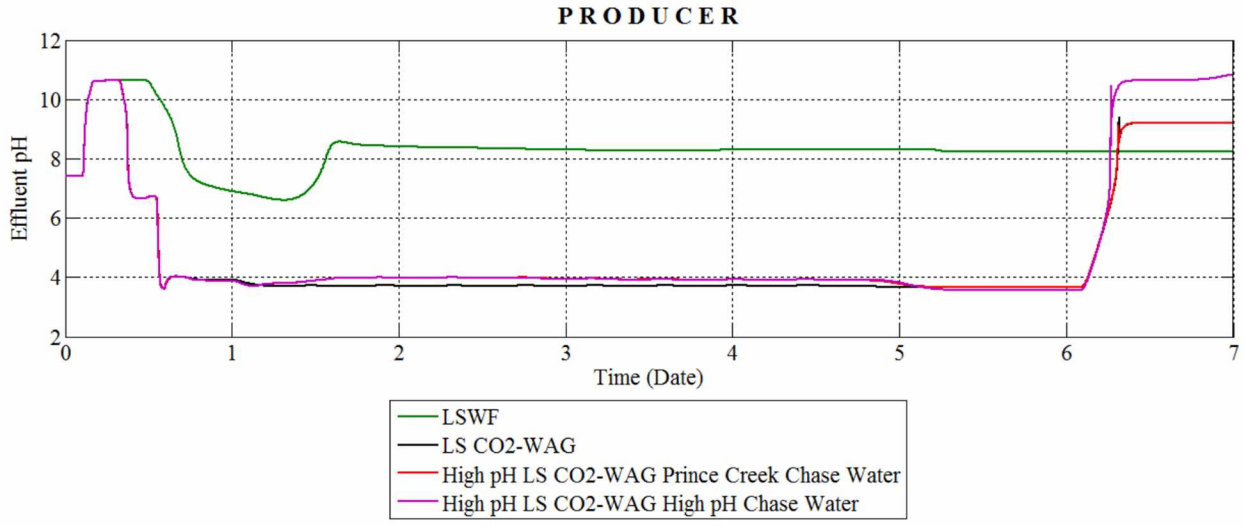

Figure 7-16 Effluent pH for the coreflood simulations

CHAPTER 8 CONCLUSIONS AND RECOMMENDATIONS

8.1 Conclusions

The results of this research show that low salinity EOR can be effectively applied to the Schrader Bluff viscous oil field. Schrader Bluff's rock and fluid properties – good permeability, presence of polar components in the reservoir fluid, adequately high formation water salinity, presence of active ions in the formation water, and low reservoir temperature – make it a desirable candidate for low salinity EOR. The presence of the low salinity Prince Creek aquifer on top of the Schrader Bluff formation also brings exciting prospects to the feasibility of this process. Furthermore, reservoir rock having up to 30% clay matrix adds to the favorableness of this approach for EOR.

This study resulted in the successful modeling of a workflow to assess hydrocarbon recovery for viscous oil through the implementation of low salinity waterflooding (LSWF), conventional CO_2-WAG, and low salinity CO_2-WAG (LSWAG). Among the EOR processes modeled, carbon dioxide alternating with low salinity water recovered highest oil – as much as 39% OOIP of the in-place oil, which currently stands at 17% OOIP (Thyne, 2016). This is 14.3 percentage points higher than waterflood and represents a 58% improvement. The 9-10% incremental recovery over waterflood using conventional CO_2 is already established (Ning et al., 2011). Any recovery over and above this value is solely attributed to the benefits of using low salinity water. What is more encouraging is the fact that enriching CO_2 using NGLs can enhance recovery by 6 percentage points (Ning et al., 2011), i.e., about 45% OOIP recovery may be achievable using enriched CO_2 as a solvent.

The simulation results also demonstrated the effectiveness of CO_2 injection for recovering viscous oil through low solvent utilization values, 6 and 4.4 Mscf/STB [1.08 and 0.79 Msm^3/sm^3] for CO_2-WAG and LSWAG, respectively. These findings corroborate the observations of Ning et al. (2011), who established the effectiveness of CO_2 as a solvent through low solvent utilization values. Because low salinity water helps recover extra oil in the long term, it helps further lower the CO_2 utilization as can be seen from the LSWAG model.

Another small but significant observation from the performance evaluation was that the 98% economic water-cut limit was never reached for the low salinity EOR models, even after 53 years of

forecast starting in 2017. For conventional waterflooding and WAG, this limit was attained at 2041 and 2064, respectively, stemming the recovery through these processes at 22.7% and 34.6% OOIP, respectively. Viscous and heavy oils are produced at high water-cuts due to unfavorable mobility ratios. However, since the main mechanism for LSWF recovery is wettability alteration, the shift from high salinity to low salinity relative permeability plays a major role in guiding fluid movement. Therefore, high oil rates can be sustained during late times of a low salinity flood for a given total bottomhole fluid limit, thereby pushing back the time to reach the economic water-cut limit for a producer.

CO_2 EOR has proven to be an attractive option for recovering oil from the shallow North Slope viscous reservoirs, but its numerical modeling for the cold Schrader Bluff conditions has been challenging. This was due to the unusual phase behavior. CO_2 under Schrader Bluff injection conditions is a liquid and therefore would have immediately achieved miscibility with crude oil. However, further away from the injection well, at increasing dilution, CO_2 lost solubility with oil and would have formed a second CO_2-rich "upper liquid" (L_2) phase to appear. This phase was observed during the PVT simulation of the CO_2-oil mixture (Figure 4-3) at about 68% CO_2 and 1,200 psi [8,273.7 kPa] block pressure. However, this L_2 phase was not seen in numerical simulation, as the simulator used for this study was unable to perform a three-phase flash. This brings in some uncertainty regarding the predictive capabilities of the simulator for CO_2-based processes, as the CO_2-rich liquid phase promotes oil recovery (Strycker and Wang, 2000). Especially near the producer blocks, where the pressure was below the bubblepoint pressure of the oil, the evolved solution gas would have coexisted with the two hydrocarbon phases making essentially a three-phase region (LLV) around those blocks. Constraining these three phases to two pseudo phases required tying the "upper liquid" (L_2) phase to either the "lower liquid" (L_1) phase or the vapor phase (V).

For the processes modeled, the independent single phases were identified based on their molar volumes (and not density) to avoid associating the L_2 phase with the L_1 phase (based on density) as it has shown to lead to very erroneous results in prediction. Therefore, through this criterion of phase identification, CO_2 was always identified as a gas phase despite its liquid-like density at reservoir conditions. When the phase behavior approached the LLV behavior, the critical molar volume changed drastically with small changes in the block pressure and compositions (CO_2 mole fractions). This caused the identified L_2 phase to flip between oil and gas during successive time steps (the

equilibrium switched between liquid-liquid and liquid-vapor equilibrium) which in turn resulted in the oscillations in pressures and saturations (Figure 5-5). This ultimately lead to time step cuts and termination of the run when the time step size became smaller than the specified minimum value.

The inability of the simulator to handle three phase hydrocarbon region was the primary reason for not monitoring the amount of CO_2 sequestered as previous studies for West Sak have shown that this can lead to very erroneous results (Nourpour Aghbash and Ahmadi, 2012).

A way around this problem was achieved by decreasing the interaction coefficients between CO_2 and the hydrocarbon components. It was seen that the three-phase region shrank substantially when the binary interaction coefficients (BICs) between CO_2 and oil components were reduced from 0.15 to 0.02 (Figure 4-3). It was also seen that reducing the BICs enhanced vapor-like properties in the solvent-oil mixture, i.e., reduced density and viscosity. Hence, the alteration in the CO_2-oil BICs significantly affected the fluid PVT behavior.

In low salinity waterflood modeling it is observed that the reactions concerning dissolution of CO_2 in water, dissociation of water, and dissolution of calcite are adequate for modeling the low salinity cation exchange (Dang et al., 2014, Dang et al., 2015). However, this research shows the importance of modeling the dissociation of cationic bicarbonates that had a considerable impact on the LSWAG process as they formed in substantial quantities in the reservoir, thereby affecting the amounts of Na^+ and Ca^{2+} available for ion exchange. The numerical simulation results, however, have uncertainties inherent in them due to lack of data for modeling the low salinity process. Lack of clay distribution and the experimental low salinity oil-water relative permeability information, especially the difference between residual oil saturation between high and low salinity waterfloods, account for the bulk of the associated uncertainty. Accurate formation water data (concentration of active divalents) was also unavailable and therefore, added to the list of uncertainty parameters.

Incorporating geochemistry in the simulation model can be advantageous not only for low salinity EOR but also for conventional secondary and tertiary processes like WAG, as chemical reactions are always taking place in the reservoir associated with injection/production activity. Apart from low salinity evaluation, other processes like sulfate scaling (Bethke, 1996), solids deposition, and geochemical changes due to thermal processes (Strycker and Wang, 2000) can also be modeled. This can make reservoir models more representative of subsurface conditions and recovery processes. The

only downside to modeling geochemistry is the added burden of computations. However, with advancements in computational technology, this is a tradeoff one may be willing to make.

For the WAG processes, the pH for the effluent stream was observed to drop around 5. Thus, corrosion due to CO_2 can be anticipated and may limit CO_2's use as an EOR solvent for operations on the North Slope (Figure 7-14). This drop of pH from 7.4 to 5 is consistent with the large amount of CO_2 mole fraction (~80%) seen in the producer fluid stream from the simulations (Figure 7-15). This pH drop could not be avoided, even after injecting high pH water. The rapid increase of CO_2 concentration due to high pressure injection probably accelerated the formation of the weak bicarbonate acid propelled by an already fast geochemical reaction. The mineral dissolution reaction that is responsible for raising the alkalinity of reservoir water proceeded at a relatively slow pace and was not able to catch up with the CO_2 induced acidity.

It has been observed that a CO_2 mole fraction up to 25% in the effluent stream can be worked with and corrosion in the wells can be contained using inhibitors. Additional studies need to be undertaken to consider different WAG designs to keep effluent CO_2 concentration below this operational limit.

8.2 Recommendations

CO_2 EOR is a complex process with the complexity increasing when modeling low temperature reservoirs like Schrader Bluff. The effect of the second hydrocarbon liquid (L_2) phase on oil recovery becomes more evident during the later life of a reservoir. Additional oil recovery up to 5 percentage points has been observed for CO_2 EOR in Schrader Bluff using a simulator capable of handling three hydrocarbon phases (Strycker and Wang, 2000). Furthermore, ignoring this L_2 phase can also give inaccurate CO_2 sequestration results (Nourpour Aghbash and Ahmadi, 2012). Therefore, with regards to accuracy of results and numerical efficiency, it is recommended to use a simulator that can handle three-phase flash like UTCOMP. UTCOMP is the in-house simulator of University of Texas at Austin. Commercial simulators do not have this capability at present.

Injection of WAG cycles requires alternating drainage and injection cycles. Therefore, three phase relative permeability becomes dependent on saturation paths and saturation history. Thus, modeling hysteresis in relative permeability becomes a key component for WAG processes. Including relative permeability hysteresis has a significant impact on oil recovery and breakthrough times. Furthermore, modeling hysteresis is important to accurately assess the amount of CO_2 immobilized by capillary

trapping and has shown to impact sequestration performance. Incorporating hysteresis in the simulation model requires the specification of the maximum trapped gas saturation. For this study, this data was not available. If this information can be obtained, then more accurate modeling can be achieved.

Another aspect of the WAG process that was not incorporated was the wettability change due to interfacial tension (IFT) effects and asphaltene deposition. It is very interesting to observe that the wettability shift during a CO_2 flood can be caused by geochemical reaction, IFT effects, and potentially more asphaltene deposition. The solid deposition may also decrease porosity and permeability in a way similar to mineral precipitation. While the geochemical (mineral dissolution and ion exchange) reactions and IFT effects may promote oil recovery, asphaltene precipitation during a CO_2 flood can shift wettability to a more oil-wet state, thereby increasing the residual oil saturation. The IFT relative permeability curve is essentially an X-shaped curve describing completely miscible conditions. As mentioned previously, the model was calibrated by matching a waterflood and WAG performance done by Ning et al. (2011). For the sake of simplicity, the IFT effects were not included during the performance match process and therefore, were also not incorporated into forecasts to maintain an unbiased ground for prediction. These can be incorporated in a future study using a miscible solvent such as CO_2.

Asphaltene deposition required properties of solid deposition to model the deposition process in the PVT simulator. Again, due to similar reasons as for IFT effects, this was not undertaken, but can be modeled in a future work where study objectives include asphaltene monitoring in the reservoir.

Through this research, it was shown that corrosion due to CO_2 might be inevitable and therefore, using a hydrocarbon miscible/semi-miscible solvent or using a combination of CO_2-hydrocarbon miscible/semi-miscible can be undertaken. The required data in this case would be the swelling test data of the solvent with crude oil. In the interest of preventing corrosion, alternate WAG designs in combination can also be tried in conjunction with the use of hydrocarbon/CO_2-hydrocarbon solvents. These may be utilizing the WAG scheme with a WAG ratio in favor of water. Sensitivity studies may be performed to see the effect of such changes in the WAG design on CO_2 concentration in the effluent stream.

Since, LSWAG has shown promise for Alaskan viscous oil recovery, an uncertainty analysis study can also be undertaken quantifying the uncertainty in low salinity parameters incorporated in the model on production performance. These include: 1) clay distribution and 2) low salinity relative permeability parameters, S_{orw}, K_{row}, K_{rw}, N_w, and N_{ow}. These can be further combined with the trapped gas saturation as another uncertainty parameter to model uncertainty in relative permeability hysteresis along with LSWF. Sensitivity studies can be performed concurrently with the low salinity uncertainty quantification, where the alteration of injection water composition (especially concentration of divalents) can be altered to see its effect on low salinity EOR performance. Finally, a detailed economic feasibility study incorporating the above-mentioned uncertainties can be coupled to numerical simulation as a robust basis for comparison for the applicability of the EOR methods tested in this study.

APPENDIX

Schrader Bluff Formation Water Initialization (PHREEQC)

```
-------------------------------------------
Beginning of initial solution calculations.
-------------------------------------------

Initial solution 1.     FORMATION WATER FROM SCHRADER BLUFF

-----------------------------Solution composition------------------------------

      Elements           Molality       Moles

      C                1.162e-02   1.162e-02
      Ca               4.680e-03   4.680e-03
      Cl               3.772e-01   3.772e-01
      Na               4.133e-01   4.133e-01

----------------------------Description of solution----------------------------

                                       pH  =   7.400      Charge balance
                                       pe  =  10.560      Adjusted to redox eq.
                            Activity of water  =   0.987
                  Ionic strength (mol/kgw)  =   3.957e-01
                       Mass of water (kg)  =   1.000e+00
                  Total alkalinity (eq/kg)  =   1.116e-02
                       Total CO2 (mol/kg)  =   1.162e-02
                         Temperature (°C)  =  23.89
                  Electrical balance (eq)  =   3.428e-02
 Percent error, 100*(Cat-|An|)/(Cat+|An|)  =   4.38
                                Iterations  =  10
                                   Total H  = 1.110617e+02
                                   Total O  = 5.555967e+01

----------------------------Distribution of species----------------------------

                                                  Log       Log       Log     mole V
   Species          Molality    Activity  Molality  Activity     Gamma   cm³/mol

   OH-              3.249e-07   2.196e-07    -6.488    -6.658    -0.170      (0)
   H+               4.967e-08   3.981e-08    -7.304    -7.400    -0.096      0.00
   H2O              5.553e+01   9.865e-01     1.744    -0.006     0.000     18.06
   HCO3-            8.539e-03   5.912e-03    -2.069    -2.228    -0.160      (0)
   CO2              5.117e-04   5.613e-04    -3.291    -3.251     0.040      (0)
   CO3-2            2.876e-05   6.447e-06    -4.541    -5.191    -0.649      (0)
Ca             4.680e-03
   Ca+2             4.430e-03   1.228e-03    -2.354    -2.911    -0.557      (0)
   CaHCO3+          1.239e-04   8.578e-05    -3.907    -4.067    -0.160      (0)
   CaCl+            8.998e-05   6.230e-05    -4.046    -4.205    -0.160      (0)
   CaCO3            1.788e-05   1.788e-05    -4.748    -4.748     0.000      (0)
   CaCl2            1.781e-05   1.781e-05    -4.749    -4.749     0.000      (0)
   CaOH+            6.207e-09   4.297e-09    -8.207    -8.367    -0.160      (0)
Cl(-1)         3.772e-01
```

Cl-	**3.655e-01**	2.403e-01	-0.437	-0.619	-0.182	(0)
HCl	2.146e-09	2.146e-09	-8.668	-8.668	0.000	(0)
Na	4.133e-01					
Na+	**3.993e-01**	2.765e-01	-0.399	-0.558	-0.160	(0)
NaCl	**1.158e-02**	1.158e-02	-1.936	-1.936	0.000	(0)
NaHCO3	**2.387e-03**	2.387e-03	-2.622	-2.622	0.000	(0)
NaCO3-	9.284e-06	6.428e-06	-5.032	-5.192	-0.160	(0)
NaOH	1.050e-08	1.050e-08	-7.979	-7.979	0.000	(0)
O(0)	6.021e-15					
O2	3.010e-15	3.303e-15	-14.521	-14.481	0.040	(0)

-------------------------------Saturation indices--------------------------------

Phase	SI**	log IAP	log K(297 K, 1 atm)	
Antarcticite	-8.28	-4.18	4.09	CaCl2:6H2O
Aragonite	**0.27**	**2.26**	**1.99**	**CaCO3**
C	-59.54	4.86	64.40	C
C(g)	-177.63	4.86	182.49	C
Ca	-121.25	19.12	140.37	Ca
Ca(g)	-146.60	19.12	165.73	Ca
Ca2Cl2(OH)2:H2O	-18.57	7.72	26.29	Ca2Cl2(OH)2:H2O
Ca4Cl2(OH)6:13H2O	-36.92	31.41	68.33	Ca4Cl2(OH)6:13H2O
Calcite	**0.42**	**2.26**	**1.84**	**CaCO3**
CH4(g)	-122.50	-125.33	-2.83	CH4
Cl2(g)	-26.30	-23.27	3.03	Cl2
CO(g)	-41.25	-44.24	-2.99	CO
CO2(g)	-1.80	-9.62	-7.82	CO2
Gaylussite	-4.88	6.29	11.16	CaNa2(CO3)2:5H2O
H2(g)	-35.95	-39.04	-3.10	H2
H2O(g)	-1.62	-0.01	1.61	H2O
Halite	-2.74	-1.18	1.56	NaCl
HCl(g)	-14.37	-8.02	6.35	HCl
Hydrophilite	-15.95	-4.15	11.80	CaCl2
Ice	-0.14	-0.01	0.13	H2O
Lime	-20.81	11.88	32.70	CaO
Monohydrocalcite	-0.44	2.25	2.69	CaCO3:H2O
Na	-57.16	10.46	67.62	Na
Na(g)	-70.72	10.46	81.18	Na
Na2CO3	-7.13	4.05	11.19	Na2CO3
Na2CO3:7H2O	-5.91	4.01	9.92	Na2CO3:7H2O
Na2O	-53.97	13.68	67.65	Na2O
Nahcolite	-2.63	-2.79	-0.15	NaHCO3
Natron	-5.56	4.00	9.56	Na2CO3:10H2O
O2(g)	-11.60	-14.48	-2.88	O2
Pirssonite	-5.02	6.30	11.32	Na2Ca(CO3)2:2H2O
Portlandite	-10.75	11.88	22.63	Ca(OH)2
Thermonatrite	-6.91	4.05	10.95	Na2CO3:H2O

**For a gas, SI = log10(fugacity). Fugacity = pressure * phi / 1 atm.
For ideal gases, phi = 1.

```
-----------------------------------------------------
Beginning of initial exchange-composition calculations.
-----------------------------------------------------

Exchange 1.

X               2.000e-02 mol
```

Species	Moles	Equiv-alents	Equivalent Fraction	Log Gamma
NaX	1.738e-02	1.738e-02	**8.690e-01**	-0.160
CaX2	1.310e-03	2.619e-03	**1.310e-01**	-0.557

```
------------------
End of simulation.
------------------
```

REFERENCES

Agarwal, R. K., Li, Y. K. and Nghiem, L. 1990. A Regression Technique With Dynamic Parameter Selection for Phase-Behavior Matching. *SPE Res Eng* **5**(1): 115-120. SPE-16343-PA. http://dx.doi.org/10.2118/16343-PA.

Ahmadi, K. and Johns, R. T. 2008. Multiple Mixing-Cell Method for MMP Calculations. *SPE J.* **16**(4): 733-742. SPE-116823-MS. http://dx.doi.org/10.2118/116823-MS.

Al Harrasi, A., Al-Maamari, R. S. and Masalmeh, S. K. 2012. Laboratory Investigation of Low Salinity Waterflooding for Carbonate Reservoirs. Abu Dhabi International Petroleum Conference and Exhibition, Abu Dhabi, UAE, 11-14 November. SPE-161468-MS. http://dx.doi.org/10.2118/161468-MS.

Alboudwarej, H., Felix, J., Taylor, S., Badry, R., Bremmer, C., Brough, B., Skeates, C., Baker, A., Palmer, D., Pattison, K., Beshry, M., Krawchuk, P., Brown, G., Calvo, R., Triana, J. A. C., Hathcock, R., Koerner, K., Hughes, T., Kundu, D., Cardenasand, J. L. and West, C. 2006. Highlighting Heavy Oil. *Oilfield Review* **18**(2): 34-53. Highlighting Heavy Oil.

Albrecht, R. A. and Marsden, S. S. 1970. Foams as Blocking Agents in Porous Media. *SPE J.* **10**(1): 51-55. SPE-2357-PA. http://dx.doi.org/10.2118/2357-PA.

Ali, S. M. F. 1974. Heavy Oil Recovery - Principles, Practicality, Potential, and Problems. SPE Rocky Mountain Regional Meeting, Billings, Montana, USA, 15-16 May. SPE-4935-MS. http://dx.doi.org/10.2118/4935-MS.

Alomair, O. A., Matar, K. M. and Alsaeed, Y. H. 2014. Nanofluids Applications for Heavy Oil Recovery. SPE Asia Pacific Oil & Gas Conference and Exhibition, Adelaide, Australia, 14-16 October. SPE-171539-MS. http://dx.doi.org/10.2118/171539-MS.

AOGCC 2012a. Prudhoe Bay Unit, Prudhoe Oil Pool. http://doa.alaska.gov/ogc/annual/current/annindex_current.html (accessed 25 July, 2015).

AOGCC 2012b. Schrader Bluff Oil Pool - Orion Development Area. http://doa.alaska.gov/ogc/annual/current/18_Oil_Pools/Prudhoe%20Bay%20-%20Oil/Prudhoe%20Bay,%20Orion%20Schrader%20Bluff%20Oil/Text_Summary.pdf (accessed 25 July, 2015).

AOGCC 2015. Milne Point Unit, Schrader Bluff Oil Pool. http://doa.alaska.gov/ogc/annual/current/18_Oil_Pools/Milne%20Pt%20-%20Oil/Milne%20Point,%20Schrader%20Bluff%20Oil/1_Oil_1.htm (accessed 15 July, 2015).

Appelo, C. A. J. and Postma, D. 2005. *Geochemistry, Groundwater and Pollution*, second edition. Amsterdam: CRC press.

Austad, T., Rezaeidoust, A. and Puntervold, T. 2010. Chemical Mechanism of Low Salinity Water Flooding in Sandstone Reservoirs. SPE Improved Oil Recovery Symposium, Tulsa, Oklahoma, USA, 24-28 April. SPE-129767-MS. http://dx.doi.org/10.2118/129767-MS.

Austad, T., Strand, S., Madland, M. V., Puntervold, T. and Korsnes, R. I. 2008. Seawater in Chalk: An EOR and Compaction Fluid. *SPE Res Eval & Eng* **11**(4): 648-654. Seawater in Chalk: An EOR and Compaction Fluid. http://dx.doi.org/10.2118/118431-PA.

Ayirala, S. C., Saleh, S. H. and Yousef, A. A. 2016. Microscopic Scale Study of Individual Water Ion Interactions at Complex Crude Oil-Water Interface: A New SmartWater Flood Recovery Mechanism. SPE Improved Oil Recovery Conference, Tulsa, Oklahoma, USA, 11-13 April. SPE-179590-MS. http://dx.doi.org/10.2118/179590-MS.

Bakshi, A. K. 1991. Computer Modeling of CO2 Stimulation in the West Sak Reservoir. M.S. Thesis, University of Alaska Fairbanks.

Beliveau, D. 2009. Waterflooding Viscous Oil Reservoirs. *SPE Res Eval & Eng* **12**(5): 689-701. SPE-113132-PA. http://dx.doi.org/10.2118/113132-PA.

Bernard, G. C., Holm, L. W. and Harvey, C. P. 1980. Use of Surfactant to Reduce CO2 Mobility in Oil Displacement. *SPE J.* **20**(4): 281-293. SPE-8370-PA. http://dx.doi.org/10.2118/8370-PA.

Bernard, G. G. and Holm, L. W. 1964. Effect of Foam on Permeability of Porous Media to Gas. *SPE J.* **4**(3): 267-274. SPE-983-PA. http://dx.doi.org/10.2118/983-PA.

Bernard, G. G. and Jacobs, W. L. 1965. Effect of Foam on Trapped Gas Saturation and on Permeability of Porous Media to Water. *SPE J.* **5**(4): 295-300. SPE-1204-PA. http://dx.doi.org/10.2118/1204-PA.

Bethke, C. 1996. *Geochemical Reaction Modeling: Concepts and Applications*, first edition: Oxford University Press.

Bidinger, C. R. and Dillon, J. F. 1991. Milne Point Schrader Bluff - Finding the Keys to Two Billion Barrels. SPE International Heavy Oil Symposium, Calgary, Alberta, Canada, 19-21 June. SPE-30289-MS. http://dx.doi.org/10.2118/30289-MS.

Carlson, L. O. 1988. Performance of Hawkins Field Unit Under Gas Drive-Pressure Maintenance Operations and Development of an Enhanced Oil Recovery Project. SPE Enhanced Oil Recovery Symposium, Tulsa, Oklahoma, USA, 16-21 April. SPE-17324-MS. http://dx.doi.org/10.2118/17324-MS.

CERI 2014. Canadian Economic Impacts of New and Existing Oil Sands Development in Alberta (2014-2038), Canadian Energy Research Institute.

Champion, J. H. and Shelden, J. B. 1989. An Immiscible WAG Injection Project in the Kuparuk River Unit. *J Pet Technol* **41**(5): 533-540. SPE-16719-PA. http://dx.doi.org/10.2118/16719-PA.

Chmielowski, J. 2013. BP Alaska Heavy Oil Production from the Ugnu Fluvial-Deltaic Reservoir. Pacific Section AAPG, SEG, and SEPM Joint Conference, 19-25 April, Monterery, California, USA. BP Alaska Heavy Oil Production from the Ugnu Fluvial-Deltaic Reservoir.

Christensen, J. R., Stenby, E. H. and Skauge, A. 2001. Review of WAG Field Exerience. *SPE Res Eval & Eng* **4**(2): 97-106. SPE-71203-PA. http://dx.doi.org/10.2118/71203-PA.

Christianson, S. H. 1977. Performance and Unitization of the Empire Abo Pool. SPE Permian Basin Oil and Gas Recovery Conference, Midland, Texas, USA, 10-11 March. SPE-6384-MS. http://dx.doi.org/10.2118/6384-MS.

Chung, F. T. H., Jones, R. A. and Burchfield, T. E. 1988. Recovery of Viscous Oil Under High Pressure by CO2 Displacement: A Laboratory Study. International Meeting on Petroleum Engineering, Tianjin, China, 1-4 November. SPE-17588-MS. http://dx.doi.org/10.2118/17588-MS.

CMOST 2015. *User Guide - Enhance & Accelerate Sensitivity Analysis, History Matching, Optimization & Unertainty Analysis*. Calgary, Alberta, Canada: Computer Modelling Group Ltd.

Couch, E. J. and Watts, J. W. 1970. Permafrost Thawing Around Producing Oil Wells. *J of Can Pet Technol* **9**(2): 107-111. PETSOC-70-02-06. http://dx.doi.org/10.2118/70-02-06.

Dang, C., Nghiem, L., Nguyen, N., Chen, Z. and Nguyen, Q. 2015. Modeling and Optimization of Low Salinity Waterflood. SPE Reservoir Simulation Symposium, Houston, Texas, USA, 23-25 February. SPE-173194-MS. http://dx.doi.org/10.2118/173194-MS.

Dang, C. T. Q., Nghiem, L. X., Chen, Z., Nguyen, N. T. B. and Nguyen, Q. P. 2014. CO2 Low Salinity Water Alternating Gas: A New Promising Approach for Enhanced Oil Recovery. SPE Improved Oil Recovery Symposium, Tulsa, Oklahoma, USA, 12-16 April. SPE-169071-MS. http://dx.doi.org/10.2118/169071-MS.

Das, S. K. 1998. Vapex - An Efficient Process for the Recovery of Heavy Oil and Bitumen. *SPE Res Eng* **3**(3): 232-237. SPE-50941-PA. http://dx.doi.org/10.2118/50941-PA.

de Bruin, W. J. 2012. Simulation of Geochemical Processes during Low Salinity Water Flooding by Coupling Multiphase Buckley-Leverett Flow to the Geochemical Package PHREEQC. MSc Thesis, TU Delft.

De Ghetto, G., Paone, F. and Villa, M. 1995. Pressure-Volume-Temperature Correlations for Heavy and Extra Heavy Oils. SPE International Heavy Oil Symposium, Calgary, Alberta, Canada, 19-21 June. SPE-30316-MS. http://dx.doi.org/10.2118/30316-MS.

Delamaide, E., Bazin, B., Rousseau, D. and Degre, G. 2014. Chemical EOR for Heavy Oil - The Canadian Experience. *J of Pet Technol* **68**(3): 81-82. SPE-0316-0081-JPT. http://dx.doi.org/10.2118/0316-0081-JPT.

Dellinger, S. E., Patton, J. T. and Holbrook, S. T. 1984. CO2 Mobility Control. *SPE J.* **24**(2): 191-196. CO2 Mobility Control. http://dx.doi.org/10.2118/9808-PA.

Dusseault, M. B. 2007. Cold Heavy-Oil Production With Sand. 'In '*Petroleum Engineering Handbook*, L. W. Lake 191-248: Society of Petroleum Engineers.

Emadi, A., Sohrabi, M., Jamiolahmady, M., Irland, S. and Robertson, G. 2011. Mechanistic Study of Improved Heavy Oil Recovery by CO2-Foam Injection. SPE Enhanced Oil Recovery Conference, Kuala Lumpur, Malaysia, 19-21 July. SPE-143013-MS. http://dx.doi.org/10.2118/143013-MS.

Enick, R. M. and Olsen, D. K. 1993. Mobility and Conformance Control for Carbon Dioxide Enhanced Oil Recovery (CO2-EOR) via Thickeners, Foams, and Gels – A Detailed Literature Review of 40 Years of Research, Department of Energy/National Energy Technology Laboratory - 2012/1540.

Fjelde, I., Omekeh, A. V. and Sokama-Neuyam, Y. A. 2014. Low Salinity Water Flooding: Effect Of Crude Oil Composition. SPE Improved Oil Recovery Symposium, Tulsa, Oklahoma, USA, 12-16 April. SPE-169090-MS. http://dx.doi.org/10.2118/169090-MS.

GEM 2015. *GEM User Guide - Compositional and Unconventional Reservoir Simulator*. Calgary, Alberta, Canada: Computer Modelling Group Ltd.

Glover, F. 1986. Future paths for integer programming and links to artificial intelligence. *Comput Oper Res* **13**(5): 533-549. Future paths for integer programming and links to artificial intelligence. http://dx.doi.org/10.1016/0305-0548(86)90048-1.

Gondouin, M. and Fox III, J. M. 1991. The Challenge of West Sak Heavy Oil: Analysis of an Innovative Approach. International Arctic Technology Conference, Anchorage, Alaska, 29-31 May. SPE-22077-MS. http://dx.doi.org/10.2118/22077-MS.

Gorell, S. B. 1988. Modeling the Effects of Trapping and Water Alternate Gas (WAG) Injection on Tertiary Miscible Displacements. SPE Enhanced Oil Recovery Symposium, Tulsa, Oklahoma, USA, 16-21 April. SPE-17340-MS. http://dx.doi.org/10.2118/17340-MS.

Graue, D. J. and Blevins, T. R. 1978. Sacroc Tertiary CO2 Pilot Project. SPE Symposium on Improved Methods of Oil Recovery, Tulsa, Oklahoma, USA, 16-17 April. SPE-7090-MS. http://dx.doi.org/10.2118/7090-MS.

Gupta, R., Smith, G. G., Hu, L., Willingham, T., Lo Cascio, M., Shyeh, J. J. and Harris, C. R. 2011. Enhanced Waterflood for Carbonate Reservoirs - Impact of Injection Water Composition. SPE Middle East Oil and Gas Show and Conference, Manama, Bahrain, 25-28 September. SPE-142668-MS. http://dx.doi.org/10.2118/142668-MS.

Hadlow, R. E. 1992. Update of Industry Experience With CO2 Injection. SPE Annual Technical Conference and Exhibition, Washington, D.C., USA, 4-7 October. SPE-24928-MS. http://dx.doi.org/10.2118/24928-MS.

Hallam, R. J., Piekenbrock, E. J., Abou-Sayed, A. S., Garon, A. M., Putnam, T. W., Weggeland, M. C. and Webb, K. J. 1992. Resource Description and Development Potential of the Ugnu Reservoir, North Slope, Alaska. *SPE Form Eval* **7**(3): 211-218. SPE-21779-PA. http://dx.doi.org/10.2118/21779-PA.

Henry, R. L., Fisher, D. R., Pennell, S. P. and Honnert, M. A. 1996. Field Test of Foam to Reduce CO2 Cycling. SPE/DOE Improved Oil Recovery Symposium, Tulsa, Oklahoma, USA, 21-24 April. SPE-35402-MS. http://dx.doi.org/10.2118/35402-MS.

Hoefner, M. L., Evans, E. M., Buckles, J. J. and Jones, T. A. 1995. CO2 Foam: Results From Four Developmental Field Trials. *SPE Res Eng* **10**(4): 273-281. SPE-27787-PA. http://dx.doi.org/10.2118/27787-PA.

Holm, L. W. and Josendal, V. A. 1982. Effect of Oil Composition on Miscible-Type Displacement by Carbon Dioxide. *SPE J.* **22**(1): 87-98. SPE-8814-PA. http://dx.doi.org/10.2118/8814-PA.

Holm, W. L. 1987. Evolution of the Carbon Dioxide Flooding Processes. *J of Pet Technol.* SPE-17134-PA. http://dx.doi.org/10.2118/17134-PA.

Honarpour, M. M., Koederitz, F. and Herbert, A. 1986. *Relative Permeability of Petroleum Reservoirs*: CRC Press Inc.

Hulm, E., Bernaski, G., Kostic, B., Lowe, S. and Matson, R. 2013. Integrated Reservoir Description of the Ugnu Heavy-Oil Accumulation, North Slope, Alaska. *Heavy-oil and oil-oand petroleum systems in Alberta and beyond* **64**: 481-508. Integrated Reservoir Description of the Ugnu Heavy-Oil Accumulation, North Slope, Alaska. http://dx.doi.org/10.1306/13371589St643558.

Jerauld, G. R., Webb, K. J., Lin, C.-Y. and Seccombe, J. 2006. Modeling Low-Salinity Waterflooding. SPE Annual Technical Conference and Exhibition, San Antonio, Texas, USA, 24-27 September. SPE-102239-MS. http://dx.doi.org/10.2118/102239-MS.

Jiang, H., Nuryaningsih, L. and Adidharma, H. 2012. The Study of Timing of Cyclic Injections in Miscible CO2 WAG. SPE Western Regional Meeting, Bakersfield, California, USA, 21-23 March. SPE-153792-MS. http://dx.doi.org/10.2118/153792-MS.

Jossi, J. A., Stiel, L. I. and Thodos, G. 1962. The Viscosity of Pure Substances in the Dense Gaseous and Liquid Phases. *AIChE J.* **8**(1): 59-63. The Viscosity of Pure Substances in the Dense Gaseous and Liquid Phases. http://dx.doi.org/10.1002/aic.690080116.

Kamath, V. A., Sharma, G. D. and Ogbe, D. O. 1995. Assessment of Resource and Recovery Potential of Ugnu Tar Sands, North Slope, Alaska. UNITAR international conference on heavy crude and tar sands on fueling for a clean and safe environment, Houston, Texas, USA, 12-17 February. Assessment of Resource and Recovery Potential of Ugnu Tar Sands, North Slope, Alaska.

Kasmaei, A. K. and Rao, D. N. 2014. Is Wettability Alteration the Main Cause for Enhanced Recovery in Low- Salinity Waterflooding? SPE Improved Oil Recovery Symposium, Tulsa, Oklahoma, USA, 12-16 April. SPE-169120-MS. http://dx.doi.org/10.2118/169120-MS.

Khataniar, S., Kamath, V. A., Patil, S. L., Chandra, S. and Inaganti, M. S. 1999. CO2 and Miscible Gas Injection for Enhanced Recovery of Schrader Bluff Heavy Oil. International Thermal Operations/Heavy Oil Symposium, Bakersfield, California, USA, 17-19 March. SPE-54085-MS. http://dx.doi.org/10.2118/54085-MS.

Klins, M. A. and Ali, S. M. F. 1982. Heavy Oil Production By Carbon Dioxide Injection. *J of Can Pet Technol*. PETSOC-82-05-06. http://dx.doi.org/10.2118/82-05-06.

Koottungal, L. 2014. 2014 Worldwide EOR Survey. http://www.ogj.com/articles/print/volume-112/issue-4/special-report-eor-heavy-oil-survey/2014-worldwide-eor-survey.html (accessed 20 July, 2015).

Kovscek, A. R., Castanier, L. M., DE, W. P. U. C. and Mehlhoff, S. 2004. Transformation of Resources to Reserves: Next Generation Heavy-Oil Recovery Techniques. Semiannual Technical Progress Report, United Stated DOE, NETL.

Kumar, R. and Mohanty, K. K. 2010. ASP Flooding of Viscous Oils. SPE Annual Technical Conference and Exhibition, Florence, Italy, 19-22 September. SPE-135265-MS. http://dx.doi.org/10.2118/135265-MS.

Kyte, J. R., Stanclift Jr., R. J., Stephan Jr., S. C. and Rapoport, L. A. 1956. Mechanism of Water Flooding in the Presences of Free Gas. *Petroleum Transactions, AIME* **207**: 215-221. SPE-536-G.

Lager, A., Webb, K. J. and Black, C. J. J. 2007. Impact of Brine Chemistry on Oil Recovery. IOR 2007-14th European Symposium on Improved Oil Recovery. Impact of Brine Chemistry on Oil Recovery.

Lager, A., Webb, K. J., Black, C. J. J., Singleton, M. and Sorbie, K. S. 2008. Low Salinity Oil Recovery - An Experimental Investigation. *Petrophysics* **49**(1): 28-35. Low Salinity Oil Recovery - An Experimental Investigation.

Land, C. S. 1968. The Optimum Gas Saturation for Maximum Oil Recovery from Displacement by Water. Fall Meeting of the Society of Petroleum Engineers of AIME, Houston, Texas, USA, 29 September-2 October. SPE-2216-MS. http://dx.doi.org/10.2118/2216-MS.

Law, S., McDonald, A., Fellows, S., Reed, J. and Sutcliffe, P. G. 2015. Influence of Clay Content and Type on Oil Recovery Under Low Salinity Waterflooding in North Sea Reservoirs. SPE Offshore Europe Conference and Exhibition, Aberdeen, Scotland, UK, 8-11 September. SPE-175506-MS. http://dx.doi.org/10.2118/175506-MS.

Lee, B. I. and Kesler, M. G. 1975. A Generalized Thermodynamic Correlation Based on Three-Parameter Corresponding States. *AIChE J.* **21**(3): 510-527. A Generalized Thermodynamic Correlation Based on Three-Parameter Corresponding States.

Li, H. Z., Zheng, S. and Yang, D. T. 2011. Enhanced Swelling Effect and Viscosity Reduction of Solvents-CO2-Heavy Oil Systems. SPE Heavy Oil Conference and Exhibition, Kuwait City, Kuwait, 12-14 December. SPE-150168-MS. http://dx.doi.org/10.2118/150168-MS.

Lie, K. 2014. *An Introduction to Reservoir Simulation using MATLAB: User Guide for the Matlab Reservoir Simulation Toolbox (MRST), SINTEF ICT.*

Lohrenz, J., Bray, B. G. and Clark, C. R. 1964. Calculating Viscosities of Reservoir Fluids From Their Compositions. *J Pet Technol* **16**(10): 1171-1176. SPE-915-PA. http://dx.doi.org/10.2118/915-PA.

Lopez, V. N. 2012. Enhanced Oil Recovery (EOR): Basic Concepts and U.S. Industry Experience. CEPAC - CSLF Capacity Building Workshop, Porto Alegre, Brazil. Enhanced Oil Recovery (EOR): Basic Concepts and U.S. Industry Experience.

Ma, T. D. and Youngren, G. K. 1994. Performance of Immiscible Water-Alternating-Gas (IWAG) Injection at Kuparuk River Unit, North Slope, Alaska. SPE Annual Technical Conference and Exhibition, New Orleans, Louisiana, USA, 25-28 September. SPE-28602-MS. http://dx.doi.org/10.2118/28602-MS.

Madarapu, R. R., Khataniar, S., Patil, S. L. and Dandekar, A. Y. 2002. A Simulation Study of Enhanced Recovery of Schrader Bluff Heavy Oil by Immiscible and Miscible Gas Injection. SPE Western Regional/AAPG Pacific Section Joint Meeting, Anchorage, Alaska, USA, 20-22 May. SPE-76776-MS. http://dx.doi.org/10.2118/76776-MS.

Mahani, H., Sorop, T., Ligthelm, D. J., Brooks, D., Vledder, P., Mozahem, F. and Ali, Y. 2011. Analysis of field responses to low-salinity waterflooding in secondary and tertiary mode in Syria. SPE EUROPEC/EAGE Annual Conference and Exhibition, Vienna, Austria, 23-26 May. SPE-142960-MS. http://dx.doi.org/10.2118/142960-MS.

Mangalsingh, D. and Jagai, T. 1996. A Laboratory Investigation of the Carbon Dioxide Immiscible Process. SPE Latin America/Caribbean Petroleum Engineering Conference, Port-of-Spain, Trinidad, 23-26 April. SPE-36134-MS. http://dx.doi.org/10.2118/36134-MS.

Martin, F. D., Stevens, J. E. and Harpole, K. J. 1995. CO2 Foam Field Verification Pilot Test at EVGSAU: Phase IIIB--Project Operations and Performance Review. *SPE Res Eng* **10**(4): 266-272. SPE-27786-PA. http://dx.doi.org/10.2118/27786-PA.

Matthews, C. S. 1983. Steamflooding. *J Pet Technol* **35**(3): 465-471. SPE-9993-PA. http://dx.doi.org/10.2118/9993-PA.

McGuire, P. L., Chatham, J. R., Paskvan, F. K., Sommer, D. M. and Carini, F. H. 2005a. Low Salinity Oil Recovery: An Exciting New EOR Opportunity for Alaska's North Slope. PE Western Regional Meeting, Irvine, California, USA, 30 March-1 April. SPE-93903-MS. http://dx.doi.org/10.2118/93903-MS.

McGuire, P. L., Redman, R. S., Jhaveri, B. S., Yancey, K. E. and Ning, S. X. 2005b. Viscosity Reduction WAG: An Effective EOR Process for North Slope Viscous Oils. SPE Western Regional Meeting, Irvine, California, USA, 30 March-1 April. SPE-93914-MS. http://dx.doi.org/10.2118/93914-MS.

McKean, T. A. M., Thomas, A. H., Chesher, J. R. and Weggeland, M. C. 1999. Schrader Bluff CO2 EOR Evaluation. SPE Western Regional Meeting, Anchorage, Alaska, USA, 26-27 May. SPE-54619-MS. http://dx.doi.org/10.2118/54619-MS.

Meyer, R. F., Attanasi, E. D. and Freeman, P. A. 2007. Heavy Oil and Natural Bitumen Resources in Geological Basins of the World, U.S. Geological Survey Open-File Report 2007-1084.

Minssieux, L. and Duquerroix, J. P. 1994. WAG Flow Mechanisms in Presence of Residual Oil. SPE Annual Technical Conference and Exhibition, New Orleans, Louisiana, USA, 25-28 September. SPE-28623-MS. http://dx.doi.org/10.2118/28623-MS.

Moffitt, P. D. and Zornes, D. R. 1992. Postmortem Analysis: Lick Creek Meakin Sand Unit Immiscible CO2 Waterflood Project. SPE Annual Technical Conference and Exhibition, Washington, D.C., USA, 4-7 October. SPE-24933-MS. http://dx.doi.org/10.2118/24933-MS.

Mokrys, I. J. and Butler, R. M. 1993. In-Situ Upgrading of Heavy Oils and Bitumen by Propane Deasphalting: The Vapex Process. SPE Production Operations Symposium, Oklahoma City, Oklahoma, USA, 21-23 March. SPE-25452-MS. http://dx.doi.org/10.2118/25452-MS.

Mungan, N. 1991. An Evaluation of Carbon Dioxide Flooding. SPE Western Regional Meeting, Long Beach, California, USA, 20-22 March. SPE-21762-MS. http://dx.doi.org/10.2118/21762-MS.

NETL 2010. Carbon Dioxide Enhanced Oil Recovery - Untapped Domestic Energy Supply and Long Term Carbon Storage Solution. *The Energy Lab*. Carbon Dioxide Enhanced Oil Recovery - Untapped Domestic Energy Supply and Long Term Carbon Storage Solution.

Ning, S. X., Jhaveri, B. S., Jia, N., Chambers, B. and Gao, J. 2011. Viscosity Reduction EOR with CO2 & Enriched CO2 to Improve Recovery of Alaska North Slope Viscous Oils. SPE Western North American Region Meeting, Anchorage, Alaska, USA, 7-11 May. SPE-144358-MS. http://dx.doi.org/10.2118/144358-MS.

Nourpour Aghbash, V. and Ahmadi, M. 2012. Evaluation of CO2-EOR and Sequestration in Alaska West Sak Reservoir Using Four-Phase Simulation Model. SPE Western Regional Meeting, Bakersfield, California, USA, 21-23 March. SPE-153920-MS. http://dx.doi.org/10.2118/153920-MS.

Nutakki, R., Nghiem, L., Li, Y. K. and George, A. 1991. Optimal Representation Of Heavy Fractions In The Simulation Of Multiple-Contact Processes. Annual Technical Meeting, Banff, Alberta, Canada, April 21 - 24. PETSOC-91-57. http://dx.doi.org/10.2118/91-57.

Oellrich, L., Plöcker, U., Prausnitz, J. and Knapp, H. 1981. Equation-of-State Methods for Computing Phase Equilibria and Enthalpies. *Int. Chem. Eng.;(United States)* **21**. Equation-of-State Methods for Computing Phase Equilibria and Enthalpies.

Orr Jr., F. M. and Silva, M. K. 1987. Effect of Oil Composition on Minimum Miscibility Pressure-Part 2: Correlation. *SPE Res Eng* **2**(4). SPE-14150-PA. http://dx.doi.org/10.2118/14150-PA.

Pan, H., Chen, Y., Sheffield, J., Chang, Y.-B. and Zhou, D. 2014. Phase Behavior Modeling and Flow Simulation for Low-Temperature CO2 Injection. SPE Annual Technical Conference and Exhibition, Amsterdam, The Netherlands, 27-29 October. SPE-170903-MS. http://dx.doi.org/10.2118/170903-MS.

Parkhurst, D. L. 1990. Ion-Association Models and Mean Activity Coefficients of Various Salts. 'In '*Chemical Modeling of Aqueous Systems II*, 3 30-43: ACS Publications.

Parkhurst, D. L. and Appelo, C. 1999. User's Guide to PHREEQC (version 2): A Computer Program for Speciation, Batch-Reaction, One-Dimensional Transport, and Inverse Geochemical Calculations. User's Guide to PHREEQC (version 2): A Computer Program for Speciation, Batch-Reaction, One-Dimensional Transport, and Inverse Geochemical Calculations.

Paskvan, F., Turak, J., Jerauld, G., Gould, T., Skinner, R. and Garg, A. 2016. Alaskan Viscous Oil: EOR Opportunity, or Waterflood Sand Control First? SPE Western Regional Meeting, Anchorage, Alaska, USA, 23-26 May. SPE-180463-MS. http://dx.doi.org/10.2118/180463-MS.

Patil, S., Dandekar, A. and Khataniar, S. 2008a. Phase Behavior, Solid Organic Precipitation, and Mobility Characterization Studies in Support of Enhanced Heavy Oil Recovery on the Alaska North Slope, University of Alaska Fairbanks.

Patil, S. B., Dandekar, A. Y., Patil, S. and Khataniar, S. 2008b. Low Salinity Brine Injection for EOR on Alaska North Slope (ANS). International Petroleum Technology Conference, Kuala Lumpur, Malaysia, 3-5 December. IPTC-12004-MS. http://dx.doi.org/10.2523/IPTC-12004-MS.

Peng, D.-Y. and Robinson, D. B. 1976. A New Two-Constant Equation of State. *Ind Eng Chem Fundam* **15**(1): 59-64. A New Two-Constant Equation of State. http://dx.doi.org/10.1021/i160057a011.

Peters, E. J. 2012. *Advanced Petrophysics: Dispersion, Interfacial Phenomena/Wettability, Capillarity/Capillary Pressure, Relative Permeability*: Live Oak Book Company.

Petroleum.co.uk 2015. Benchmark Oils. http://www.petroleum.co.uk/benchmarks (accessed 15 July, 2015).

PetroWiki 2015a. CHOPS operational and monitoring issues. http://petrowiki.org/index.php?title=CHOPS_operational_and_monitoring_issues&oldid=51585 (accessed 15 July, 2015).

PetroWiki 2015b. Compositional effects during immiscible gas injection. http://petrowiki.org/index.php?title=Compositional_effects_during_immiscible_gas_injection&oldid=47218 (accessed 20 July, 2015).

Pospisil, G. 2011. Heavy Oil Challenges & Opportunities North Slope Alaska. http://www.aoga.org/wp-content/uploads/2011/01/8.-Pospisil-Heavy-Viscous-Oil.pdf (accessed 18 July, 2015).

RezaeiDoust, A., Puntervold, T., Strand, S. and Austad, T. 2009. Smart water as wettability modifier in carbonate and sandstone: A discussion of similarities/differences in the chemical mechanisms. *Energy & fuels* **23**(9): 4479-4485. Smart water as wettability modifier in carbonate and sandstone: A discussion of similarities/differences in the chemical mechanisms. http://dx.doi.org/10.1021/ef900185q@proofing.

Rojas, G. A. and Ali, S. M. F. 1988. Dynamics of Subcritical CO2/Brine Floods for Heavy-Oil Recovery. *SPE Res Eng* **3**(1): 35-44. SPE-13598-PA. http://dx.doi.org/10.2118/13598-PA.

Sammon, P. H., Kurihara, M. and Jialing, L. 2001. Applying High-Resolution Numerical Schemes in Reservoirs Described by Complex Corner-Point Grids. SPE Reservoir Simulation Symposium, Houston, Texas, USA, 11-14 February. SPE-66344-MS. http://dx.doi.org/10.2118/66344-MS.

Sánchez-Rodríguez, J., Gachuz-Muro, H. and Sohrabi, M. 2015. Application of Low Salinity Water Injection in Heavy Oil Carbonate Reservoirs. EUROPEC 2015, Madrid, Spain, 1-4 June. SPE-174391-MS. http://dx.doi.org/10.2118/174391-MS.

Sankur, V., Creek, J. L., Di Julio, S. S. and Emanuel, A. S. 1986. A Laboratory Study of Wilmington Tar Zone CO2 Injection Project. *SPE Res Eng*. SPE-12751-PA. http://dx.doi.org/10.2118/12751-PA.

Schlumberger 2015. Minimum Miscibility Pressure. http://www.glossary.oilfield.slb.com/Terms/m/minimum_miscibility_pressure.aspx (accessed 15 July, 2015).

Seccombe, J. C., Lager, A., Webb, K. J., Jerauld, G. and Fueg, E. 2008. Improving Waterflood Recovery: LoSalTM EOR Field Evaluation. SPE Symposium on Improved Oil Recovery,, Tulsa, Oklahoma, USA, 20-23 April. SPE-113480-MS. http://dx.doi.org/10.2118/113480-MS.

Seright, R. 2010. Potential for Polymer Flooding Reservoirs With Viscous Oils. *SPE Res Eval & Eng* **13**(4): 730-740. SPE-129899-PA. http://dx.doi.org/10.2118/129899-PA.

Shahid, M., Shaharudin, M., Jalan, S., Masoudi, R. and Othman, M. B. 2013. Chemical EOR: Challenges for Full Field Simulation. SPE Enhanced Oil Recovery Conference, Kuala Lumpur, Malaysia, 2-4 July. SPE-165247-MS. http://dx.doi.org/10.2118/165247-MS.

Sharma, B. C., Khataniar, S., Patil, S. L., Kamath, V. A. and Dandekar, A. Y. 2002. A Simulation Study of Novel Thermal Recovery Methods in the Ugnu Tar Sands Reservoir, North Slope, Alaska. SPE Western Regional/AAPG Pacific Section Joint Meeting, Anchorage, Alaska, USA, 20-22 May. SPE-76729-MS. http://dx.doi.org/10.2118/76729-MS.

Sharma, G. D., Kamath, V. A., Khataniar, S. and Patil, S. L. 1995. Study on Hydrocarbon Miscible Solvent Slug Injection Process for Improved Recovery of Heavy Oil from Schrader Bluff Oil Pool, Milne Point Unit, Alaska, US Department of Energy.

Shelton, J. L. and Schneider, F. N. 1975. The Effects of Water Injection on Miscible Flooding Methods Using Hydrocarbons and Carbon Dioxide. *SPE J.* **15**(3): 217-226. SPE-4580-PA. http://dx.doi.org/10.2118/4580-PA.

Skauge, A., Dale, E. I. and Bergen, U. 2007. Progress in Immiscible WAG Modeling. SPE/EAGE Reservoir Characterization and Simulation Conference, Abu Dhabi, UAE, 28-31 October. SPE-111435-MS. http://dx.doi.org/10.2118/111435-MS.

Smalley, P. C., Goodwin, N. S., Dillon, J. S., Bidinger, C. R. and Drozd, R. J. 1997. New Tools Target Oil Quality Sweetspots in Viscous Oil Accumulations. *SPE Res Eng* **12**(3): 157-162. SPE-36652-PA. http://dx.doi.org/10.2118/36652-PA.

Spivak, A., Garrison, W. H. and Nguyen, J. P. 1990. Review of an Immiscible CO2 Project, Tar Zone, Fault Block V, Wilmington Field, California. *SPE Res Eng* **5**(2): 155-162. SPE-17407-PA. http://dx.doi.org/10.2118/17407-PA.

Stephenson, D. J., Graham, A. G. and Luhning, R. W. 1993. Mobility Control Experience in the Joffre Viking Miscible CO2 Flood. *SPE Res Eng* **8**(3): 183-188. Mobility Control Experience in the Joffre Viking Miscible CO2 Flood. http://dx.doi.org/10.2118/23598-PA.

Strycker, A. and Wang, S. 1999. Gas Injection for Schrader Bluff, National Petroleum Technology Office, US Department of Energy Report TRWPT-CRADA-003-2.

Strycker, A. and Wang, S. 2000. Recovery Processes for Schrader Bluff, Alaska, U.S. Department of Energy and BP Exploration Inc. Report TRWPT/CRADA-004.

Talbi, K. and Maini, B. B. 2003. Evaluation of CO2 Based Vapex Process for the Recovery of Bitumen from Tar Sand Reservoirs. SPE International Improved Oil Recovery Conference in Asia Pacific, Kuala Lumpur, Malaysia, 20-21 October. SPE-84868-MS. http://dx.doi.org/10.2118/84868-MS.

Tanner, C. S., Baxley, P. T., Crump, J. G., III and Miller, W. C. 1992. Production Performance of the Wasson Denver Unit CO2 Flood. SPE/DOE Enhanced Oil Recovery Symposium, Tulsa, Oklahoma, USA, 22-24 April. SPE-24156-MS. http://dx.doi.org/10.2118/24156-MS.

Targac, G. W., Redman, R. S., Davis, E. R., Rennie, S. B., McKeever, S. O. and Chambers, B. C. 2005. Unlocking the Value in West Sak Heavy Oil. SPE International Thermal Operations and Heavy Oil Symposium, Calgary, Alberta, Canada, 1-3 November. SPE-97856-MS. http://dx.doi.org/10.2118/97856-MS.

Taylor, C. O. and Seamount Jr., D. T. 2002. Conservation Order No. 477, Milne Point Field - Milne Point Unit, Schrader Bluff Oil Pool. Anchoage, AK, USA, Alaska Oil and Gas Conservation Commission.

Thyne, G. 2016. Wettability Alteration in Reservoirs: How it Applies to Alaskan Oil Production. SPE Western Regional Meeting, Anchorage, Alaska, USA, 23-26 May. SPE-180370-MS. http://dx.doi.org/10.2118/180370-MS.

Truesdell, A. H. and Jones, B. F. 1974. WATEQ, A Computer Program for Calculating Chemical Equilibria of Natural Waters. *J. Res. US Geol. Surv* **2**(2): 233-248. WATEQ, A Computer Program for Calculating Chemical Equilibria of Natural Waters.

Twu, C. H. 1984. An Internally Consistent Correlation for Predicting the Critical Properties and Molecular Weights of Petroleum and Coal-Tar Liquids. *Fluid Phase Equilib* **16**(2): 137-150. An Internally Consistent Correlation for Predicting the Critical Properties and Molecular Weights of Petroleum and Coal-Tar Liquids.

Walsh, M. P., Negahban, S. and Gupta, S. P. 1989. An Analysis of Water Shielding in Water-Wet Porous Media. SPE Annual Technical Conference and Exhibition, San Antonio, Texas, USA, 8-11 October. SPE-19652-MS. http://dx.doi.org/10.2118/19652-MS.

Werner, M. R. 1987. Tertiary and Upper Cretaceous Heavy-Oil Sands, Kuparuk River Unit Area, Alaskan North Slope: Section V. Exploration Histories. *SG 25: Exploration for Heavy Crude Oil and Natural Bitumen*: 537-547. Tertiary and Upper Cretaceous Heavy-Oil Sands, Kuparuk River Unit Area, Alaskan North Slope: Section V. Exploration Histories.

Whitson, C. H., Soreide, I. and Anderson, T. 1989. C7+ Characterization of Related Equilibrium Fluids Using the Gamma Distribution. 'In '*C7+ Fraction Characterization*, G. A. Mansoori and L. G. Chorn. New York, N.Y.: Taylor & Francis Pub. Co.

WINPROP 2015. *User Guide - Phase Behavor & Fluid Property Program*. Calgary, Alberta, Canada: Computer Modelling Group Ltd.

Wolery, T. J. 1992. *EQ3/6: A Software Package for Geochemical Modeling of Aqueous Systems: Package Overview and Installation Guide (version 7.0)*: Citeseer.

Yousef, A. A., Al-Saleh, S. and Al-Jawfi, M. S. 2012. The Impact of the Injection Water Chemistry on Oil Recovery from Carbonate Reservoirs. SPE EOR Conference at Oil and Gas West Asia, Muscat, Oman, 16-18 April. SPE-154077-MS. http://dx.doi.org/10.2118/154077-MS.

Yousef, A. A., Al-Saleh, S., Al-Kaabi, A. U. and Al-Jawfi, M. S. 2010. Laboratory Investigation of Novel Oil Recovery Method for Carbonate Reservoirs. Canadian Unconventional Resources and International Petroleum Conference, Calgary, Alberta, Canada, 19-21 October. SPE-137634-MS. http://dx.doi.org/10.2118/137634-MS.

Yu, J., Liu, N., Li, L. and Lee, R. L. 2012. Generation of Nanoparticle-Stabilized Supercritical CO2 Foams. Carbon Management Technology Conference, Orlando, Florida, USA, 7-9 February. CMTC-150849-MS. http://dx.doi.org/10.7122/150849-MS.